POROUS GRAPHITIC CARBON FOR SEPARATIONS OF METABOLITES

Daniel Benjamin Lunn

A dissertation submitted to the faculty at the University of North Carolina at Chapel Hill in partial fulfillment of the requirements for the degree of Doctor of Philosophy in the Department of Chemistry.

Chapel Hill
2017

Approved by:

James W. Jorgenson

Mark H. Schoenfisch

J. Michael Ramsey

Joseph Templeton

Jillian L. Dempsey

ABSTRACT

Daniel Benjamin Lunn: Porous Graphitic Carbon for Separations of Metabolites
(Under the direction of James Jorgenson)

The analysis of the low molecular weight metabolites produced from cellular activity has a broad range of applications in systems biology. One method used to characterize these complex samples is liquid chromatography-mass spectrometry. Traditionally, reversed phase separations using n-octadecyl (C18) bonded silica stationary phases have been used for metabolite samples. Human metabolite samples contain a significant population of polar metabolites, which are not well retained on reversed phase columns. As an alternative to bonded silica, porous graphitic carbon (PGC) stationary phases have been shown to be useful for the analysis of polar and non-polar solutes. PGC offers alternative retention mechanisms combining dispersion interactions with electrostatic interactions. Experiments here explore the applicability of PGC for separations of metabolites using long packed capillary columns.

When moving to capillary scale separations, it is common to use large volume injections relative to the column volume. Due to the lack of retention on C18 bonded silica, these injections will cause polar metabolites to elute as broad peaks early in the gradient. PGC offers significantly increased retention for model metabolites when compared to C18 bonded silica, and PGC also would be suitable for focusing large volume injections. When performing gradient separations with long capillary columns run times can be very long. If a solute has rapid diffusion in the stationary phase during these runs, the bands could elute as broad peaks. It was found that PGC possesses a low level of stationary phase diffusion across a range of temperature and retention conditions, allowing for sharp peaks to elute even after long gradients. Using gradient prediction models, it was found that experimental PGC gradient separations behaved as predicted based on retention data. Long capillary

columns packed with PGC particles produce less efficient columns than C18 bonded silica. As the main interest in PGC was its ability to retain polar metabolites, this was not of particular concern. Application of these columns to liquid chromatography-mass spectrometry of urinary metabolites showed that PGC offered increased peak capacity, largely due to the ability to separate the metabolites over a significantly wider range of mobile phase strengths.

ACKNOWLEDGEMENTS

I would first like to thank Dr. Jorgenson, with whom I have had the privilege of working under for my time in graduate school. His brilliance and enthusiasm for science are remarkable. His guidance along the way has been invaluable in the completion of the work contained within this dissertation. I am thankful for all of my friends that have helped me through graduate school, in particular my Thursday lunch crew. Those hour-long breaks were a welcome respite each week to just escape lab when it is so easy to get absorbed by work. The last year or so hasn't been the same without you all. I'm thankful for all my fellow lab members past and present including Justin Godinho, Stephanie Moore, Jim Grinias, James Treadway, Katie Moeller, and Kelsey Miller. Their conversations about work, life, and random non-sense have been essential throughout the years.

Waters Corporation has been invaluable in the completion of this work. Their discussions over the years have been very insightful on a variety of my projects, many of which did not make it into this thesis. They also have been critical in the supply of parts and consumables to keep the instruments running smooth on a daily basis.

I am thankful for my professors at Luther College, Doug Schumacher and Dr. Carolyn Mottley. They introduced me to analytical instrumentation and were very blunt with me about what graduate school really was like, which helped prepare me for the utter grind that these years have been.

I must thank my girlfriend, Sarah; who has been incredibly encouraging and supportive these last few years. When we first met, I was in a low point of my graduate school career. She was confident in me, even when I was not in myself and I am forever grateful for this. Finally, I must thank my family for molding me into the person I am today. It is the work ethic, handiness, and sheer hardheadedness that I was instilled with from a young age, that got me here today.

TABLE OF CONTENTS

LIST OF TABLES

LIST OF FIGURES

LIST OF ABBREVIATIONS

2-MHA	2-methylhippuric acid
3-MHA	3-methylhippuric acid
4-MHA	4-methylhippuric acid
A/D	Analog-to-digital
AA	Ascorbic acid
Ag/AgCL	Silver/silver chloride
BEH	Bridged-ethyl hybrid
BQ	1,4-Benzoquinone
C18	n-Octadecyl
CLSM	Confocal laser scanning microscopy
EMG	Exponentially-modified Gaussian
ESI	Electrospray ionization
FA	Formic acid
GC-MS	Gas chromatography-mass spectrometry
HA	Hippuric acid
HILIC	Hydrophobic interaction liquid chromatography
HPLC	High performance liquid chromatography
HQ	Hydroquinone
i.d.	Inner diameter
IFF	Isocratic-focusing factor
ISM	Iterative statistical moments
KCl	Potassium chloride
LC	Liquid chromatography
LC-MS	Liquid chromatography-mass spectrometry
MA	Mandelic acid

MeCN	Acetonitrile
MeOH	Methanol
MP	Mobile phase
MS	Mass Spectrometry
m/z	Mass-to-charge ratio
NMR	Nuclear magnetic resonance
o.d.	Outer diameter
PDA	Photodiode array
PGC	Porous graphitic carbon
POISe	Performance optimizing injection sequence
PREG	Polar retention effect on graphite
qToF	Quadrupole time-of-flight
RSD	Relative standard deviation
SEM	Scanning electron microscopy
TASF	Temperature assisted solute focusing
TFA	Trifluoroacetic acid
UHPLC	Ultra-high pressure liquid chromatography
UPLC	Ultra-performance liquid chromatography
UV	Ultraviolet
Vis	Visible

LIST OF SYMBOLS

A	Eddy diffusion van Deemter term
A_{peak}	Amplitude of Exponentially Modified Gaussian function peak fit
a	Reduced eddy diffusion van Deemter term
a_{curve}	Parameter allowing for observed curvature in the fit of retention data
B	Longitudinal diffusion van Deemter term
B_{sol}	Solute dependent term largely determined by molecular weight
b	Reduced longitudinal diffusion van Deemter term
C	Resistance to mass transfer van Deemter term
c	Reduced resistance to mass transfer van Deemter term
D_{eff}	Effective diffusion coefficient
$D_{eff,2MHA}$	Effective diffusion coefficient of 2-methylhippuric acid
$D_{eff,acetone}$	Effective diffusion coefficient of acetone
D_m	Diffusion coefficient of an analyte in the mobile phase
$D_{m,0}$	Frequency factor of mobile phase diffusion
$D_{m,2MHA}$	Diffusion coefficient of an 2-methylhippuric acid in the mobile phase
$D_{m,acetone}$	Diffusion coefficient of an acetone in the mobile phase
D_s	Stationary phase diffusion coefficient
$D_{s,0}$	Frequency factor of surface diffusion
d_c	Column inner diameter
$d_{inj,0}$	Distance that an unretained analyte travels over the course of injection loading
$d_{inj,a}$	Distance that a retained analyte travels over the course of injection loading
d_p	Particle diameter
E_m	Activation energy of molecular diffusion in the mobile phase

E_s	Activation energy of molecular diffusion in the stationary phase
F	Volumetric flow rate
$f(t)$	Measured peak signal in the time domain
$\Delta G°$	Standard Gibbs free-energy
G	Gradient compression factor
g	Gradient slope
H	Height equivalent of a theoretical plate
$\Delta H°$	Standard enthalpy of transfer from mobile to stationary phase
h	Reduced plate height
$h_{\min}$	Minimum reduced plate height
IFF_{BEH}	Isocratic-focusing factor on C18 BEH column
IFF_{PGC}	Isocratic-focusing factor on Hypercarb column
K_0	Frequency factor of adsorption
K	Analyte partition coefficient
K_{inj}	Term describing the injection profile
k'_{00}	Retention factor of an analyte in 100% water
$k'_{00,BEH}$	Retention factor of an analyte in 100% water for C18 BEH column
$k'_{00,PGC}$	Retention factor of an analyte in 100% water for Hypercarb column
k'	Analyte retention factor
k'_a	Analyte retention factor in a specific mobile phase composition
$k'_{a,BEH}$	Analyte retention factor in a specific mobile phase composition for C18 BEH column
$k'_{a,PGC}$	Analyte retention factor in a specific mobile phase composition for Hypercarb column
k_B	Boltzmann constant
k'_{init}	Retention factor in gradient initial conditions

k'_{total}	Combined term defininining the retention of a solute for error propogation
L	Length of a chromatographic column
M_A	Molecular weight of a solute
N	Number of theoretical plates
N_{max}	Number of theoretical plates at the optimum velocity
$N_{max,1m}$	Number of theoretical plates at the optimum velocity for a 1 m Hypercarb column
$N_{max,2m}$	Number of theoretical plates at the optimum velocity for a 2 m Hypercarb column
n_c	Peak capacity
$n_{c,1m}$	Peak capacity for a 1 m Hypercarb column
$n_{c,2m}$	Peak capacity for a 2 m Hypercarb column
ΔP	Required pressure drop
ΔP_{opt}	Pressure required to reach the optimum linear velocity of a column
Q_{st}	Isosteric heat of adsorption
R	Gas constant
r_H	Hydrodynamic radius of a solute
S	Constant dependent on solute molecular weight
$\Delta S°$	Standard entropy of transfer from mobile to stationary phase
T	Absolute temperature
$t_{1/2}$	Time to reach 50% of maximum signal intensity
t	Time
t_{delay}	Gradient delay time
t_{expt}	Experimentally measured retention time
t_G	Gradient length in time
t_g	Length of gradient separation window

t_{inj}	Time it takes to load a fixed injection volume
t_m	Column deadtime
t_{pred}	Predicted retention time
t_R	Retention time of an analyte
t_{stop}	Stop time
Δt	Time between detected peaks
u	Linear velocity of the mobile phase
u_a	Solute linear velocity
V_a	Total volume a solute band occupies after injection loading
$V_{a,BEH}$	Total volume a solute band occupies after injection loading on C18 BEH column
$V_{a,PGC}$	Total volume a solute band occupies after injection loading on Hypercarb column
V_{dwell}	Dwell volume
V_f	Solvent Free volume
V_{inj}	Injection volume
V_m	Volume of mobile phase in the column
V_{max}	Maximum allowable injection volume
V_S	Volume of stationary phase in the column
v	Reduced linear velocity
w_p	Average peak width
β	Surface diffusion fraction of isosteric heat of adsorption
γ_m	Mobile phase obstruction (tortuosity) factor
γ_s	Stationary phase obstruction (tortuosity) factor
ε_i	Interparticle porosity of the column
ε_t	Total column porosity

η	Mobile phase viscosity
θ	Term related to the amount of allowable performance loss from injection
λ_{diff}	Distance between two equilibrium positions for diffusion
$\sigma_{1+k'}$	Standard deviation of the term, retention factor plus one
$\sigma_{ax,L}^2$	Spatial variance of a peak due to longitudinal diffusion
$\sigma_{D_{eff}}$	Standard deviation of the analyte effective diffusion coefficient
$\sigma_{D_{eff}-\psi}$	Standard deviation of the analyte effective diffusion coefficient minus the mobile phase contribution to effective diffusion
$\sigma_{D_{eff,acetone}}$	Standard deviation of the effective diffusion contribution for acetone
$\sigma_{D_{eff,2MHA}}$	Standard deviation of the effective diffusion for 2-methylhippuric acid
$\sigma_{D_{eff,2MHA}-\psi}$	Standard deviation of the analyte effective diffusion coefficient minus the mobile phase contribution to effective diffusion for 2-methylhippuric acid
σ_{D_m}	Standard deviation of the analyte diffusion coefficient in the mobile phase
$\sigma_{D_{m,acetone}}$	Standard deviation of the diffusion coefficient of acetone in the mobile phase
$\sigma_{D_{m,2MHA}}$	Standard deviation of the diffusion coefficient of 2-methylhippuric acid in the mobile phase
$\sigma_{d_c^2}$	Standard deviation of the square of the column diameter
σ_{d_c}	Standard deviation of the column diameter
$\sigma_{k'}$	Standard deviation of the retention factor
$\sigma_{k'_{total}}$	Standard deviation of the combined term defining the retention of a solute for error propagation
σ_{diff}^2	Temporal variance due to longitudinal molecular diffusion
σ_{fit}	Sigma parameter from Exponentially Modified Gaussian function peak fit
σ_{slope}	Standard deviation of the slope of a trend line

$\sigma_{slope,acetone}$	Standard deviation of the slope for acetone
$\sigma_{slope,2MHA}$	Standard deviation of the slope for 2-methylhippuric acid
σ_{t1}^2	Temporal variance of first detected peak
σ_{t2}^2	Temporal variance of second detected peak
σ_t^2	Temporal variance of a peak
$\sigma_{\Delta t}$	Standard deviation of the migration time between detected peaks
$\sigma_{t,EMG}^2$	Variance of peak fit with Exponentially Modified Gaussian function
σ_{t_m}	Standard deviation of the deadtime
$\sigma_{t\_net}^2$	Accumulated temporal variance between detectors
σ_{t_R}	Standard deviation of the retention time
$\sigma_{t_R - t_m}$	Standard deviation of the time difference between retention time and deadtime
σ_{γ_m}	Standard deviation of the mobile phase obstruction factor
$\sigma_{\gamma_m D_m}$	Standard deviation of the mobile phase obstruction factor times mobile phase phase diffusion coefficient
$\sigma_{\gamma_m D_{m,2MHA}}$	Standard deviation of the mobile phase obstruction factor times mobile phase phase diffusion coefficient for 2-methylhippuric acid
$\sigma_{\gamma_s D_s}$	Standard deviation of the stationary phase obstruction factor times stationary phase diffusion coefficient
$\sigma_{\gamma_s D_s}$	Standard deviation of the stationary phase obstruction factor times stationary phase diffusion coefficient
$\sigma_{\frac{\gamma_s D_s}{\gamma_m D_m}}$	Standard deviation of the stationary phase contribution divided by the mobile phase contribution
$\sigma_{\frac{\sigma_{\gamma_s D_s}}{\gamma_m D_{m,2MHA}}}$	Standard deviation of the stationary phase contribution divided by the mobile phase contribution for 2-methylhippuric acid
$\sigma_{\Delta\sigma_{t\_net}^2}$	Standard deviation of the accumulated temporal variance
σ_ψ	Standard deviation of the mobile phase diffusion contribution to the effective diffusion coefficient

τ_{diff}	Rate constant of diffusion
τ_{fit}	Tau parameter from Exponentially Modified Gaussian function peak fit
Φ	Flow resistance
ϕ	Phase ratio
φ	Fraction of mobile phase consisting of organic content
$\Delta\varphi$	Change in organic content over the gradient
ψ	Mobile phase diffusion contribution to the effective diffusion coefficient

CHAPTER 1. INTRODUCTION

1.1 Metabolomics

1.1.1 Scope of Metabolomics Analysis

The field of metabolomics encompasses the detection, quantification, and identification of small molecules (molecular weight < 1,200 Da) produced during cellular processes in biological samples.[1] This systems biology level approach of studying metabolism has provided insight into the processes of drug discovery, disease biomarker detection, and toxicology.[2–6] The metabolome encompasses a wide variety of compounds including, among other things, amino acids, lipids, fatty acids, vitamins, and carbohydrates. For humans alone, there are over 40,000 confirmed metabolites.[7] Analysis of metabolites can be classified into a number of different strategies based on the desired information about the sample. These strategies include targeted analysis, global profiling, clinical diagnostics, and metabolic fingerprinting.[8]

A general metabolomics workflow can be found in Figure 1-1. The specifics of each step will be determined by the sample, analysis method, and goal of the experiment. For detailed metabolomics studies, hundreds to thousands of samples must be collected and analyzed.[6] Small differences in metabolic profile are often being investigated, making the stability of these samples and reproducibility of the preparation steps of the utmost importance.[9,10] Even timing of sample collection can play a role in the final result of the analysis as the metabolite sample collected at any moment in time is simply a snapshot of the metabolic profile and is subject to variation over the course of a single day. Although natural variability between people is expected to be more significant, the details of the collection, storage, and sample preparation steps and their impact on the analysis should not be overlooked.[11]

1.1.2 Analytical Techniques used for Metabolomics

Metabolomic samples provide a complex analytical problem. Compared to proteomics and transcriptomics, metabolomics offers a much more diverse range of compounds.[12] With only 20 amino acid building blocks for the proteome and four nucleotide bases for the transcriptome, the structural variability is limited.[12] Increased structural variation leads to more chemical variability in metabolites, as seen by the range in polarities between metabolites such as carbohydrates and lipids. Another complicating factor is that the metabolic profile expressed within a human is not just dependent on their genetics, but also a number of other factors including, but not limited to, diet, chemical exposures, gender, and age.[13–16] These factors produce a number of exogenous and endogenous compounds that are in flux not only over the course of a human lifetime, but also over the course of a single day. The concentration range of species in metabolite samples can also span 9-orders of magnitude (mM to pM), requiring sensitive detection of low abundance species.[12]

To date, the most common analytical methods used for metabolomics analysis are nuclear magnetic resonance (NMR) spectroscopy, gas chromatography-mass spectrometry (GC-MS), and liquid chromatography-mass spectrometry (LC-MS).[12] Due to the complexity of the human metabolome, no single method can provide analysis of all metabolites.[17] These techniques provide complimentary information, and can be used in combination to get a more complete picture of the metabolite profile at the time of sampling.

NMR provides the ability to do analysis of metabolite samples with little to no sample preparation in a highly reproducible and non-destructive manner.[18,19] ^{1}H NMR is most often used as the majority of metabolites will contain hydrogen atoms, allowing simultaneous detection of a large number of species. Due to the complexity of samples, a single NMR spectrum could produce thousands of signals, providing a great deal of structural information about metabolites after significant data processing is performed.[20] Metabolites can be quantified directly by the addition of an internal standard.[21] The big drawback of NMR is its relatively high limit of detection (~10 μM), meaning that many metabolites will go undetected.[8]

GC-MS allows for the separation and detection of wide range of low molecular weight and volatile metabolites with low limits of detection. A derivitization step using silylating reagents is needed to allow for sufficient volatility of the polar species.[11] The resulting chromatograms can contain hundreds of peaks, which can be correlated to metabolite identifications using deconvolution software and spectral database searching.[22] Although GC-MS has been widely utilized for metabolomics, it does have several shortcomings. First, due to the volatility needed for analysis, GC-MS is inherently biased against high molecular weight and non-volatile species.[12] Also, the additional derivitization step needed for polar species adds sample preparation time and is potentially a source of variability if not done in a repeatable fashion.[23] Consistency of the derivitization step has been improved by the development of automated systems, although the process can still lead to multiple peaks for a single compound due to partial, or incomplete derivitization.[11,23]

LC-MS is capable of analyzing metabolites with a wide range of properties and low limits of detection with the added benefit of not requiring any sample derivitization. Traditionally, reversed phase separations using n-octadecyl (C18) bonded silica particles are used for metabolomics.[24–26] The popularity of reversed phase separations is due to its well-understood properties as well as the simplicity of use. Reversed phase columns utilize a hydrophobic particle surface in conjunction with aqueous mobile phases containing low levels of organic content (acetonitrile or methanol).[27] Compounds interact with the stationary phase and are retained based on increasing hydrophobicity. Due to the wide range of polarities present in metabolite samples, it is often necessary to utilize gradient separations, where the organic content in the mobile phase is increased over the course of the run. The pitfall with reversed phase columns is their inability to sufficiently retain polar species.[28,29] These species will not interact strongly with the C18 layer, ultimately leading to compounds eluting at the pace of the mobile phase or as very wide bands early in the gradient. Metabolite samples are typically derived from aqueous fluids, therefore many of their constituents will be highly polar and when analyzed with a reversed phase column, a loss of information may occur.

Due to the number of polar metabolites that are difficult to analyze using C18-bonded

columns, hydrophilic interaction liquid chromatography (HILIC) has become more popular for applications such as the analysis of urinary metabolites.[29–31] HILIC utilizes a polar stationary phase (bare silica, aminopropyl modified, or diol modified are common) in conjunction with aqueous mobile phases containing a high level of acetonitrile to allow retention and separation of polar species.[32] The retention mechanism for HILIC is complex and involves a layer of water that is bound to the particle surface, into which solutes will partition. Although HILIC is able to analyze polar compounds, any metabolite with a moderate amount of hydrophobicity will be unretained. Similar to C18 bonded columns; HILIC columns are not capable of separating the whole range of polarities that are expected in metabolite samples. Therefore, HILIC and reversed phase separations are considered to be complementary in the information that they provide.[32,33] As an alterative to these C18 bonded and HILIC columns, porous graphitic carbon has been shown able to retain both non-polar and polar species using a single chromatographic column, potentially providing similar information in decreased analysis time.[34]

1.2 Porous Graphitic Carbon

1.2.1 Origin of Porous Graphitic Carbon in Chromatography

Initial interest in carbon as a chromatographic stationary phase was spurred by the knowledge that silica is unstable under basic conditions and high temperatures.[27,35] Since the 1970's, many attempts to produce a chromatographically useful carbon stationary phase have been made. Early on, the primary issues that were encountered were a lack of mechanical stability as well as poor chromatographic performance.[36–38] The poor performance was thought to be due to the presence of micropores and surface defects, which caused slow mass transfer kinetics. In 1980, Knox and Gilbert filed a patent detailing the preparation of a material that would later be called porous graphitic carbon (PGC).[39,40] These PGC particles were made by first introducing a mixture of phenol and hexamine into a spherical porous silica template, which was then polymerized. Heating of the particles up to 1000 °C pyrolized the polymer and after the dissolution of the silica substrate, left a carbon structure that is the negative of the silica template. Graphitization was then performed at temperatures

> 2500 °C under inert conditions, which ordered the carbon structure and eliminated micropores that were previously present. This material was commercialized under the trade name of Hypercarb, and is now available in 7 μm, 5 μm, and 3 μm particle sizes. In 1991, two other groups published alternative methodologies for the production of porous graphitic particles.[41,42] These materials were commercialized as BTR Carbon and TSK-gel Carbon-500. Although the synthetic pathways used to produce these three forms of porous graphitic carbon are different, they all are expected to have similar properties and so they will all be grouped under the title of PGC throughout the following Chapters.

Further studies by Knox, Kaur, and Millward into Hypercarb allowed insight into the structure of the PGC surface.[43] PGC particles are composed of intertwined stacks of graphitic sheets of sp^2 hybridized carbon atoms, giving the surface a flat structure. The atoms within a single sheet are held together by covalent bonds, while the layers of sheets interact by van der Waals forces. PGC particles are considered two-dimensional graphite, which differs from three-dimensional graphite in that it no longer has regular orientation of the layered graphite sheets. The basal plane of the PGC, or the plane parallel to the graphitic sheets, is atomically flat and has a satisfied valence throughout, making it highly polarizable.[44] The carbon atoms on the edge plane, or the plane perpendicular to the sheets, posses an unsatisfied valence and are thought to be sites where oxidizable functional groups could exist.[45] While bonded silica based stationary phases are unstable under basic and high temperature conditions, PGC, being composed completely of carbon, is stable across the full range of pH as well as temperatures up to 200 °C.[46–48]

1.2.2 Retention Mechanisms of PGC

Since its development, a number of studies on the retention properties and mechanisms of PGC have been published.[49–51] The retention mechanisms have been found to be a combination of dispersive and electrostatic interactions.[45] Separations of neutral hydrocarbons suggest that PGC offers retention properties similar to traditional reversed phase stationary phases for these species.[50,51] PGC has been shown to have higher methylene selectivity than C18-bonded columns, meaning that

the addition of a methylene group to a compound produces a larger change in retention on PGC. Overall, the retention of non-polar species tend to be higher on PGC, and has been shown to be due in part to the flat surface favoring strong adsorption of the solutes.

Although PGC is composed solely of carbon, it does not strictly act like a reversed phase system. Early on it was realized that the electronic distribution of the solute impacted its retention.[51] Ross and Knox classified these electrostatic interactions with polar compounds as the polar retention effect on graphite (PREG).[47] As mentioned previously, the basal plane of the graphite sheets contain delocalized electrons, making the surface highly polarizable. When a polar compound approaches the surface, the electron cloud will form an image force based on the electron density of the polar group. Figure 1-2 is a diagram of the induced dipoles that would be produced on the PGC due to positively and negatively charged groups nearing the surface. As the strength of electrostatic interactions is dependent on the distance between the bodies, it is expected that the orientation of polar functional groups in relation to the graphite surface play a role in retention.[52] Although the combination of the dispersive interaction and PREG mechanism allow increased retention of both polar and non-polar species when compared to traditional reversed phase systems, it comes at the cost of added complexity for understanding the interplays of these mechanisms.

1.2.3 Application of PGC Columns

The main areas of interest that PGC particles have been applied are in the separations of polar analytes and structurally similar analytes. Due to the increased retention of polar compounds with the PREG mechanism, PGC columns have been successfully applied to neurotransmitters, carbohydrates, organic explosives, and glycans.[53–56] Since the graphite surface is flat, the three-dimensional configuration of the analyte as it approaches the surface can impact its retention.[52] More planar molecules are able to reach closer to the surface and interact more strongly, allowing for the separation of structural isomers that differ in their ability to come in contact with the flat graphite surface.[57] The differences in retention between PGC and reversed phase columns have also led to several publications reporting two-dimensional separations utilizing the PGC and C18 bonded

stationary phases.[58,59] The utility of PGC to separate polar, non-polar, and structurally similar species with a single column makes it a unique material for a variety of separations. Despite these unique properties, widespread adoption of PGC has been limited due to the complexities of its retention mechanism making the prediction of the elution of solutes a challenge, along with inherent redox properties which have been shown to influence separations (discussed in Chapter 2).[34]

1.3 Chromatographic Theory

1.3.1 Chromatographic Efficiency

In order to perform quality separations of complex metabolite samples, it is vital to have a highly efficient column. Although gradient separations are typically used with metabolomics samples, it is still useful to determine the efficiency of a column using isocratic separations. While flowing down a chromatographic column under isocratic conditions, a solute band experiences a variety broadening processes that ultimately sum to the final peak profile. The efficiency is determined by direct measurement of the peak profile and its corresponding number of theoretical plates (N).[27]

$$N = \frac{t_R^2}{\sigma_t^2} \qquad \text{Equation 1-1}$$

Here, t_R is the analyte retention time and σ_t^2 is the temporal variance of the measured peak. N provides a dimensionless value describing the overall performance for a single solute, but provides no context of the column used to perform the separation. In order to compare packed columns, the height equivalent of a theoretical plate (H) is a more useful term as it scales N to the column length (L).

$$H = \frac{L}{N} \qquad \text{Equation 1-2}$$

H allows for comparison of performance of two columns, independent of their overall length.

1.3.2 van Deemter Equation

It is known that broadening processes vary with the mobile phase linear velocity (u) as the solute band travels through the column. The velocity dependence of these processes can be easily understood through the van Deemter equation.[27]

$$H = A + \frac{B}{u} + Cu \qquad \text{Equation 1-3}$$

Here, the A-term describes the contribution of eddy dispersion, the B-term describes the contributions of longitudinal diffusion, and the C-term describes the resistance to mass transfer within the column. Equation 1-3 clearly shows that the broadening processes vary with u and that they are additive to H, which can be visualized in Figure 1-3.

Although the van Deemter equation allows understanding the plate height variation with mobile phase velocity, it falls short in allowing direct comparison of columns packed with different particle sizes (d_p) as well as varying analyte diffusion coefficients in the mobile phase (D_m). For this reason, terms for the reduced plate height (h) and reduced velocity (v) are often calculated using Equations 1-4 and 1-5.[60]

$$h = \frac{H}{d_p} \qquad \text{Equation 1-4}$$

$$v = \frac{u d_p}{D_m} \qquad \text{Equation 1-5}$$

These terms can also be substituted into Equation 1-3 to form the reduced van Deemter equation.

$$h = a + \frac{b}{v} + cv \qquad \text{Equation 1-6}$$

Here, a, b, and c are the reduced forms of the broadening terms discussed above. Again, the use of Equation 1-6 allows for direct comparison of the performance of columns of varying lengths, packed with different particle sizes, as well as differing analyte/mobile phase combinations. Detailed mathematical discussion of the van Deemter terms is beyond the scope of this work, but the basic principles of the contributions will be discussed here.[61–64]

1.3.3 *A*-term Broadening

Also know eddy dispersion, the A-term describes the broadening that occurs due to the presence of multiple flow paths that an analyte could travel through in the packed bed of the column. Alternative paths mean that analyte molecules will experience differing path lengths and velocities,

leading to a broadening of the band. Giddings' work described a more complex picture of eddy dispersion involving five different regimes that account for A-term broadening: transchannel, short-range interchannel, long-range interchannel, transparticle and transcolumn.[61] The difference between these regimes is the distance scale upon which they operate within a packed bed. Although the A-term is considered to be independent of flow in the van Deemter equation, these regimes all will be partially dependent on linear velocity.[63,64] The flow dependence can manifest as an apparent increase in C-term, disguising the overall contribution of the A-term.[64] By improving the homogeneity of the packed bed, the range of flow paths can be reduced, thus stressing the importance of packing a uniform bed structure.[62]

1.3.4 B-term Broadening

The B-term describes broadening due to longitudinal diffusion within the column, coming about from the relaxation of concentration gradients within the solute band. Increasing linear velocity will reduce the contribution from longitudinal diffusion. There are number of diffusional processes that occur within the column that will broaden the solute band. Diffusion in the mobile phase can occur in the interstices of the particles as well as within the pores of fully porous or superficially porous particles. The mobile phase within the particle pores is also known as the stagnant mobile phase. In practice, the diffusion coefficients in the mobile phase and stagnant mobile phase are some fraction of D_m as obstructions due to the particle packed bed as well as possible steric constriction within the particle pores limit diffusion.[61] A third, and often ignored, source of diffusion is that within the stationary phase of the packing material.[27] Even when in a retained state, solute molecules can still diffuse along the particle surface, with this contribution becoming potentially more significant for highly retained analytes that spend a lot of time in the stationary phase.[65]

1.3.5 C-term Broadening

The C-term, or the resistance to mass transfer, is related to the transfer of solute molecules between regions of the column. All liquid chromatography (LC) separations will have contributions

from the mobile and stationary phases, but if porous particles are used, a contribution from the stagnant mobile phase will also be included. Stationary phase resistance to mass transfer comes about due to the time it takes for solutes to diffuse into and out of the stationary phase.[27] Mobile phase resistance to mass transfer is related to the transit of analyte from the interparticle volumes to the particle surface.

1.3.6 Effect of Particle Size on Performance

When looking to improve separations, one route to achieve this is by utilizing packing material of differing size. In particular the A and C-terms scale with d_p and d_p^2, respectively.[27] This means that by utilizing smaller particles, H will decrease accordingly. Figure 1-4 shows the change in H that is expected when using 5 μm, 3 μm, and 1 μm particles. Another observation is that as particle size decreases, the linear velocity at which the minimum plate height is observed is shifted higher. Improvements in column performance when moving to smaller particles is what led to the development of ultrahigh pressure liquid chromatography (UHPLC) in our lab. The pressure required to flow through a packed bed can be found using the Kozeny-Carman equation:[27]

$$\Delta P = \left(\frac{185u\eta L}{d_p^2}\right)\left(\frac{1-\varepsilon_i}{\varepsilon_i}\right) \qquad \text{Equation 1-7}$$

where ΔP is the required pressure drop, η is the mobile phase viscosity, and ε_i is the fraction of column volume in the interstices between particles. As the linear velocity needed to achieve the minimum plate height is related to $\frac{1}{d_p}$, the pressure required to operate at the optimum linear velocity (ΔP_{opt}) is related to d_p by:[66]

$$\Delta P_{opt} \propto \frac{1}{d_p^3} \qquad \text{Equation 1-8}$$

Equation 1-8 makes clear that the improved performance of small particles comes at the cost of greatly increased pressure requirements. The development of systems capable of performing isocratic separations at these elevated pressures led to a number of studies showing the packing of capillary columns with particles as small as 1 μm and operating them pressures up to 100,000 psi.[67]

1.3.7 Gradient UHPLC Separations

As mentioned previously, when analyzing complex samples, gradient methods are preferred due to their ability to elute a wide range of compounds in a reasonably short time frame. A common measure of efficiency of these complex gradient separations is the peak capacity (n_c), or the number of peaks that can be fit in a separation window with a resolution of one.[68]

$$n_c = \frac{t_g}{w_p} + 1 \qquad \text{Equation 1-9}$$

Here t_g is the gradient separation window, or the time between the first and last peak, and w_p is average width of the peaks throughout that separation window. It is also expected that $n_c \propto \sqrt{N}$, so higher performing columns should produce higher peak capacities.[27] The two most common methods to improve N are by utilizing longer columns (Equation 1-2) and packing with smaller particles. In order to use the high efficiency columns produced for UHPLC separations, instrumentation capable of performing gradient separations above the 400 bar (5,800 psi) limit of traditional high performance liquid chromatography (HPLC) instruments were needed. Multiple manufacturers have now released commercial instruments capable of gradient separations up to 15,000 psi (1,000 bar). Shen *et al.* demonstrated a system capable of running two-meter columns packed with 3 µm C18-bonded particles that was able to detect > 5,000 metabolites from a *Shewanella oneidensis* (a bacterium) in a 2,000 minute gradient separation at pressures of 20,000 psi.[69] Recently, a modified gradient UHPLC system was developed in our lab. This system allowed pre-loaded gradient separations to be performed up to 45,000 psi and can be seen in Figure 1-5.[70] Utilizing this gradient system with long columns packed with sub-2 µm particles allowed a peak capacity of 800 to be achieved in 700 minutes for proteomic samples.[71]

1.4 Dissertation Overview

The work presented in this dissertation is focused on improving separations of metabolites with the implementation of long capillary columns packed with porous graphitic carbon. It is thought that PGC could be useful due to its alternative retention mechanism increasing retention of polar

analytes, offering an alternative to traditional reversed phase packing materials. As the smallest commercially available Hypercarb particles are 3 μm, the best way to improve the peak capacity of metabolite separations with PGC is to increase the column length. Columns of one and two-meters in length are possible due to the pressure limits available with the modified gradient UHPLC system. Before capillary columns are introduced, it is important to understand the fundamentals of how PGC columns perform with model metabolites. Chapter 2 investigates the retention and injection focusing properties of Hypercarb. Chapter 3 looks into the stationary phase diffusion properties of Hypercarb, which are vital for the long gradient separations that would be used with these capillary columns. Chapter 4 utilizes the retention data obtained in Chapter 2 in order to model gradient separations to assure that the experimental separations with PGC act as predicted. Finally, Chapter 5 culminates in the packing, characterization and application of long capillary columns packed with PGC for the analysis of urinary metabolites. Along the way, comparisons will be continuously made to traditional C18 bonded stationary phases, as they are the most popular phases used today for reversed phase separations.

1.5 FIGURES

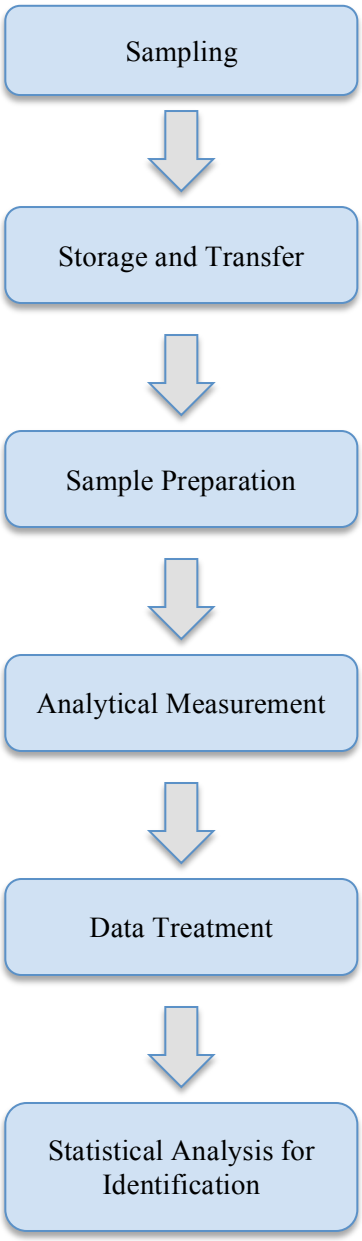

Figure 1-1. Workflow of a standard metabolomics experiment. The specific steps within each process will vary depending on the sample, analysis method, as well as the overall goal of the analysis.

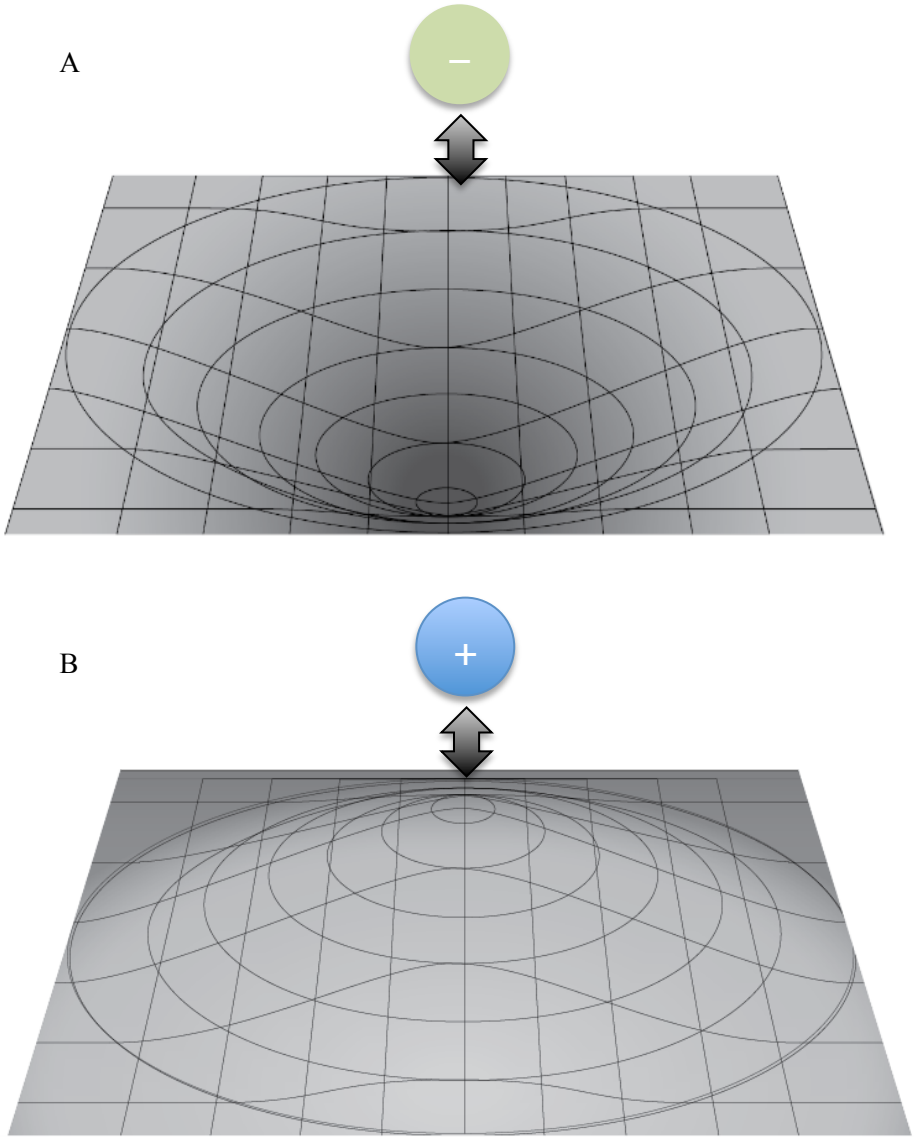

Figure 1-2. Diagram showing the impact of PREG on the electron density when a negatively (A) and positively (B) charged species approach the PGC surface. Image forces are produced due to the attraction/repulsion of valence electrons on the particle surface to the analyte.

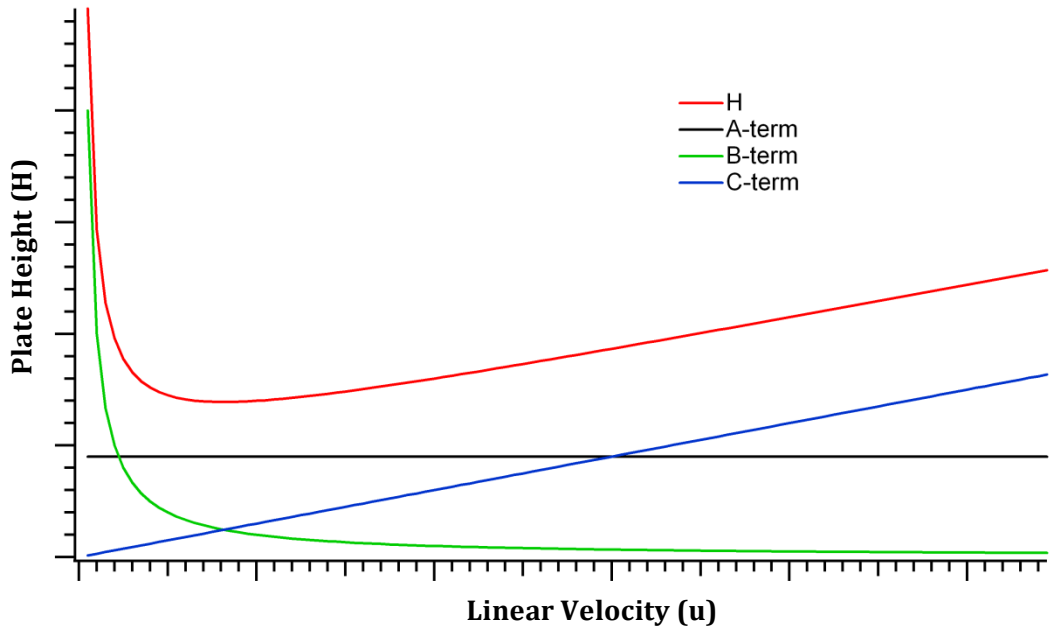

Figure 1-3. Contributions of the A, B, and C-terms to the overall plate height, as a function of linear velocity. These contributions are derived from Equation 1-3.

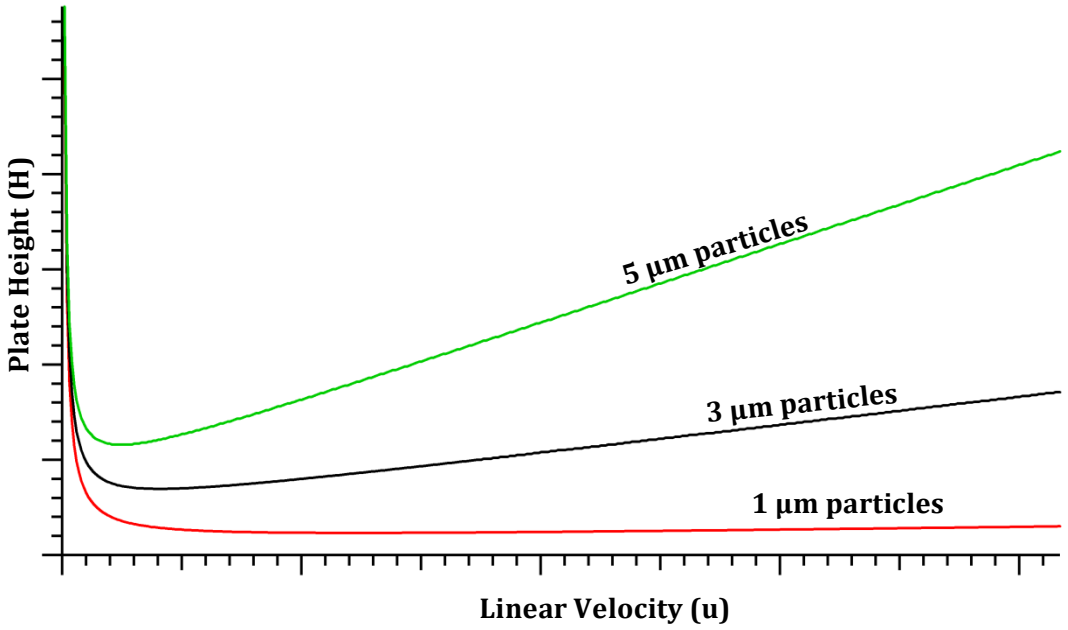

Figure 1-4. Theoretical plots of plate height vs. linear velocity for columns packed with 5 µm, 3 µm, and 1 µm particles. It is seen that as the particle diameter decreases, plate height decreases and the minimum plate height shifts to higher linear velocities.

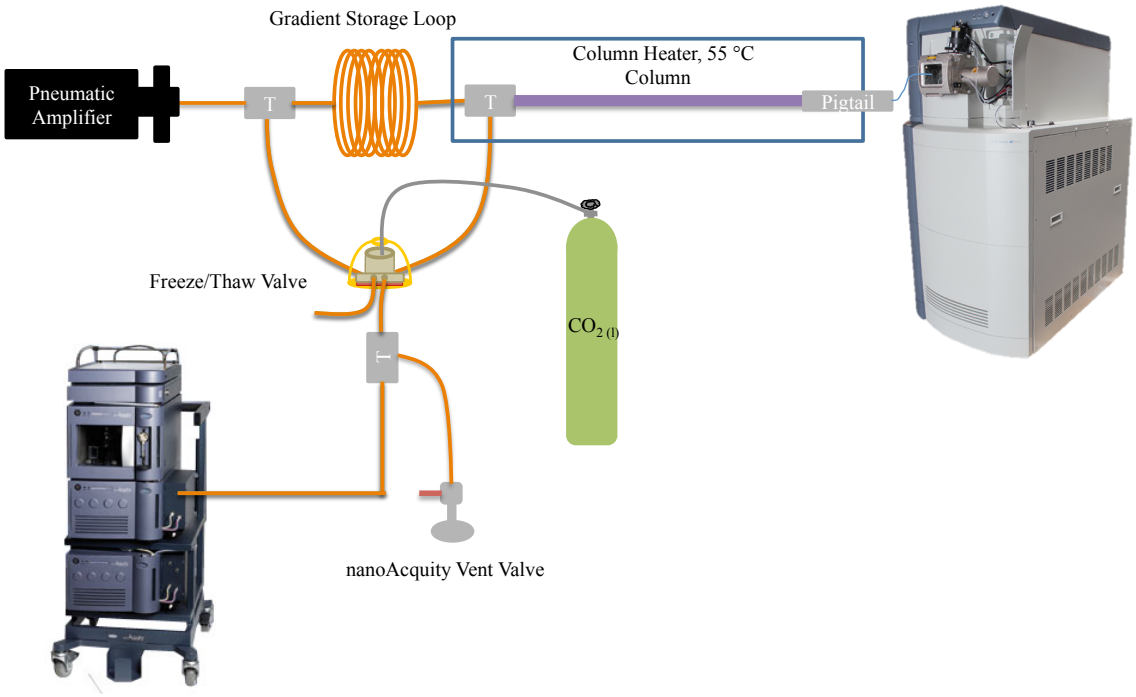

Figure 1-5. Schematic of the gradient UHPLC system used for capillary LC-MS analysis. This figure was used with permission from the author.[70]

REFERENCES

(1) Nobeli, I.; Ponstingl, H.; Krissinel, E. B.; Thornton, J. M. J Mol Biol **2003**, 334, 697–719.

(2) Spagou, K.; Wilson, I. D.; Masson, P.; Theodoridis, G.; Raikos, N.; Coen, M.; Holmes, E.; Lindon, J. C.; Plumb, R. S.; Nicholson, J. K.; Want, E. J. Anal. Chem. **2011**, 83, 382–390.

(3) Ryan, D.; Robards, K.; Ryan, D.; Robards, K. Anal. Chem. **2006**, 78, 7954–7958.

(4) Wishart, D. S. Nat. Rev. Drug Discov. **2016**, 15, 473–484.

(5) Kell, D. B. Curr. Opin. Microbiol. **2004**, 7, 296–307.

(6) Mamas, M.; Dunn, W. B.; Neyses, L.; Goodacre, R. Arch. Toxicol. **2011**, 85, 5–17.

(7) Wishart, D. S.; Jewison, T.; Guo, A. C.; Wilson, M.; Knox, C.; Liu, Y.; Djoumbou, Y.; Mandal, R.; Aziat, F.; Dong, E.; Bouatra, S.; Sinelnikov, I.; Arndt, D.; Xia, J.; Liu, P.; Yallou, F.; Bjorndahl, T.; Perez-Pineiro, R.; Eisner, R.; Allen, F.; Neveu, V.; Greiner, R.; Scalbert, A. Nucleic Acids Res. **2013**, 41, D801–D807.

(8) Wiedmer, S. K.; Hyotylainen, T. Chromatogr. Methods Metabolomics **2013**, No. 18, 1–10.

(9) Wiedmer, S. K.; Hyötyläinen, T. In Chromatographic Methods in Metabolomics; Wiedmer, S. K., Hyötyläinen, T., Eds.; The Royal Society of Chemistry, **2013**;11–39.

(10) Gika, H. G.; Theodoridis, G. A.; Wilson, I. D. J. Chromatogr. A **2008**, 1189, 314–322.

(11) Roessner, U.; Wagner, C.; Kopka, J.; Trethewey, R. N.; Willmitzer, L. Plant J. **2000**, 23, 131–142.

(12) Dunn, W. B.; Ellis, D. I. TrAC - Trends Anal. Chem. **2005**, 24, 285–294.

(13) Lenz, E. M.; Bright, J.; Wilson, I. D.; Morgan, S. R.; Nash, A. F. P. J. Pharm. Biomed. Anal. **2003**, 33, 1103–1115.

(14) Rezzi, S.; Ramadan, Z.; Fay, L. B.; Kochhar, S. Journal of Proteome Research. **2007**,513–525.

(15) Holmes, E.; Loo, R. L.; Cloarec, O.; Coen, M.; Tang, H.; Maibaum, E.; Bruce, S.; Chan, Q.; Elliott, P.; Stamler, J.; Wilson, I. D.; Lindon, J. C.; Nicholson, J. K. Anal. Chem. **2007**, 79, 2629–2640.

(16) Stella, C.; Beckwith-Hall, B.; Cloarec, O.; Holmes, E.; Lindon, J. C.; Powell, J.; Van Der Ouderaa, F.; Bingham, S.; Cross, A. J.; Nicholson, J. K. J. Proteome Res. **2006**, 5, 2780–2788.

(17) Phinney, K. W.; Ballihaut, G.; Bedner, M.; Benford, B. S.; Camara, J. E.; Christopher, S. J.; Davis, W. C.; Dodder, N. G.; Eppe, G.; Lang, B. E.; Long, S. E.; Lowenthal, M. S.; McGaw, E. A.; Murphy, K. E.; Nelson, B. C.; Prendergast, J. L.; Reiner, J. L.; Rimmer, C. A.; Sander, L. C.; Schantz, M. M.; Sharpless, K. E.; Sniegoski, L. T.; Tai, S. S. C.; Thomas, J. B.; Vetter, T. W.; Welch, M. J.; Wise, S. A.; Wood, L. J.; Guthrie, W. F.; Hagwood, C. R.; Leigh, S. D.; Yen, J. H.; Zhang, N. F.; Chaudhary-Webb, M.; Chen, H.; Fazili, Z.; Lavoie, D. J.; McCoy, L. F.; Momin, S. S.; Paladugula, N.; Pendergrast, E. C.; Pfeiffer, C. M.; Powers, C. D.;

Rabinowitz, D.; Rybak, M. E.; Schleicher, R. L.; Toombs, B. M. H.; Xu, M.; Zhang, M.; Castle, A. L. Anal. Chem. **2013**, 85, 11732–11738.

(18) Gowda, G. A. N.; Raftery, D. **2015**, 260, 144–160.

(19) Lindon, J. J. C.; Holmes, E.; Nicholson, J. K. Anal. Chem. **2003**, 75, 384A–391A.

(20) Smolinska, A.; Blanchet, L.; Buydens, L. M.; Wijmenga, S. S. Anal Chim Acta **2012**, 750, 82–97.

(21) Markley, J. L.; Brüschweiler, R.; Edison, A. S.; Eghbalnia, H. R.; Powers, R.; Raftery, D.; Wishart, D. S. Current Opinion in Biotechnology. **2017**,34–40.

(22) Koek, M. M.; Jellema, R. H.; van der Greef, J.; Tas, A. C.; Hankemeier, T. Metabolomics. **2011**,307–328.

(23) Zarate, E.; Boyle, V.; Rupprecht, U.; Green, S.; Villas-Boas, S. G.; Baker, P.; Pinu, F. R. Metabolites **2017**, 7, 1.

(24) Lutz, U.; Lutz, R. W.; Lutz, W. K. Anal. Chem. **2006**, 78, 4564–4571.

(25) Robertson, D. G.; Reily, M. D.; Baker, J. D. Journal of Proteome Research. **2007**, 526–539.

(26) Wilson, I. D.; Plumb, R.; Granger, J.; Major, H.; Williams, R.; Lenz, E. M. J. Chromatogr. B Anal. Technol. Biomed. Life Sci. **2005**, 817, 67–76.

(27) Neue, U. D. HPLC Columns: Theory, Technology, and Practice; Wiley-VCH, Inc: New York, 1997.

(28) Idborg, H.; Zamani, L.; Edlund, P.; Schuppekoistinen, I.; Jacobsson, S. J. Chromatogr. B **2005**, 828, 9–13.

(29) Cubbon, S.; Bradbury, T.; Wilson, J.; Thomas-Oates, J. Anal. Chem. **2007**, 79 (23), 8911–8918.

(30) Kloos, D. P.; Lingeman, H.; Niessen, W. M. A.; Deelder, A. M.; Giera, M.; Mayboroda, O. A. J. Chromatogr. B Anal. Technol. Biomed. Life Sci. **2013**, 927, 90–96.

(31) Tang, D.; Zou, L.; Yin, X.; Ong, C. N. Mass Spectrom. Rev. **2016**, 35, 574–600.

(32) Song, H.; Adams, E.; Desmet, G.; Cabooter, D. J. Chromatogr. A **2014**, 1369, 83–91.

(33) Theodoridis, G. A.; Michopoulos, F.; Gika, H. G.; Plumb, R. S.; Wilson, I. D. In Chromatographic Methods in Metabolomics; Wiedmer, S. K., Hyötyläinen, T., Eds.; The Royal Society of Chemistry, **2013**; pp 64–83.

(34) West, C.; Elfakir, C.; Lafosse, M. J. Chromatogr. A **2010**, 1217, 3201–3216.

(35) Vanhoenacker, G.; Sandra, P. J. Chromatogr. A **2005**, 1082, 193–202.

(36) Colin, H.; Guiochon, G. J. Chromatogr. A **1976**, 126, 43–62.

(37) Colin, H.; Guiochon, G. J Chromatogr **1977**, 137, 19.

(38) Poole, S. K.; Poole, C. F. Anal. Commun. **1997**, 34, 247–251.

(39) Knox, J.; Gilbert, M. T. UK Patent 7939449, **1980**.

(40) Gilbert, M. T.; Knox, J. H.; Kaur, B. Chromatographia **1982**, 16, 138–146.

(41) Obayashi, T.; Ozawa, T. K. European Patent 0458548A, **1990**.

(42) Ichikawa, H.; Yokoyama, A.; Kawai, T.; Moriyama, H.; Komiya, K.; Kato, Y. European Patent 0458176A, **1990**.

(43) Knox, J. H.; Kaur, B.; Millward, G. R. R. J. Chromatogr. A **1986**, 352, 3–25.

(44) Lu, T.; Olesik, S. V. Anal. Chem. **2015**, 87, 3616–3622.

(45) Pereira, L. J. Liq. Chromatogr. Relat. Technol. **2008**, 31, 1687–1731.

(46) Barrett, D. A.; Pawula, M.; Knaggs, R. D.; Shaw, P. N. Chromatographia **1998**, 47, 667.

(47) Knox, J. H.; Ross, P. In Advances in Chromatography, Vol 37; Brown, P. R., Grushka, E., Eds.; Marcel Dekker: New York, 1997; 73–161.

(48) Marin, S. J.; Jones, B. A.; Felix, W. D.; Clark, J. In Journal of Chromatography A; 2004; Vol. 1030, 255–262.

(49) Kříž, J.; Adamcová, E.; Knox, J. H.; Hora, J. J. Chromatogr. A **1994**, 663, 151–161.

(50) Möckel, H. J.; Braedikow, A.; Melzer, H.; Aced, G. J. Liq. Chromatogr. **1991**, 14, 2477–2498.

(51) Tanaka, N.; Tanigawa, T.; Kimata, K.; Hosoya, K.; Arai, T. J. Chromatogr. A **1991**, 549, 29–41.

(52) Wan, Q. H.; Shaw, P. N.; Davies, M. C.; Barrett, D. A. J. Chromatogr. A **1995**, 697, 219–227.

(53) Thiébaut, D.; Vial, J.; Michel, M.; Hennion, M. C.; Greibrokk, T. J. Chromatogr. A **2006**, 1122, 97–104.

(54) Melmer, M.; Stangler, T.; Premstaller, A.; Lindner, W. J. Chromatogr. A **2010**, 1217, 6092–6096.

(55) Holmgren, E.; Carlsson, H.; Goede, P.; Crescenzi, C. J. Chromatogr. A **2005**, 1099, 127–135.

(56) Zhou, S.; Dong, X.; Veillon, L.; Huang, Y.; Mechref, Y. Anal. Bioanal. Chem. **2017**, 409, 453–466.

(57) Wan, Q.-H.; Davies, M. C.; Shaw, P. N.; Barrett, D. A. Anal. Chem. **1996**, 68, 437–446.

(58) Leira, E.; Botana, A.; Cela, R. J. Chromatogr. A **1996**, 724, 67–78.

(59) Sawatsubashi, T.; Tsukahara, C.; Baba, K.; Ohi, E.; Shinoda, A.; Miura, N. J. Chromatogr. A **2008**, 1177, 138–149.

(60) Snyder, L. R.; Kirkland, J. J.; Dolan, J. W. Introduction to Modern Liquid Chromatography, 3rd ed.; John Wiley & Sons, Inc.: Hoboken, 2010.

(61) Giddings, J. C. Dynamics of Chromatography; Marcel Dekker: New York, 1965.

(62) Gritti, F.; Guiochon, G. Anal. Chem. **2013**, 85, 3017–3035.

(63) Gritti, F.; Guiochon, G. Journal of Chromatography A. **2012**, 2–40.

(64) Gritti, F.; Guiochon, G. Journal of Chromatography A. **2013**, 1–13.

(65) Neue, U. D.; Marchand, D. H.; Snyder, L. R. J. Chromatogr. A **2006**, 1111, 32–39.

(66) MacNair, J. E.; Lewis, K. C.; Jorgenson, J. W. Anal. Chem. **1997**, 69, 983–989.

(67) Patel, K. D.; Jerkovich, A. D.; Link, J. C.; Jorgenson, J. W. Anal. Chem. **2004**, 76, 5777–5786.

(68) Neue, U. D. J. Chromatogr. A **2005**, 1079, 153–161.

(69) Shen, Y.; Zhang, R.; Moore, R. J.; Kim, J.; Metz, T. O.; Hixson, K. K.; Zhao, R.; Livesay, E. A.; Udseth, H. R.; Smith, R. D. Anal. Chem. **2005**, 77, 3090–3100.

(70) Moore, S. M. Separation and Identification Techniques for Membrane Proteins Using Ultra-High Pressure Liquid Chromatography Coupled to Mass Spectrometry, University of North Carolina at Chapel Hill, 2016.

(71) Grinias, K. M.; Godinho, J. M.; Franklin, E. G.; Stobaugh, J. T.; Jorgenson, J. W. J. Chromatogr. A **2016**, 1469, 60–67.

CHAPTER 2. INVESTIGATIONS IN THE RETENTION OF MODEL METABOLITES ON POROUS GRAPHITIC CARBON

2.1 Introduction

2.1.1 Thermodynamics of Chromatography

Although different modes of chromatography come about due to different retention mechanisms, they all share common principles in thermodynamics of retention. The most convenient descriptor of retention for comparison amongst different columns is the retention factor (k').

$$k' = \frac{t_R - t_m}{t_m} \qquad \text{Equation 2-1}$$

Here, t_R is the solute retention time and t_m is the column deadtime as determined by an unretained solute. k' data can allow for the investigation of some important thermodynamic properties associated with retention. The level of retention of a solute is dictated by its partition coefficient (K) from the mobile phase (MP) into the stationary phase. The partition coefficient is related to k' by:

$$k' = K\phi \qquad \text{Equation 2-2}$$

where ϕ is the phase ratio of the column. Phase ratio is the ratio of the volume of stationary phase (V_S) to the volume of mobile phase (V_m) within the column.

$$\phi = \frac{V_S}{V_m} \qquad \text{Equation 2-3}$$

The partition coefficient can be related to the standard Gibbs free-energy ($\Delta G°$) associated with the partition from mobile phase to stationary phase by:

$$\Delta G° = -RT \ln K \qquad \text{Equation 2-4}$$

where R is the gas constant and T is the absolute temperature. The Gibbs free energy is a function of the standard enthalpy ($\Delta H°$) and entropy ($\Delta S°$) associated with a solute moving from the mobile

phase to the stationary phase.

$$\Delta G° = \Delta H° - T\Delta S° \qquad \text{Equation 2-5}$$

By combining Equations 2-2, 2-4, and 2-5 the retention factor can now be related to column temperature by the van't Hoff equation.

$$\ln k' = \frac{-\Delta H°}{RT} + \frac{\Delta S°}{R} + \ln \phi \qquad \text{Equation 2-6}$$

Plots of $\ln k'$ vs $\frac{1}{T}$ will normally form linear plots for a neutral solute, allowing determination of $\Delta H°$ and $\Delta S°$. These values of $\Delta H°$ and $\Delta S°$ can give insights into the retention mechanisms that govern the interactions between solute and stationary phase, as well as the effect that temperature has on the overall retention of a species.[1–3] In reversed phase separations, increasing temperature will usually lead to decreased retention. When compared to the change in retention due to mobile phase composition, temperature has been seen to influence retention to a lesser extent. The basic trend is that it takes a 5 °C increase in temperature to equal the change in retention due to a 1% increase in organic content in the mobile phase.[4]

2.1.2 Importance of Pre-concentration and Focusing in Separations

Polar samples can be difficult to analyze with traditional reversed phase columns due to their lack of retention.[5–7] Analytes with low k' will elute very early in a gradient, in some cases at the mobile phase breakthrough time.[8,9] As we are ultimately concerned with the separation of metabolites using capillary UHPLC in particular, this lack of retention for polar metabolites could cause the loss of useful metabolomic information. Due to their inherently small volumes, capillary columns benefit from large volume sample injections that allow for sufficient loading of low abundance species for ease of detection. This is especially important for metabolites as species can range in concentration from mmol to pmol within a single sample.[10]

When using capillary columns with gradient elution, it is common for the injection volume to be larger than the column volume. When using small injection volumes, the majority of band dispersion is due to the column (assuming minimal other extracolumn volumes), leading to a

Gaussian peak shape. As injection volume is increased, increases in peak height are seen initially without a change in peak width.[11,12] As the injection volume is increased even further it will reach a point where peak width will begin to increase. This phenomenon is known as volume overload. When pushed even further, the detected peak will resemble a Gaussian peak combined with the rectangular profile of the injection in that it has a Gaussian profile at the front and rear edges, but is flat on top. The injection volume at which overloading becomes an issue is strongly dependent on the sample, column, and conditions used for the separation.[8,13] As a basic starting point, the maximum allowable volume injected (V_{max}) for a solute before volume overload is seen can be estimated by:[14]

$$V_{max} = \frac{\theta K_{inj} \varepsilon_t \pi L d_c^2 (k' + 1)}{4\sqrt{N}} \qquad \text{Equation 2-7}$$

where θ is related to the specified level of allowed performance loss due to peak width increases (θ^2) from injection volume, K_{inj} is a term describing the shape of the injection profile ($K_{inj} = 4$ for ideal rectangular injection), ε_t is the total column porosity, and d_c is the column inner diameter. A couple of observations can be made from this equation. As k' increases, the maximum volume that can be injected without overloading also increases, making it desirable to have very high retention under injection conditions in order to form as narrow a solute band as possible. The solute band velocity slows down as molecules are spending more time in the stationary phase where there aren't moving with the flow of mobile phase, ultimately narrowing the band compared to the original injection volume.

The second observation is that as the column diameter is decreased, the required injection volume decreases by d_c^2. This requirement for smaller injections is due to the fact that the column volume in total decreases as well as the amount of packing material within the column. This is where the move to capillary scale separations becomes a challenge. For analytes with low retention, injections in the low nL range would be needed to prevent volume overload on a 75 μm inner diameter (i.d.) x 15 cm long column.[14] In practice, this is difficult as commercial UHPLC instruments are not capable of producing such a small injection. In order to limit volume overload on capillary

columns it is necessary to have sufficient retention of solutes under injection conditions.[15] For gradient elution, which is most often used for metabolite separations, injections occur in weak solvents. These conditions will ideally allow for the solutes to have high k' and form narrow injected bands on the column inlet, ultimately leading to narrow peaks upon elution. As discussed earlier, polar compounds are not retained well on traditional reversed phase columns even under weak mobile phase conditions, risking significant volume overloading and loss of information.

A number of different methods have been shown to improve the ability to focus large volume injections. "On-column focusing" refers to a injecting a sample in a weaker solvent than the mobile phase being used for the separation.[15,16] This increases the retention of the compounds in the sample relative to if it was in the mobile phase, and in turn improves the ability to focus the injection on the head of the column. Closely related to this is the performance optimizing injection sequence (POISe) method, which injects a volume of weak solvent along with the sample in mobile phase.[17] POISe differs from "on-column" focusing in that there is no need to prepare the sample in a weak mobile phase. The sample and weak mobile phase plugs mix as they are in transit from the injector to the column. This mixing causes the solutes to be in a weaker solvent than their original, increasing the retention and focusing that the solutes will experience once they reach the column head.

Since it is ultimately a state of increased retention that allows for improved injection focusing, it is also possible to manipulate temperature to improve focusing. This technique, called temperature assisted solute focusing (TASF), uses a setup where a short region of the column inlet is cooled to 5 °C while the rest of the column is kept at an elevated temperature.[18] As the column temperature decreases, retention of most analytes in reversed phase LC increases. When an injection hits the column inlet at 5 °C, the k' is higher than it would have been if at the same temperature as the rest of the column. This causes the wide injection band to focus significantly. Once the injection is loaded, the inlet region is rapidly heated to the column temperature and the focused solute bands are released. Using this method, near identical peak widths were seen for injection volumes ranging from 50–1000 nL, whereas separations performed without TASF were seen to broaden 2.5-fold over the

same range.[18] Further improvements have been made to TASF by utilizing even lower trapping temperatures as well as using a two-stage TASF, where the injection is focused sequentially by two cooled regions, allowing for improvement in peak shape in both isocratic and gradient separations.[19,20]

2.1.3 Redox Properties of PGC

Due to its alternative retention mechanisms, PGC has found a niche in the analysis of polar compounds, though this retention can get complicated due to the presence of surface oxides. The manufacturer of Hypercarb suggests that the heat treatment (~2,500 °C) under inert atmosphere should produce a material that is essentially void of surface functionality of any kind.[21] However, it has been shown previously that commercially available PGC columns have inherent redox properties.[22,23] Through redox titrations it was found that the Hypercarb surface has an approximate surface coverage of 0.1 mol% or 4 x 10^{-11} mol/cm^2 of oxidisable groups.[24] With approximately 0.4% of the PGC surface being edge atoms with unsatisfied valence, this means that potentially 25% of edge atoms could host surface oxide groups.[24] It is expected that these groups would be similar to those seen on traditional graphite electrodes such as carbonyl, lactone, quinone, carboxylic acid and phenol groups.[25,26]

Using redox titrations, it was also found that the particles have an inherent redox potential of approximately +0.35 V vs. Ag/AgCl.[24] This oxidative capability has allowed for a PGC column to be used as an on-line redox derivatization unit, by converting a Co(II) complex to Co(III) complex.[27] Within this study, treatment of the PGC column with a reducing agent changed redox properties of the column, allowing it to now reduce Co(III) to Co(II) complexes. This initial finding opened the doors for a number of researchers to study the redox properties of PGC, many of which have found that by tuning the redox state using chemical or electrochemical methods, it is possible to tune the retention and selectivity of species.[22,28–30] Although these redox properties allow for unique control of retention with PGC, it also adds complexity to the use of PGC compared to traditional reversed phase materials.

2.2 Experimental Methods

2.2.1 Chemicals

For the purpose of isocratic characterization of columns, HPLC grade methanol (MeOH) and acetone were used as received from Fisher Scientific (Waltham, MA). Deionized water was obtained using a Barnstead Nanopure ultrapure water system (Dubuque, IA). Formic acid (FA, LC-MS grade) and L-ascorbic acid (AA) were used as received from Sigma Aldrich (St. Louis, MO). The test mixture used to evaluate the retention characteristics contained mandelic acid (MA), hippuric acid (HA), 2-methylhippuric acid (2-MHA), 3-methylhippuric acid (3-MHA), and 4-methylhippuric acid (4-MHA), all of which were used as received from Sigma Aldrich (St. Louis, MO).

2.2.2 Instrumentation and Chromatographic Columns

Isocratic separations were carried out on an Acquity ultraperformance liquid chromatography (UPLC) system equipped with a photodiode array (PDA) detector from Waters Corporation (Milford, MA). The Acquity has a Binary Solvent Manager capable of delivering flow rates up to 2 mL/min with a maximum pressure of 15,000 psi. The Acquity Sample Manager contains a six-port injection valve that delivers analyte injections onto the column, which sits in a thermostated oven capable of reaching 65 °C. For all experiments shown here, 5 µL injections were used. To ensure proper sampling of the peak shape, the acquisition rate of the photodiode array detector was set such that a minimum of 40 data points were taken across a peak. The columns used in this study were: a Hypercarb column (4.6 mm x 100 mm, 3 µm particles) from Thermo Fisher Scientific (Waltham, MA) and a C18-modified bridged-ethyl hybrid column (BEH, 2.1 mm x 50 mm,1.7 µm particles) from Waters Corp.

2.2.3 Measurement of Retention of Metabolite Standards

In order to study the retention characteristics of Hypercarb and C18 BEH columns, isocratic separations of a series of model metabolites were performed over a wide range of water/MeOH + 0.1% FA mobile phase compositions at 30 °C. This test mixture was composed of mandelic acid, hippuric acid, 2-methylhippuric acid, 3-methylhippuric acid, and 4-methylhippuric acid. Acetone and

ascorbic acid were used as deadtime markers for the Hypercarb and C18 BEH columns, respectively. At least triplicate measurements were made for all mobile phase conditions used.

Initially, the Hypercarb column showed significant day-to-day drift in retention of metabolites. A pre-treatment process was adopted in which the Hypercarb column was washed for at least 90 column volumes with the desired mobile phase (water/MeOH + 0.1% FA) for use, with 10 mM ascorbic acid added. The ascorbic acid was then flushed off the column using the standard mobile phase (water/MeOH + 0.1% FA) for at least 30 column volumes. This washing process brought the graphite surface to a reproducible redox state before retention measurements were made each day. This pre-treatment step was not needed for the C18 BEH column as the silica surface should have no redox properties and the observed retention times were repeatable.

2.2.4 Effect of Temperature on the Retention of Metabolites with C18 BEH and Hypercarb

In order to study the effect of temperature on the retention of the model metabolites, retention measurements were made using the Hypercarb and C18 BEH columns over a range of temperatures (30-65 °C) and mobile phase (water/MeOH + 0.1% FA) conditions for each column. Triplicate injections were made of the metabolites under each condition. This allowed the evaluation of how temperature effected the retention of analytes, under a variety of k' conditions. As the Acquity system does not pre-heat mobile phase before the column, it was necessary to perform the separations at elevated temperatures (> 40 °C) at lower flow rates. This should prevent the cold mobile phase flowing into the column from causing a wide spread axial temperature gradient. The Hypercarb column underwent AA pre-treatment and re-equilibration steps multiple times throughout the day, essentially any time the column oven temperature was changed. This was done in order to minimize any potential changes in the surface redox properties when varying the temperature and to provide a repeatable state for each group of measurements.

2.3 Results and Discussion

2.3.1 Effect of Ascorbic Acid Wash on Model Metabolite Retention

Initially, the retention times of the standard metabolites drifted significantly day-to-day. The

source of this variability was unknown, but it was suspected that the surface chemistry of the Hypercarb was to blame. With the knowledge that surface redox chemistry plays a significant role in the retention characteristics of Hypercarb, we started to look for ways to control the redox state of the particles.[22,24,31] Previous studies utilized sodium sulfite doped mobile phases to reduce the PGC surface,[32] but due to the high level of MeOH in the conditions used in this work, solubility of sulfite was limited. Ascorbic acid, which is more soluble in the conditions used, has been shown to be a chemical reductant of graphene oxide, so it was thought that it could be used to reset the Hypercarb surface redox state on a daily basis similar to sulfite.[33] Figure 2-1 shows a comparison of the repeatability of retention of the metabolite mixture before and after AA treatment was started. Significant improvement in repeatability was seen using the AA pre-treatment. The wash seems to regenerate the carbon surface to a consistent state, which leads to much more repeatable retention times day-to-day. This consistency is vital in chromatographic separations, as many replicate injections of a sample are often needed. The other observation was that the k' of the metabolites, especially the most retained, was also decreased significantly with AA washing. This suggests that the metabolites interact strongly with the small percentage of oxidized groups on the particle surface, since the reduction drastically decreases their retention. This is in line with previous observations that further oxidation of the original particles leads to greatly increased retention for dopamine and its metabolite, 3,4-dihydroxyphenylacetic acid.[24] It should be noted that previous studies have shown that the treatment of PGC with a reducing agent has differing effects depending on the analyte properties, with reduction causing decreased retention for anions, having little effect on neutral compounds, and increasing the retention of cations.[32]

When looking at the stability of the redox state after the AA wash, it is useful to look at how the retention times vary throughout a single day after the wash. Figure 2-2 shows a series of runs performed across a single day, after AA treatment, for 5/95 (v/v) water/MeOH + 0.1% FA (A) and 35/65 (v/v) water/MeOH + 0.1% FA (B). In 5/95 water/MeOH + 0.1% FA, little drift was seen over the course of the four runs. In 35/65 water/MeOH + 0.1% FA, however, a significant amount of drift

was seen. In general, as the number of runs increased, the retention of the metabolites increased. This also seems to have a larger effect on more retained solutes. As mentioned previously, the AA washing step significantly decreased the retention of the metabolites by reducing the PGC surface. The tendency for peaks to become more retained as the number of runs increases, suggests that the PGC surface is slowly being oxidized back to its original state. This is likely due to dissolved oxygen in the mobile phase oxidizing the PGC surface as it flows through the column. A similar trend was seen in the literature, but with PGC that had been previously oxidized with potassium permanganate, slowly returning to the original redox state over time as mobile phase flowed through the column.[24] PGC seems to naturally tend towards an equilibrium redox state based on the mobile phase conditions it is exposed to. As the stability of the surface redox state seemed to change relatively rapidly over the course of the day, especially for high k' compounds, it became apparent the importance of consistently performing AA washing steps at least once a day, or multiple times a day for conditions of high retention.

Figure 2-3 shows the retention of the metabolites on a new, identical Hypercarb column (4.6 mm x 100 mm, 3 μm) that was prepared using the AA pre-treatment step. If Figure 2-3 is compared to Figure 2-1 (B), it can be seen that there is a slight difference in the retention times of the metabolites. Looking at simply the 4-MHA peak, the original column had a retention time around 8 minutes, while the new column is around 9 minutes. It is unclear as to why these difference in retention were seen. While the reduction process with AA should, ideally, bring the PGC to a repeatable state, it is still led to differing times on these columns. It is possible that there were slight variations in the particle batches used to pack the columns, which could ultimately lead to different retention or surface chemistry. Although it seemed that little could be done to give identical retention on the two columns, it was good to know that variability between the physical columns themselves was seen and could be a possibility in the future.

2.3.2 Effect of Mobile Phase Composition on the Retention of Metabolite Standards

Now that AA washes were shown to improve retention repeatability for the metabolite

mixture on Hypercarb, interest was turned to seeing how the retention changed under various mobile phase conditions. The metabolite mixture was separated isocratically over a range of water/MeOH + 0.1% FA compositions at 30 °C with both the C18 BEH and Hypercarb columns. As a comparison of the retention difference between Hypercarb and C18 BEH, Figure 2-4 shows a plot of k' vs fraction of MeOH in the mobile phase for 4-MHA, which is essentially the most retained analyte on both columns under the conditions used. Hypercarb, with its alternative mechanism for retaining polar compounds and ability to have π-π interactions with the aromatic ring of 4-MHA, shows significantly increased retention over the C18 BEH column.[25] Even in 90/10 (v/v) water/MeOH + 0.1% FA, which is close to the initial conditions of most reversed phase gradients, the C18 BEH column provides a k' of approximately 25 for 4-MHA while Hypercarb shows a similar level of retention in 65% methanol. Keep in mind that this is the most retained compound of the mixture on both columns, so all other species will have even lower k'. As mentioned previously, this lack of retention is a limiting factor for the gradient separations of polar metabolites with C18 bonded columns.

Due to the high level of retention for several of the test compounds on Hypercarb, it was not reasonable to measure k' under still weaker mobile phase conditions. In order to project the retention of these test compounds to the conditions that would be expected under initial gradient conditions, it was necessary to fit the experimental data with an empirical model. It has been shown that the assumption of a linear relationship between the logarithm of k' and organic content is an oversimplification, and that experimental data across a wide range of solvent compositions will show some curvature.[34] Neue's equation is used here to fit the observed curvature.[34]

$$\ln(k') = \ln(k'_{00}) + 2\ln(1 + a_{curve}\varphi) - \frac{B_{sol}\varphi}{1 + a_{curve}\varphi} \qquad \text{Equation 2-8}$$

Here, k'_{oo} is the retention factor in 100% water, φ is the fraction of organic in the mobile phase, B_{sol} is a solute dependent term largely determined by molecular weight, and a_{curve} is a term that allows for curvature. Figure 2-5 shows the Hypercarb (A) and BEH (B) retention data for all of the standard metabolites, fit with Equation 2-8. Table 2-1 compares the k'_{00} factors for the five model analytes on

Hypercarb versus C18 BEH. With the exception of mandelic acid, k'_{00} values on Hypercarb are between 3,000 and 11,000, and offer more than 100-fold greater retention than C18 BEH under the same 100% aqueous mobile phase conditions. It is also noteworthy that the PGC and C18 BEH columns show slightly differing selectivity with the elution order of the pairs 2-MHA/HA and 3-MHA/4-MHA being swapped on the two columns. PGC is known to be useful for separations of structurally similar solutes as slight differences in structure will lead to differences in their ability to be in contact with the flat PGC surface and in turn alter their retention.[35] This improved ability to differentiate between isomers allows baseline resolution of 3-MHA and 4-MHA on Hypercarb, while they are not resolved on the C18 BEH column due to the fluid-like carbon chains.

2.3.3 Implications of Improved Retention on PGC for Injection Focusing

As mentioned previously, when using capillary columns where total column volume is often smaller than the injection volume, volume overloading can be a problem. Under these conditions the injection process is similar to an isocratic separation performed in the injection solvent. As an analyte with low k' is loaded onto the column, it is swept along faster than a more retained analyte, ultimately leading to a broader band after the injection is loaded. More retained analytes are focused at the inlet due to strong interactions with stationary phase, decreasing the band width compared to injection width. One way that the ability for columns to focus analytes can quantitatively be compared is with the isocratic-focusing factor (IFF) as discussed by Sanchez, Anspach, and Farkas.[17] When an injection is loaded with the sample in the mobile phase of initial gradient conditions, the solute band linear velocity (u_a) as it travels through the column can be found by:

$$u_a = \frac{u}{1 + k'_a} \qquad \text{Equation 2-9}$$

where u is the mobile phase linear velocity and k'_a is the analyte retention factor in the mobile phase that the sample is dissolved in. The time (t_{inj}) it takes to load a fixed injection volume (V_{inj}) onto a column is related to the volumetric flow rate (F).

$$t_{inj} = \frac{V_{inj}}{F}$$ Equation 2-10

The time of injection can then be used in conjunction with the band velocity to determine the distance that the injection front traveled over the course of an injection for a retained ($d_{inj,a}$) and unretained solute ($d_{inj,0}$).

$$d_{inj,a} = t_{inj} * u_a = \frac{V_{inj}}{F} * \frac{u}{1+k\prime_a}$$ Equation 2-11

$$d_{inj,0} = t_{inj} * u = \frac{V_{inj}}{F} * u$$ Equation 2-12

When the front of a retained solute band encounters the head of the column, its velocity is reduced due to interaction with the stationary phase.[8] This allows the tail end of the band to catch up to the front, ultimately decreasing the overall width. An unretained analyte, however, will travel at the velocity of the mobile phase, leading to a band as wide as the injection itself. The IFF is the ratio of the distance traveled by a retained solute to an unretained.[17]

$$IFF = \frac{d_{inj,a}}{d_{inj,0}} = \frac{\frac{V_{inj}}{F} * \frac{u}{1+k\prime_a}}{\frac{V_{inj}}{F} * u} = \frac{1}{1+k\prime_a}$$ Equation 2-13

Equation 2-13 shows that as k'_a increases the IFF decreases. This can then be related to the total volume that a solute band occupies (V_a) by:

$$V_a = \frac{V_{inj}}{1 + k'_a}$$ Equation 2-14

As metabolite samples may have a large portion of relatively polar compounds, it is necessary to use very aqueous (~95% water) conditions to load samples onto reversed phase columns. Table 2-2 shows the values for k'_a, IFF, and V_a for the standard metabolites assuming a sample solvent of 95/5 (v/v) water/MeOH + 0.1% FA, for both the C18 BEH and Hypercarb columns. The values for k'_a were found using extrapolations of C18 BEH and Hypercarb retention data fit with Equation 2-8 (Figure 2-5). As expected, k'_a is significantly higher for all analytes on Hypercarb than on C18 BEH, leading to all values of IFF on PGC (IFF_{PGC}) for the metabolites to be lower than IFF on C18 BEH (IFF_{BEH}). If we assume a 2 µL injection, which is common for commercial capillary LC-MS

instruments with low concentration samples, the values of the overall band volumes can be found. Again, the focused band volume on PGC ($V_{a,PGC}$) is significantly smaller than the band volume on C18 BEH ($V_{a,BEH}$). By taking the ratio, $\frac{V_{a,BEH}}{V_{a,PGC}}$, the overall fold increase in focusing expected using Hypercarb instead of C18 BEH can be found. Outside of the least retained analyte, MA, it is expected that Hypercarb would provide between 80-200-fold improvement in injection focusing when the metabolites are injected in gradient initial conditions of 95/5 water/MeOH + 0.1% FA. With this enhanced level of retention, these compounds will pre-concentrate as soon as they arrive at the head of the Hypercarb column, allowing the use of larger volume injections with Hypercarb while still minimizing volume overload of the most retained analytes. The use of larger injection volumes with Hypercarb is vital for metabolite samples since many of the compounds of interest are present at very low concentrations, making injecting and focusing large volumes vital for loading more of these analytes and ultimately increasing sensitivity when running capillary scale LC-MS.[10]

2.3.3 Influence of Temperature on the Retention of Metabolites

By studying retention of a series of compounds at a number of temperatures, it is possible to not only determine the effect of temperature on retention, but also look into the thermodynamics of retention. Traditionally a homologous series of solutes is used to test thermodynamic properties involved with retention mechanisms, so it is difficult to say things with certainty using the small series of metabolites used here, but general trends will be noted.[36–38] The retention of the standard metabolites was measured at a series of temperatures between 30 – 65 °C using both the C18 BEH and Hypercarb columns. These measurements were performed under a number of different water/MeOH + 0.1% FA mobile phase compositions in order to achieve a range of k'. Figure 2-6 shows an example van't Hoff plot of the metabolites on both C18 BEH and Hypercarb. Based on Equation 2-6, the slope of these trend lines is $\frac{-\Delta H^{\circ}}{R}$. With the exception of MA on Hypercarb in 5/95 and 15/85 (v/v) water/MeOH + 0.1% FA, all trend lines showed good linearity with $R^2 > 0.94$, with the majority having $R^2 > 0.99$. MA under those conditions was only slightly retained beyond the

column deadtime, which led to problems with accurate determination of retention times and k'. For this reason, MA data sets will be left out of further discussion.

Tables 2-3 and 2-4 show the effect of mobile phase compositions on the retention and $\Delta H°$ for the metabolites on C18 BEH and Hypercarb. As $\Delta H°$ is derived from the slope of the van't Hoff plot, it gives insight into the effect of temperature on the retention of the metabolites. For both C18 BEH and PGC, the values of $\Delta H°$ are negative. This value indicates that the transition from mobile to stationary phase is exothermic and that retention will decrease with higher temperatures. This trend is normally seen with reversed phase separations, but it has been reported previously that the separation of oligosaccharides on PGC will display positive values for $\Delta H°$ and increasing retention with higher temperatures.[39,40] When looking at the change in enthalpy as retention increases, it seems that Hypercarb experiences a larger change in $\Delta H°$ than C18 BEH. For C18 BEH, $\Delta H°$ for HA and 2-MHA are seen to be mostly constant for the conditions used here while 3-MHA and 4-MHA get increasingly exothermic. All $\Delta H°$ values on PGC gets increasingly exothermic as retention increases. In general, $\Delta H°$ values for an analyte on C18 BEH are more exothermic than those seen on Hypercarb, under the conditions measured. This suggests that increasing temperature will have a larger impact on the retention for the C18 BEH column than the PGC column, but due to the trend of $\Delta H°$ changing more rapidly with retention on PGC, this may not hold true under weaker mobile phase conditions.

The intercept of van't Hoff plots can be used to determine some additional thermodynamic information about solute retention. The intercept equals $\frac{\Delta S°}{R} + \ln \phi$. Traditionally, phase ratios are difficult to calculate for bonded reversed phase columns. V_m can been found a number of ways including measuring the deadtime of an unretained solute, monitoring for a baseline disturbance when injecting a deuterated mobile phase, and measuring the difference in weight of the column when filled with solvents of varying density.[41] V_S is more difficult to determine as the stationary phase-mobile phase boundary is not sharp and can change due to the ability of the C18 later to absorb some of the

organic component of the mobile phase.[41–43] This causes the stationary phase to "swell" and increases V_S. Even knowing that V_S may change with mobile phase composition, it is still most often estimated based solely on the physical properties of the packing material in the column such as carbon load (due to C18 chains), density of bonded alkyl chain and total weight of material in the column.[44] This will provide a single value describing the column phase ratio, independent of chromatographic conditions. As the stationary phase for the PGC column is composed of a solid-liquid interface, the phase ratio is not expected to change with organic content in the mobile phase.

Although ϕ is not known for the C18 BEH and Hypercarb columns used here, it will be arbitrarily assumed that $\phi = 1$ for both columns. This makes the contribution of the phase ratio zero, and attributes all of the intercept to $\Delta S°$. Obviously, this is an oversimplification and is not physically true for these columns, but it will allow for rough estimations of $\Delta S°$. If the phase ratio for the columns were set to any fixed value, as most studies assume, $\ln \phi$ would be a constant. This would lead to all $\Delta S°$ values being offset by a constant, still allowing for trends in $\Delta S°$ to emerge. Tables 2-5 and 2-6 show the corresponding entropy data calculated from the van't Hoff plots for C18 BEH and Hypercarb. It was seen that all values of $\Delta S°$ were negative, signifying that the entropy change due to transfer from the mobile phase into the stationary phase was entropically unfavorable and the system became more ordered. For C18 BEH, although the values are all negative, they are moving closer to zero as retention increases, suggesting that the transfer from mobile phase to stationary phase is then causing increased disorder. For reversed phase separations, it is thought that the mobile phase contributes significantly to the retention mechanism by hydrophobic interactions.[45] When a non-polar solute is dissolved in the mobile phase, solvent molecules near the solute create a very ordered structure. The transition of the solute from the mobile phase to the stationary phase would cause this ordered structure to relax and increase disorder.[36] This is in line with what is seen here for C18 BEH, since as k' is increased, the $\Delta S°$ is seen to move closer to zero. For Hypercarb, $\Delta S°$ values suggest the system is becoming increasingly ordered as retention increases. It is unclear as to why this trend

occurs, but it could be an indication of the alternative retention mechanism for PGC compared to C18 BEH.

The values of $\Delta S°$ and $\Delta H°$ can be used with Equation 2-5 to calculate their contributions to $\Delta G°$. Figures 2-7 and 2-8 show plots of the contributions of $-T\Delta S°$ and $\Delta H°$ to $\Delta G°$ for C18 BEH and Hypercarb across a range of retention conditions, for all analytes. For these plots, column temperature was assumed to be 30 °C for the calculation of $-T\Delta S°$. For 2-MHA and HA on C18 BEH, $\Delta H°$ is seen to stay relatively constant, and $-T\Delta S°$ causes the majority of the change in $\Delta G°$. 3-MHA and 4-MHA look slightly different with $\Delta H°$ becoming slightly more exothermic while $-T\Delta S°$ stills decreases. These contributions to $\Delta G°$ as retention increases are similar, but seem to slightly favor $-T\Delta S°$ being the majority contributor. This suggests that entropy could be the more significant factor impacting $\Delta G°$ for retention on the C18 BEH column. PGC shows a difference in the contributions of $-T\Delta S°$ and $\Delta H°$, again suggesting a potential difference in the retention mechanism between the phases. $-T\Delta S°$ is seen to increases slightly over the retention range, while $\Delta H°$ becomes significantly more exothermic. This suggests that retention on PGC is heavily enthalpy controlled. Again, it is important to note that traditional thermodynamic measurements are performed using a homologous series, so these inferences are simply applicable to the small set of compounds used here. That said, it has been found previously, using a homologous series, that enthalpy contributed much more significantly that entropy for the retention process on PGC, which is in agreement with the work presented here.[46]

2.4 Conclusions

In this chapter, a number of experiments were performed to better understand the retention and thermodynamic differences between PGC and C18 bonded stationary phases. Hypercarb showed significantly increased retention for all metabolites studied compared to C18 BEH, with many of the metabolites showing more than 100-fold greater retention. This increase in retention is vital as the ultimate goal is to use PGC for the separation of metabolites using capillary UHPLC, where injection volumes are often larger than the column volume. Without sufficient retention in initial gradient

conditions, volume overload will occur, leading to broad peaks and a loss of metabolomic information. With the retention differences for Hypercarb and C18 BEH, it is predicted that when injected in initial gradient conditions, the volume of the injected bands for the model metabolites will be focused by upwards of 80-fold for the more retained solutes on PGC compared to C18 BEH, reducing any issues with volume overloading. By studying the effect of temperature on the retention of the metabolite standards, it was seen that temperature had a larger effect on C18 BEH than PGC. Both phases showed decreasing retention with increasing temperature. This data was then used to study the thermodynamics of retention. It is known that PGC and C18 bonded columns have different retention mechanisms, and the differences in the trends of $\Delta H°$ and $-T\Delta S°$ seen here seem to suggest the same idea. The data suggest that retention on Hypercarb is controlled by enthalpic contributions, but more in-depth studies would be need needed to give comprehensive discussion of these processes and this is beyond the scope of the work.

The redox characteristics of the PGC surface were also investigated. Based on initial investigations, the surface redox state seemed to vary from day-to-day as seen by varying retention of the model metabolites. By treating the column with a reducing agent, ascorbic acid, the retention times of the metabolites decreased and stabilized after the treatment. As mobile phase was passed through the column over the course of a day after AA treatment, retention times were seen to drift to longer times. This impact was magnified as k' of the analyte increased. This drift is in line with previous studies suggesting that some component of the mobile phase, likely dissolved O_2, oxidizes the surface over time. This study showed the importance of controlling the surface redox state for isocratic separations. It is suggested that redox treatment be performed each day before use in order to create a more repeatable redox state of the surface and ultimately repeatable retention of solutes.

2.5 TABLES

Analyte	$k'_{00,PGC}$	$k'_{00,BEH}$	$\frac{k'_{00,PGC}}{k'_{00,BEH}}$
MA	47	9.6	4.9
2-MHA	3300	23	140
HA	5800	15	390
3-MHA	13000	61	210
4-MHA	11000	61	180

Table 2-1. Projected retention of standard metabolites in 100% water (k'_{00}) on Hypercarb (4.6 mm x 100 mm, 3 µm) and C18 BEH (2.1 mm x 50 mm, 1.7 µm) columns as well as the ratio of $\frac{k'_{00,PGC}}{k'_{00,BEH}}$. Retention was measured over a range of mobile phase compositions consisting of (v/v) mixtures of water/MeOH + 0.1% FA at 30 °C. Experimental retention data was then fit with Equation 2-8 to find k'_{00}. $k'_{00,PGC}$ and $k'_{00,BEH}$ are the retention factors in 100% water for Hypercarb and C18 BEH.

Analyte	$k'_{a,PGC}$	IFF_{PGC}	$V_{a,PGC}$ (nL)	$k'_{a,BEH}$	IFF_{BEH}	$V_{a,BEH}$ (nL)	$\frac{V_{a,BEH}}{V_{a,PGC}}$
MA	29.5	3.28×10^{-2}	65.6	6.86	1.27×10^{-1}	255	3.9
2-MHA	1360	7.35×10^{-4}	1.47	15.3	6.13×10^{-2}	123	83.5
HA	2330	4.29×10^{-4}	0.86	10.0	9.07×10^{-2}	181	211
3-MHA	6360	1.57×10^{-4}	0.31	38.2	2.55×10^{-2}	51.0	162
4-MHA	5660	1.77×10^{-4}	0.35	38.0	2.56×10^{-2}	51.3	145

Table 2-2. Data predicting the injection focusing capabilities of packed capillary C18 BEH and Hypercarb columns assuming a 2 µL injection of standard metabolites in 95/5 (v/v) water/MeOH + 0.1% FA. k'_a data obtained by fitting the experimental retention data on Hypercarb (4.6 mm x 100 mm, 3 µm) and C18 BEH (2.1 mm x 50 mm, 1.7 µm) columns at 30 °C with Equation 2-8. $k'_{a,PGC}$ and $k'_{a,BEH}$ are the retention factors in injected sample solvent for Hypercarb and C18 BEH.

	HA		2-MHA		4-MHA		3-MHA	
MP (v/v)	k'	$\Delta H°$ (kJ/mol)	k'	$\Delta H°$ (kJ/mol)	k'	$\Delta H°$ (kJ/mol)	k'	$\Delta H°$ (kJ/mol)
60/40	0.70	-13.3	1.08	-12.5	1.67	-14.4	1.75	-14.5
75/25	2.00	-13.6	3.15	-12.7	5.82	-15.9	6.05	-16.1
85/15	4.55	-13.4	7.27	-12.2	15.3	-17.1	15.7	-17.1
92.5/7.5	10.1	-14.2	16.4	-12.8	37.4	-18.3	38.0	-18.2

Table 2-3. Mobile phase composition, k' (at 30 °C), and $\Delta H°$ for C18 BEH (2.1 mm x 50 mm, 1.7 μm). Values for k' and $\Delta H°$ were determined from van't Hoff plots, where retention was measured at a range of temperatures. Multiple mobile phase (MP) compositions were used in order to monitor $\Delta H°$ under various retention conditions. Mobile phases were (v/v) compositions of water/MeOH + 0.1% FA.

	2-MHA		HA		3-MHA		4-MHA	
MP (v/v)	k'	$\Delta H°$ (kJ/mol)	k'	$\Delta H°$ (kJ/mol)	k'	$\Delta H°$ (kJ/mol)	k'	$\Delta H°$ (kJ/mol)
5/95	0.81	-3.1	1.82	-5.5	4.52	-7.9	5.79	-8.2
15/85	1.24	-4.3	2.54	-6.5	7.03	-8.9	8.92	-9.1
25/75	2.04	-7.0	3.86	-8.9	11.8	-11.4	14.8	-11.7
40/60	5.26	-9.7	8.90	-11.1	31.9	-13.7	39.7	-14.1

Table 2-4. Mobile phase composition, k' (at 30 °C), and $\Delta H°$ for Hypercarb (4.6 mm x 100 mm, 3 μm). Values for k' and $\Delta H°$ were determined from van't Hoff plots, where retention was measured at a range of temperatures. Multiple mobile phase (MP) compositions were used in order to monitor $\Delta H°$ under various retention conditions. Mobile phases were (v/v) compositions of water/MeOH + 0.1% FA.

	HA		2-MHA		4-MHA		3-MHA	
MP (v/v)	k'	$\Delta S°$ (J/molK)	k'	$\Delta S°$ (J/molK)	k'	$\Delta S°$ (J/molK)	k'	$\Delta S°$ (J/molK)
60/40	0.70	-46.8	1.08	-40.7	1.67	-43.1	1.75	-43.2
75/25	2.00	-39.1	3.15	-32.3	5.82	-37.9	6.05	-38.1
85/15	4.55	-31.4	7.27	-23.4	15.3	-33.5	15.7	-33.6
92.5/7.5	10.1	-27.7	16.4	-19.0	37.4	-30.2	38.0	-29.8

Table 2-5. Mobile phase composition, k' (at 30 °C), and $\Delta S°$ for C18 BEH (2.1 mm x 50 mm, 1.7 μm). Values for k' and $\Delta S°$ were determined from van't Hoff plots, where retention was measured at a range of temperatures. $\Delta S°$ was calculated from the intercept of those plots assuming $\phi = 1$. Multiple mobile phase (MP) compositions were used in order to monitor $\Delta S°$ under various retention conditions. Mobile phases were (v/v) compositions of water/MeOH + 0.1% FA.

	2-MHA		HA		3-MHA		4-MHA	
MP (v/v)	k'	$\Delta S°$ (J/molK)	k'	$\Delta S°$ (J/molK)	k'	$\Delta S°$ (J/molK)	k'	$\Delta S°$ (J/molK)
5/95	0.81	-12.1	1.82	-13.3	4.52	-13.5	5.79	-12.3
15/85	1.24	-13.8	2.54	-14.8	7.03	-14.7	8.92	-14.6
25/75	2.04	-17.3	3.86	-18.1	11.8	-17.6	14.8	-16.9
40/60	5.26	-18.6	8.90	-20.2	31.9	-16.9	39.7	-15.3

Table 2-6. Mobile phase composition, k' (at 30 °C), and $\Delta S°$ for Hypercarb (4.6 mm x 100 mm, 3 μm). Values for k' and $\Delta S°$ were determined from van't Hoff plots, where retention was measured at a range of temperatures. $\Delta S°$ was calculated from the intercept of those plots assuming $\phi = 1$. Multiple mobile phase (MP) compositions were used in order to monitor $\Delta S°$ under various retention conditions. Mobile phases were (v/v) compositions of water/MeOH + 0.1% FA.

2.6 FIGURES

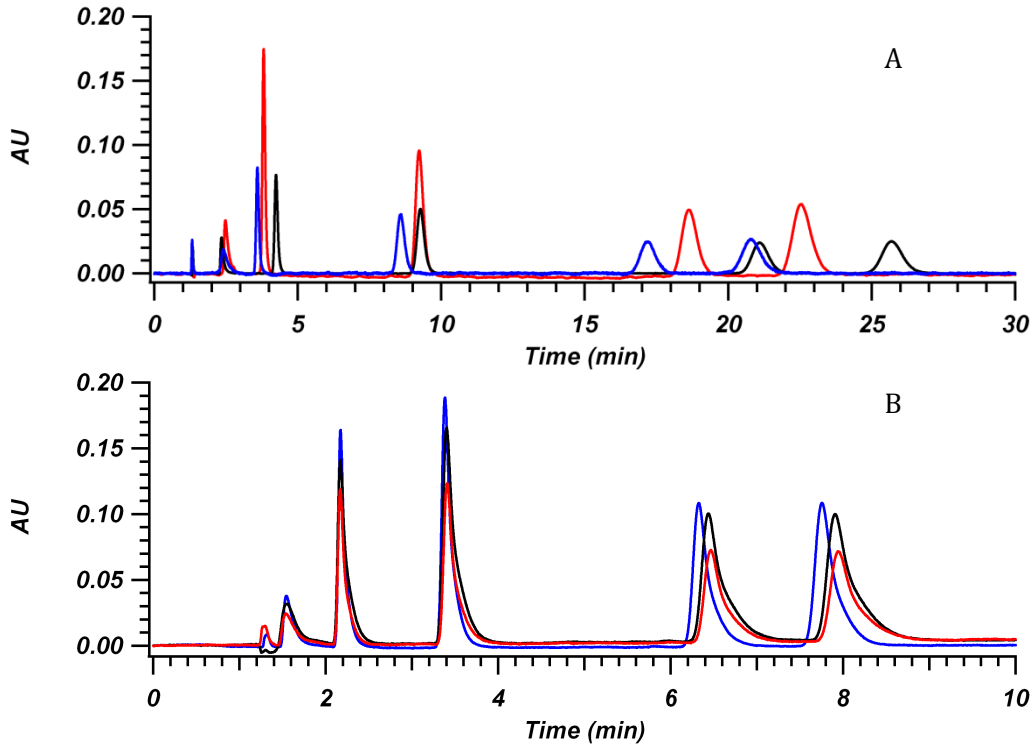

Figure 2-1. Chromatograms showing the change in day-to-day repeatability for the standard test mixture before (A) and after (B) treatment using 10 mM ascorbic acid. Column was 4.6 mm x 100 mm packed with 3 µm Hypercarb. Mobile phase conditions were 5/95 (v/v) water/MeOH + 0.1% FA at a flow rate of 1 mL/min and 30 °C. For (A), measurements were taken over the course of 2 weeks at day 1 (red), day 4 (black) and day 14 (blue). For (B), ascorbic acid treatment was performed before use each day by flowing 10 mM ascorbic acid in mobile phase overnight. Before measurements, ascorbic acid was washed off the column by flushing with mobile phase. Measurements were taken over a similar time span as in (A). Elution order: mandelic acid, 2-MHA, hippuric acid, 3-MHA, and 4-MHA. UV Detection: 240 nm.

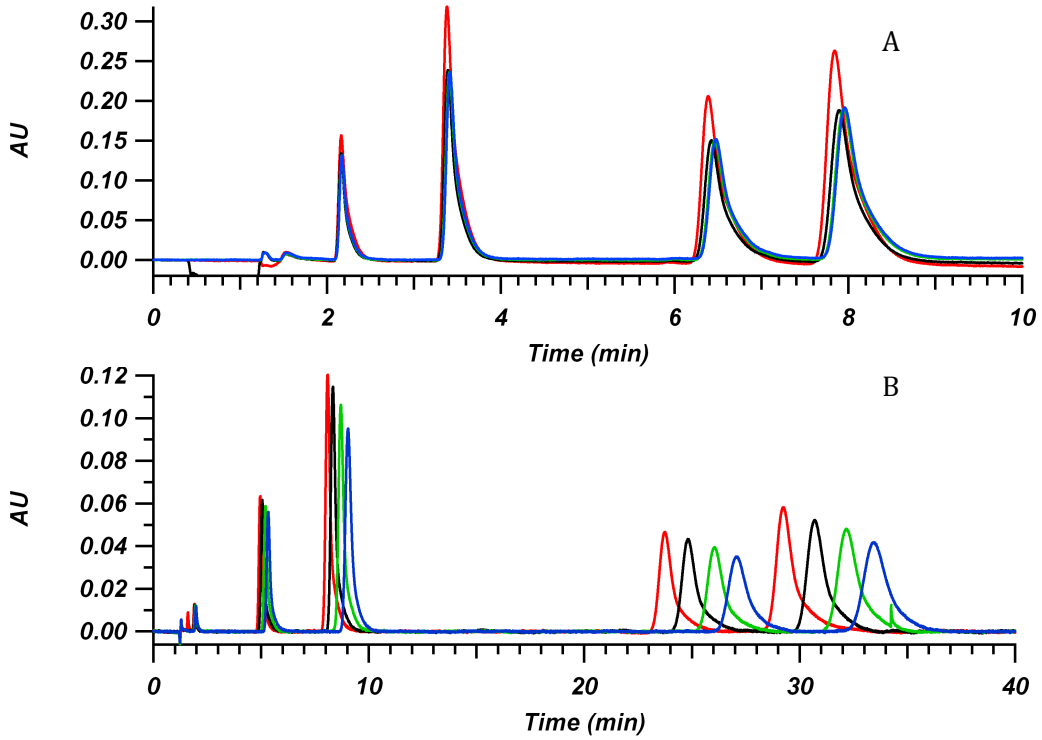

Figure 2-2. Chromatograms showing the drift in retention over the course of a single day for 5/95 (v/v) water/MeOH + 0.1% FA (A) and 35/65 (v/v) water/MeOH + 0.1% FA (B) after AA treatment of a Hypercarb column (4.6 mm x 100 mm, 3 µm). Measurements made at a flow rate of 1 mL/min and at 30 °C. Four repeated measurements were taken in sequential order of injection 1 (red), injection 2 (black), injection 3 (green), and injection 4 (blue). Ascorbic acid treatment was performed before use by flowing 10 mM ascorbic acid in mobile phase overnight. Before measurements, ascorbic acid was washed off column by flushing with mobile phase. Elution order: mandelic acid, 2-MHA, hippuric acid, 3-MHA, and 4-MHA. UV Detection: 240 nm.

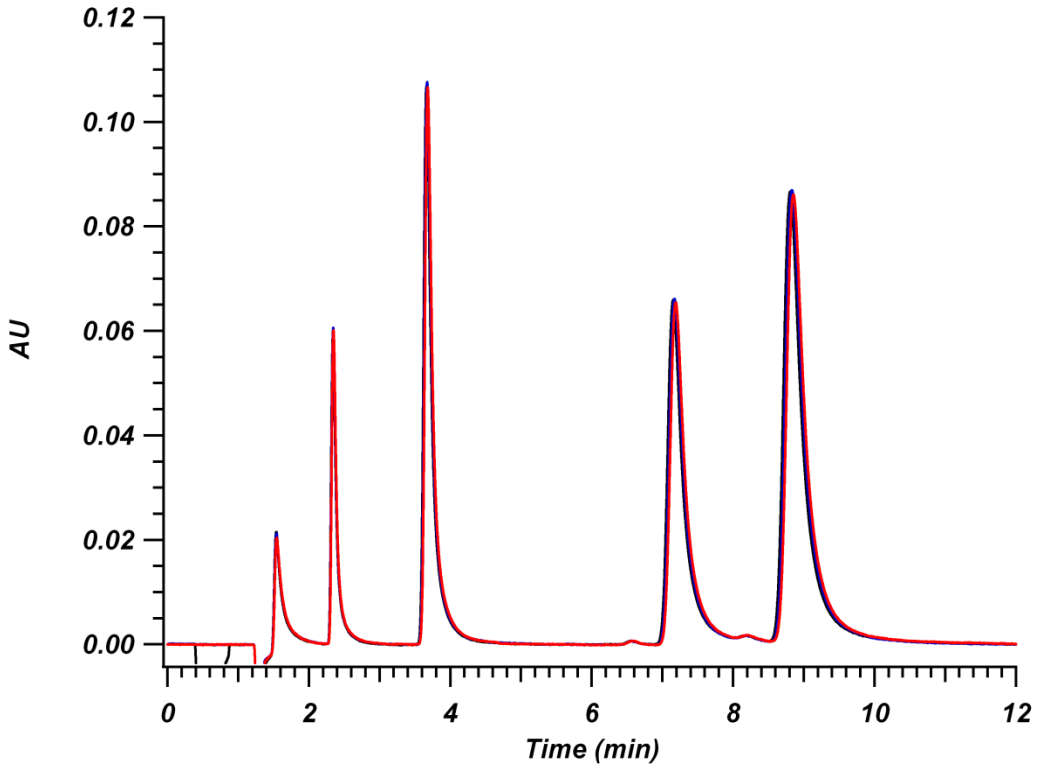

Figure 2-3. Chromatograms showing the change in day-to-day repeatability over three days for the standard test mixture after treatment using 10 mM ascorbic acid using a new Hypercarb column. Column was 4.6 mm x 100 mm packed with 3 µm Hypercarb. Mobile phase conditions were 5/95 (v/v) water/MeOH + 0.1% FA at a flow rate of 1 mL/min and 30 °C. Three measurements were taken over the course of 2 weeks and are overlaid here. Column used was new out of box and a different one than used for Figure 2-1 (B).

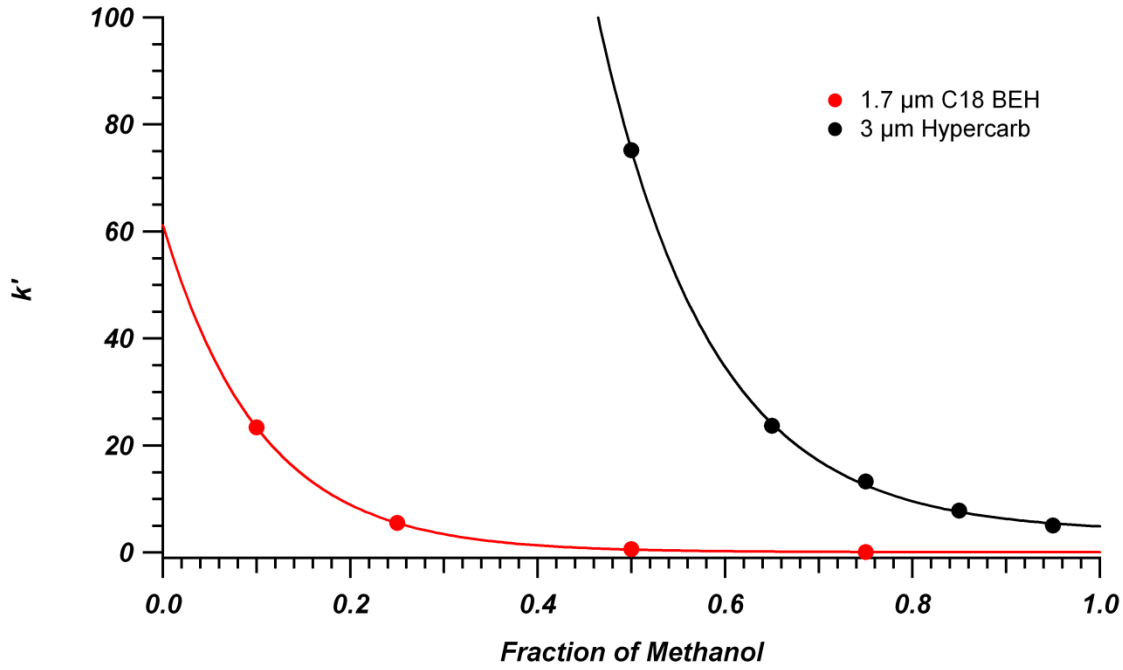

Figure 2-4. Retention factor of 4-methylhippuric acid on C18 BEH (red) and Hypercarb (black) columns as a function of methanol volume fraction in the mobile phase. Columns were 2.1 mm x 50 mm packed with 1.7 µm C18 BEH and 4.6 mm x 100 mm packed with 3 µm Hypercarb. Mobile phases consisted of mixtures of (v/v) water/MeOH + 0.1% FA at 30 °C. Experimental data fit with exponential curves.

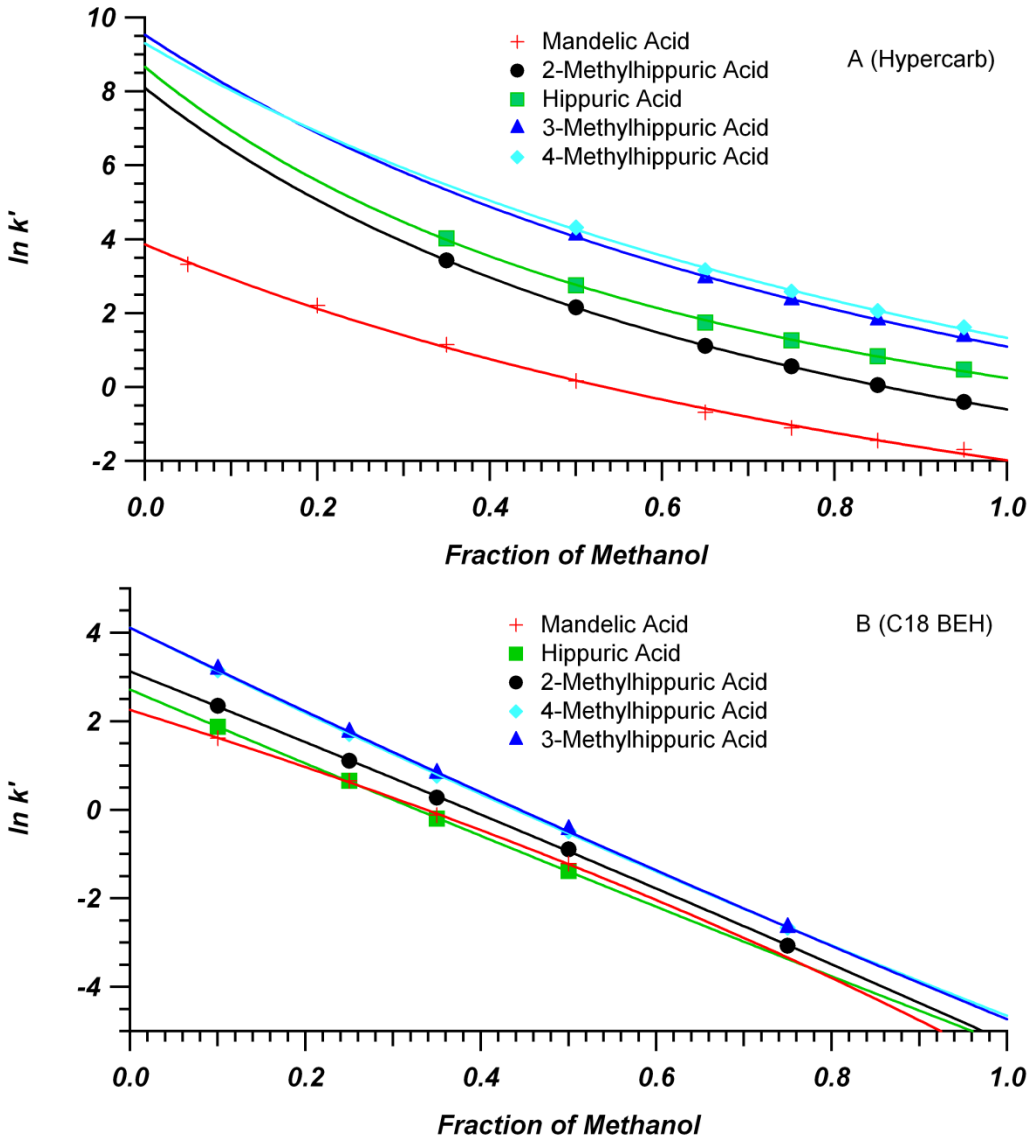

Figure 2-5. Plot of natural log of retention factors of the model metabolites as a function of methanol volume fraction in the mobile phase on the Hypercarb (A) column (4.6 mm x 100 mm, 3 µm) and C18 BEH (B) column (2.1 mm x 50 mm, 1.7 µm). Measurements made in (v/v) water/MeOH + 0.1% FA mobile phases at 30 °C. Experimental data fit with Equation 2-8.

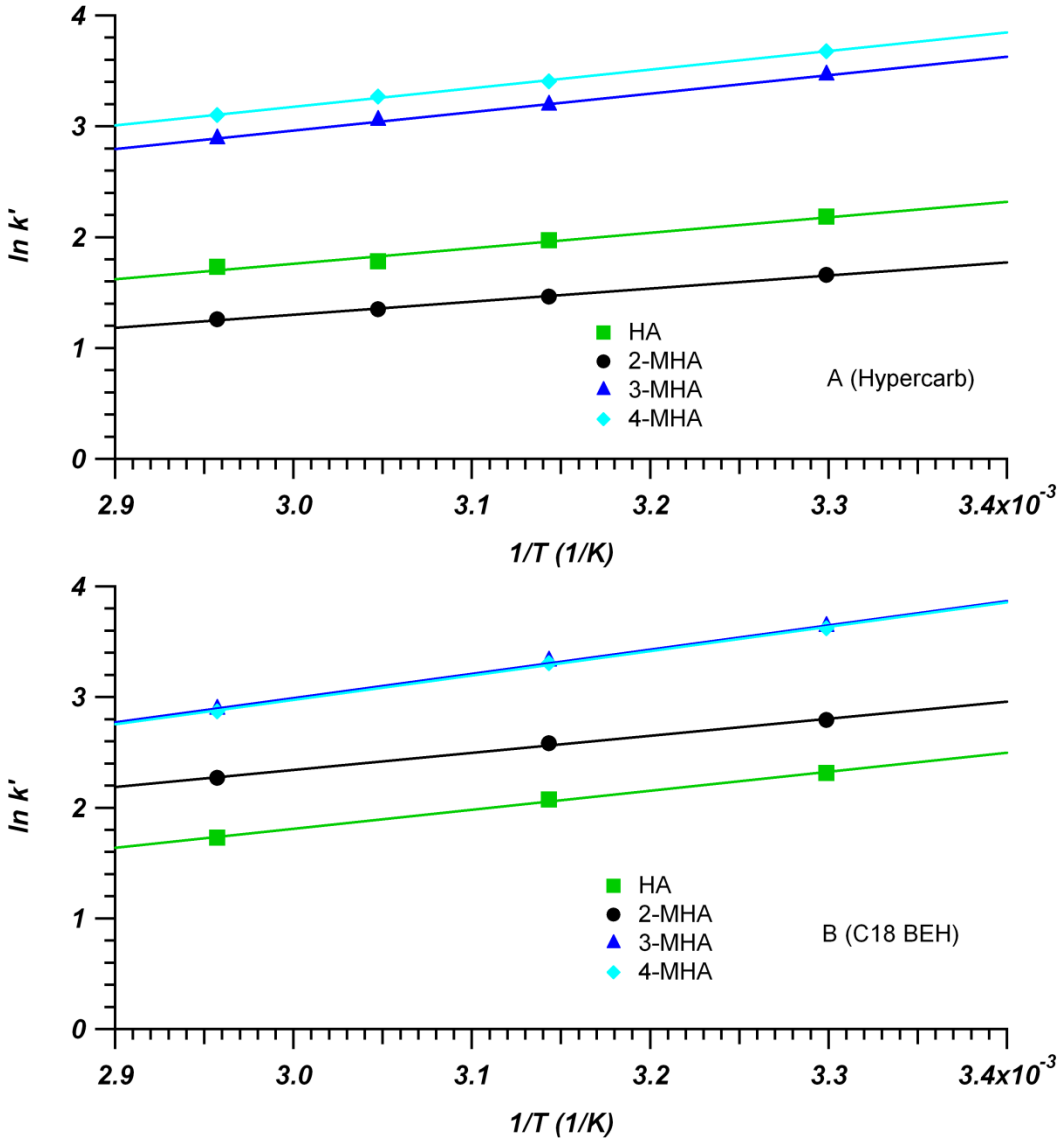

Figure 2-6. van't Hoff plots of standard metabolites for Hypercarb (A, 4.6 mm x 100 mm, 3 µm) and C18 BEH (B, 2.1 mm x 50 mm, 1.7 µm) columns. Mobile phase compositions were 40/60 water/MeOH + 0.1% FA for Hypercarb and 92.5/7.5 water/MeOH + 0.1% FA for C18 BEH. Retention was measured at a number of temperatures between 30 °C and 65 °C. Based on Equation 2-6, the slope is equal to $\frac{-\Delta H^{\circ}}{R}$ while the intercept is equal to $\frac{\Delta S^{\circ}}{R} + \ln \phi$.

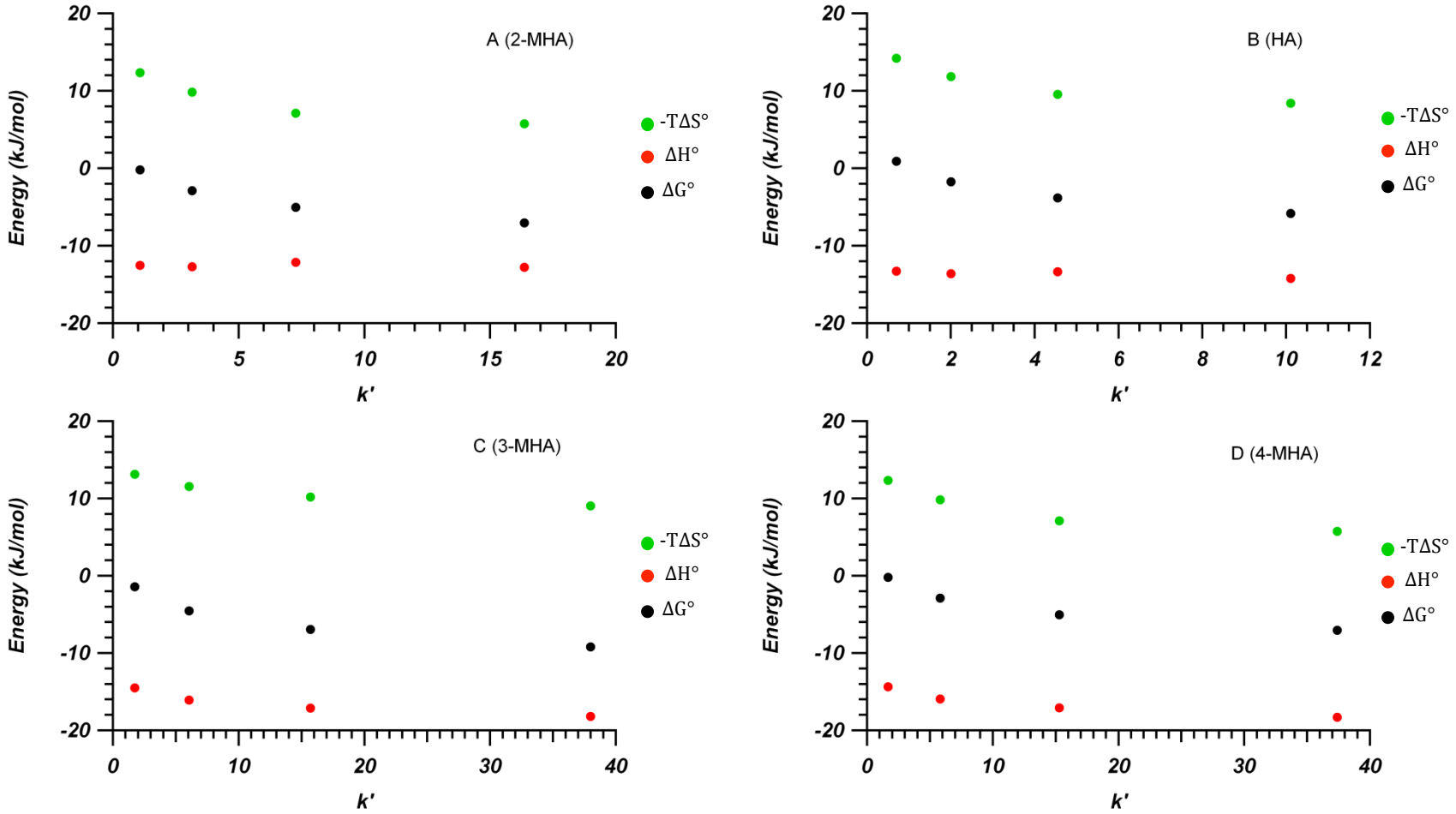

Figure 2-7. Plots showing the change in $\Delta G°$, $\Delta H°$, and $-T\Delta S°$ for 2-MHA (A), HA (B), 3-MHA (C) and 4-MHA (D) on a C18 BEH (2.1 mm x 50 mm, 1.7 µm) column at various k'. k' values were determined at 30 °C (also used for T). Values for $\Delta G°$ determined using data from Tables 2-3 and 2-5 along with Equation 2-5.

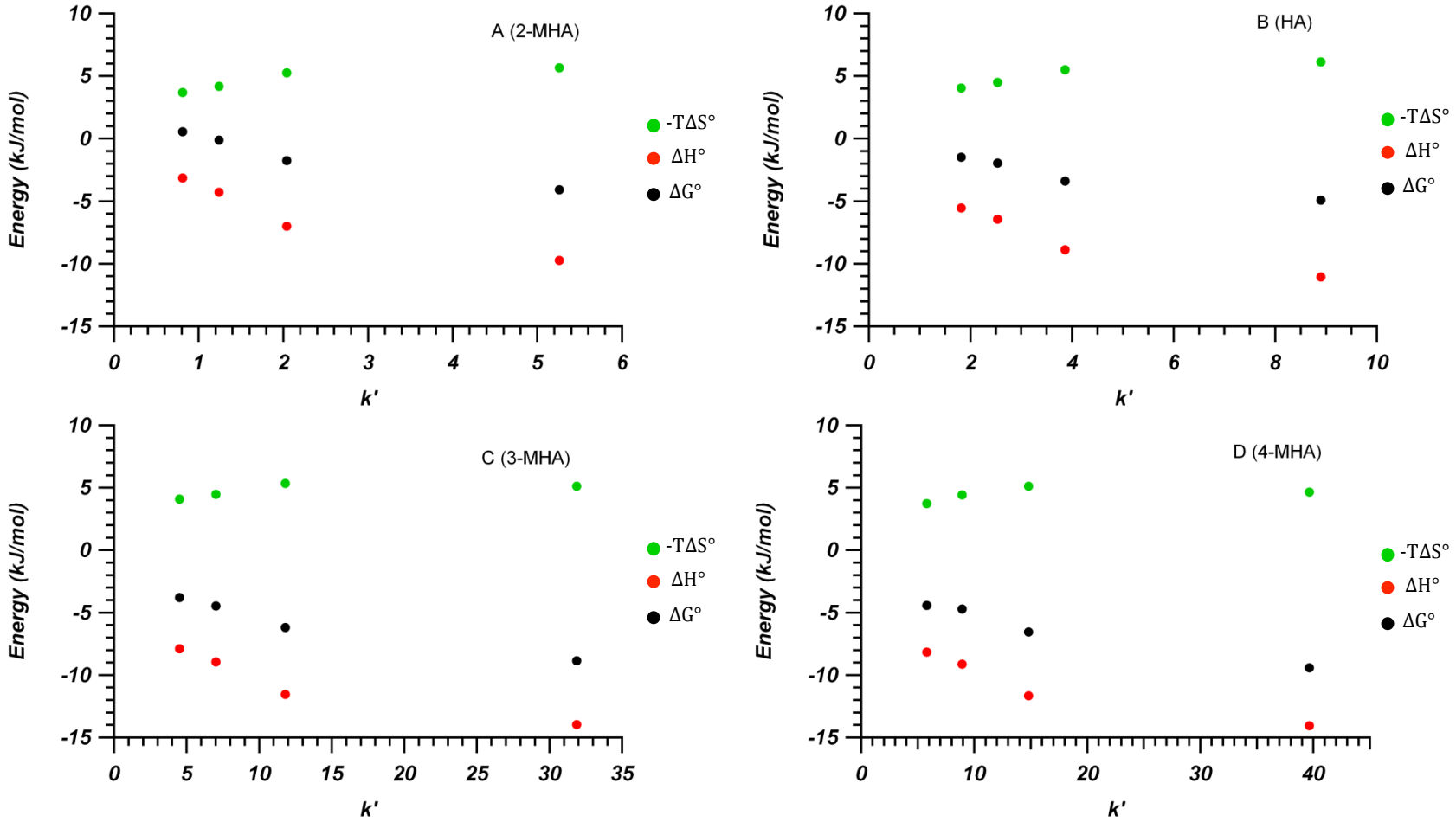

Figure 2-8. Plots showing the change in $\Delta G°$, $\Delta H°$, and $-T\Delta S°$ for 2-MHA (A), HA (B), 3-MHA (C) and 4-MHA (D) on a Hypercarb (4.6 mm x 100 mm, 3 µm) column at various k'. k' values were determined at 30 °C (also used for T). Values for $\Delta G°$ determined using data from Tables 2-4 and 2-6 along with Equation 2-5.

REFERENCES

(1) Cole, L. A.; Dorsey, J. G. Anal. Chem. **1992**, 64, 1317–1323.

(2) Rafferty, J. L.; Siepmann, J. I.; Schure, M. R. J. Chromatogr. A **2011**, 1218, 2203–2213.

(3) Akapo, S. O.; Simpson, C. F. Chromatographia **1997**, 44, 135–144.

(4) Zhu, C.; Goodall, D. M.; Wren, S. A. C. LCGC Asia Pacific **2005**, 8, 48–59.

(5) Idborg, H.; Zamani, L.; Edlund, P.; Schuppekoistinen, I.; Jacobsson, S. J. Chromatogr. B **2005**, 828, 9–13.

(6) Tang, D.; Zou, L.; Yin, X.; Ong, C. N. Mass Spectrom. Rev. **2016**, 35, 574–600.

(7) Cubbon, S.; Bradbury, T.; Wilson, J.; Thomas-Oates, J. Anal. Chem. **2007**, 79 (23), 8911–8918.

(8) Gilar, M.; McDonald, T. S.; Johnson, J. S.; Murphy, J. P.; Jorgenson, J. W. J. Chromatogr. A **2015**, 1390, 86–94.

(9) Stevenson, P. G.; Bassanese, D. N.; Conlan, X. A.; Barnett, N. W. J. Chromatogr. A **2014**, 1337, 147–154.

(10) Dunn, W. B.; Ellis, D. I. TrAC - Trends Anal. Chem. **2005**, 24, 285–294.

(11) Dolan, J. LCGC North Am. **2014**, 32, 780–785.

(12) Neue, U. D. HPLC Columns: Theory, Technology, and Practice; Wiley-VCH, Inc: New York, 1997.

(13) Layne, J.; Farcas, T.; Rustamov, I.; Ahmed, F. In Journal of Chromatography A; 2001; Vol. 913, pp 233–242.

(14) Chervet, J. P.; Ursem, M.; Salzmann, J. P. Anal. Chem. **1996**, 68, 1507–1512.

(15) Mills, M. J.; Maltas, J.; Lough, W. J. J. Chromatogr. A **1997**, 759, 1–11.

(16) Groskreutz, S. R.; Weber, S. G. J. Chromatogr. A **2015**, 1409, 116–124.

(17) Sanchez, A. C.; Anspach, J. A.; Farkas, T. J. Chromatogr. A **2012**, 1228, 338–348.

(18) Groskreutz, S. R.; Weber, S. G. J. Chromatogr. A **2014**, 1354, 65–74.

(19) Groskreutz, S. R.; Weber, S. G. J. Chromatogr. A **2016**, 1474, 95–108.

(20) Wilson, R. E.; Groskreutz, S. R.; Weber, S. G. Anal. Chem. **2016**, 88, 5112–5121.

(21) Knox, J.; Gilbert, M. T. UK Patent 7939449, 1980.

(22) Shibukawa, M.; Unno, A.; Oyashiki, Y.; Miura, T.; Nagoya, A. Anal. Commun. **1997**, 34,

397–400.

(23) Rinne, S.; Holm, A.; Lundanes, E.; Greibrokk, T. J. Chromatogr. A **2006**, 1119 (1–2), 285–293.

(24) Törnkvist, A.; Markides, K. E.; Nyholm, L. Analyst **2003**, 128, 844–848.

(25) West, C.; Elfakir, C.; Lafosse, M. J. Chromatogr. A **2010**, 1217, 3201–3216.

(26) R.L. McCreery. Chem. Rev. **2008**, 108, 2646–2687.

(27) Shibukawa, M.; Unno, A.; Miura, T.; Nagoya, A.; Oguma, K. Anal. Chem. **2003**, 75, 2775–2783.

(28) Takeuchi, T.; Kojima, T.; Miwa, T. J. High Resol. Chromatogr. **2000**, 23 (10), 590–594.

(29) Melmer, M.; Stangler, T.; Premstaller, A.; Lindner, W. J. Chromatogr. A **2010**, 1217 (39), 6097–6101.

(30) Saitoh, K.; Koichi, K.; Yabiku, F.; Noda, Y.; Porter, M. D.; Shibukawa, M. J. Chromatogr. A **2008**, 1180 (1–2), 66–72.

(31) Pabst, M.; Grass, J.; Fischl, R.; Le, R.; Jin, C.; Borth, N.; Altmann, F. Anal. Chem. **2010**, 82, 9782–9788.

(32) Shibukawa, M.; Terashima, H.; Nakajima, H.; Saitoh, K. Analyst **2004**, 129, 623–628.

(33) Fernandez-Merino, M. J.; Guardia, L.; Parades, J. I.; Villar-Rodil, S.; Solis-Fernandez, P.; Martinez-Alonso, A.; Tascon, J. M. D. J. Phys. Chem. C **2010**, 114, 6426–6432.

(34) Neue, U. D. Chromatographia **2006**, 63, S45–S53.

(35) Wan, Q.-H.; Davies, M. C.; Shaw, P. N.; Barrett, D. A. Anal. Chem. **1996**, 68 (3), 437–446.

(36) Ranatunga, R. P. J.; Carr, P. W. Anal. Chem. **2000**, 72, 5679–5692.

(37) Möckel, H. J.; Braedikow, A.; Melzer, H.; Aced, G. J. Liq. Chromatogr. **1991**, 14 (13), 2477–2498.

(38) Tanaka, N.; Tanigawa, T.; Kimata, K.; Hosoya, K.; Arai, T. J. Chromatogr. A **1991**, 549, 29–41.

(39) Melmer, M.; Stangler, T.; Premstaller, A.; Lindner, W. J. Chromatogr. A **2010**, 1217, 6092–6096.

(40) Pabst, M.; Altmann, F. Anal. Chem. **2008**, 80 (19), 7534–7542.

(41) Moldoveanu, S.; David, V. J. Chromatogr. A **2015**, 1381, 194–201.

(42) Caiali, E.; David, V.; Aboul-Enein, H. Y.; Moldoveanu, S. C. J. Chromatogr. A **2016**, 1435, 85–91.

(43) Chester, T. L.; Coym, J. W. J. Chromatogr. A **2003**, 1003, 101–111.

(44) Sentell, K. B.; Dorsey, J. G. J. Liq. Chromatogr. **1988**, 11 (9–10), 1875–1885.

(45) Dorsey, J. G.; Dill, K. a. Chem. Rev. **1989**, 89, 331–346.

(46) Zhang, Y.; McGuffin, V. L. J. Liq. Chromatogr. Relat. Technol. **2007**, 30, 1551–1575.

CHAPTER 3. INVESTIGATION OF SURFACE DIFFUSION OF MODEL METABOLITES ON POROUS GRAPHITIC CARBON

3.1 Introduction

3.1.1 Factors Impacting Peak Width in Gradient Elution

During gradient elution, the composition of the mobile phase is varied over the course of the separation, allowing the analysis of a large range of solutes in a single run. A number of factors influence the width of the peaks once they elute from the column. As discussed in Chapter 2, the retention of the analyte in gradient initial conditions has a large impact on the peak width when using large volume injections, but usually initial conditions are chosen to ensure an acceptable level of retention. As a solute band travels during the gradient, the tail of the band is in a slightly stronger mobile phase than the front of the band, leading to the tail traveling at a slightly faster velocity and catching up to the front. This velocity difference leads to an overall narrowing of the peak width for a comparative isocratic separation, by a gradient compression factor (G).[1]

$$G = \frac{[1 + p + (p^2/3)]^{1/2}}{1 + p} \qquad \text{Equation 3-1}$$

$$p = \frac{2.3k'_{init}g}{k'_{init} + 1} \qquad \text{Equation 3-2}$$

Here, k'_{init} is the solute retention factor in the gradient initial conditions and g is the gradient slope that the solute experiences. The gradient slope for a solute can be defined as:[2]

$$g = S\Delta\varphi\frac{t_m}{t_G} \qquad \text{Equation 3-3}$$

where S is a constant largely related to the solute's molecular weight, $\Delta\varphi$ is the change in organic content over the gradient, and t_G is the gradient length in time. The previous equations show that the impact of gradient compression becomes more significant with increasing gradient steepness.

In practice, a number of other factors may prevent the expected peak width from being realized.[3] Post-column connecting tubing and detectors can contribute to extra-column band broadening. Pre-column volumes normally don't impact gradient separations as long as k'_{init} is high. Another influence is that the column performance may vary with k', whereas the predictions of peak width are based on constant N for the column. Neue, Marchand, and Snyder also suggested that surface diffusion along the particle stationary phase could contribute to wider than expected peaks.[1] When an analyte with high k'_{init} reaches the head of the column, its migration stops almost immediately due to interaction with the stationary phase. Although the solute band is not migrating with the flow of mobile phase, solute molecules are still free to longitudinally diffuse through the stationary phase, potentially leading to increased peak width.[2,4,5] The impact of surface diffusion is expected to be most significant during long and shallow gradient separations as they allow more time for surface diffusion to occur, as well as less effective gradient compression.[1]

3.1.2 Surface Restricted Diffusion in Chromatography

As mentioned above, the contribution of surface diffusion for an analyte is in the form of a molecular diffusion coefficient and is related to the total variance due to longitudinal molecular diffusion ($\sigma^2_{ax,L}$) by:[6]

$$\sigma^2_{ax,L} = 2\gamma_m D_m t_m + 2\gamma_s D_s k' t_m \qquad \text{Equation 3-4}$$

where γ is the obstruction factor, related to the tortuosity of the path hindering diffusion, and D is the solute diffusion coefficient. The subscripts m and s are used to designate contributions from the mobile and stationary phases. $\sigma^2_{ax,L}$ is the sum of the parallel contributions of diffusion in the mobile and stationary phases. The contributions from the mobile and stationary phases will sum to an overall effective diffusion coefficient that a solute band is experiencing (D_{eff}) during a time (t), simplifying Equation 3-4.[7]

$$\sigma^2_{ax,L} = 2D_{eff}t \qquad \text{Equation 3-5}$$

Combining Equations 3-4 and 3-5 yields the individual contributions of stationary and mobile phase

diffusion to the effective diffusion coefficient.[7]

$$D_{eff} = \frac{\gamma_m D_m}{1+k'} + \frac{k'\gamma_s D_s}{1+k'} \qquad \text{Equation 3-6}$$

Using Equation 3-6, if k' increases, then the contribution from $\gamma_s D_s$ begins to dominate D_{eff} thus illustrating how it could become an issue if surface diffusion is high under gradient initial conditions.

The most widely accepted model for surface diffusion in reversed phase chromatography is the surface restricted diffusion model, developed by Miyabe and Guiochon.[8,9] This model assumes that stationary phase diffusion is analogous to molecular diffusion in the mobile phase, but now occurring in the potential field of the stationary phase. The process of diffusion through the mobile phase is considered an activated process.[8]

$$D_m = D_{m,0} \exp\left(\frac{-E_m}{RT}\right) \qquad \text{Equation 3-7}$$

Here $D_{m,0}$ is the frequency factor of molecular diffusion in the mobile phase and E_m is the activation energy of molecular diffusion. E_m is related to the process of hole making in the mobile phase, which is required for diffusion. E_m is correlated to the evaporation energy of the solvent system. D_m can also be described in terms of absolute rate theory:[10]

$$D_m = \lambda_{diff}^2 \, \tau_{diff} \qquad \text{Equation 3-8}$$

where λ_{diff} is the distance between two equilibrium positions and τ_{diff} is the rate constant of diffusion.[8]

$$\tau_{diff} = \left(\frac{1}{V_f^{1/3}}\right)\left(\frac{k_B T}{2\pi M_A}\right) \exp\left(\frac{-E_m}{RT}\right) \qquad \text{Equation 3-9}$$

Here, V_f is the free volume of the solvent, which is related to the solvent molar volume and evaporation energy, k_B is the Boltzmann constant, and M_A is the molecular weight of the solute. The combination of Equations 3-7, 3-8, and 3-9 allow estimation of $D_{m,0}$ by:[8]

$$D_{m,0} = \left(\frac{\lambda_{diff}^2}{V_f^{1/3}}\right)\left(\frac{k_B T}{2\pi M_A}\right)^{1/2} \qquad \text{Equation 3-10}$$

The values of λ_{diff}, M_A, and V_f are dependent on the solute and solvent system used, but values of $D_{m,0}$ generally fall in the range of 3 x 10^{-3} to 2 x 10^{-2} cm^2/s for reversed phase LC.

As mentioned previously, the surface restricted diffusion model assumes that stationary diffusion is similar to mobile phase diffusion, but now in the potential field of the surface.[9]

$$E_s = E_m + \beta(-Q_{st}) \qquad \text{Equation 3-11}$$

Here E_s is the required activation energy for surface diffusion and β is some fraction of the isosteric heat of adsorption (Q_{st}). Equation 3-11 provides insight into the energetic processes that must occur for stationary phase diffusion to occur.[11] First a hole must be made for the solute, assumed here to be equivalent to a hole making process in the mobile phase (E_m), but in the potential field of the surface. Then the solute must break a certain energy barrier related to its retention ($\beta(-Q_{st})$), in order to hop into the hole. The process of hole making and hopping steps in the potential field of adsorption is at the core of the surface restricted diffusion model and as such, D_s takes on a similar form as Equation 3-7.[8]

$$D_s = D_{s,0} \exp\left(\frac{-E_s}{RT}\right) = D_{s,0} \exp\left(\frac{-(E_m + \beta(-Q_{st}))}{RT}\right) \qquad \text{Equation 3-12}$$

The values for $D_{s,0}$ (surface diffusion frequency factor) and $D_{m,0}$ are expected to be similar, but λ_{diff}, M_A, and V_f cannot be estimated accurately in the potential field of the surface thus making determination of $D_{s,0}$ difficult.

By dividing Equation 3-12 by 3-7, the ratio of $\frac{D_s}{D_m}$ can be determined.[8]

$$\frac{D_s}{D_m} = \left(\frac{D_{s,0}}{D_{m,0}}\right)\left[\exp\left(\frac{Q_{st}}{RT}\right)\right]^{\beta} \qquad \text{Equation 3-13}$$

Using the van't Hoff equation, the isosteric heat of adsorption can be related to the partition equilibrium constant (K) by:

$$K = K_0 \exp\left(\frac{-Q_{st}}{RT}\right) \qquad \text{Equation 3-14}$$

where K_0 is the frequency factor of adsorption, or the value of K when Q_{st} = 0 kJ/mol. Combining

Equations 3-13 and 3-14 yields the relationships between $\frac{D_s}{D_m}$ and K.

$$\frac{D_s}{D_m} = \left(\frac{D_{s,0}}{D_{m,0}}\right)\left[\frac{K_0}{K}\right]^{\beta} \qquad \text{Equation 3-15}$$

Since $K \propto k'$, $\frac{D_s}{D_m}$ will decrease with increasing retention of a solute. This trend is important as it should limit the amount of broadening that can occur over the course of a gradient separation since analytes tend to have a high k' until the mobile phase reaches a strength needed to elute the peak.

The surface restricted diffusion model has been shown to hold true for a number of reversed phase chromatography systems including C18 bonded particles as well as monolithic columns.[9,11,12] To the best of my knowledge, the study of surface diffusion on porous graphitic carbon stationary phases has not been previously investigated. As our interest is to utilize long capillary columns with long gradient run times, it is necessary for us to understand the surface diffusion properties of the PGC particles.

3.2 Experimental Methods

3.2.1 Chemicals

Methanol (MeOH, HPLC grade), acetone (HPLC grade), potassium chloride (KCl) and L-ascorbic acid were purchased from Fisher Scientific (Fair Lawn, NJ). Deionized water was obtained using a Barnstead Nanopure ultrapure water system (Dubuque, IA). Formic acid (FA), mandelic acid (MA), hippuric acid (HA), 2-methylhippuric acid (2-MHA), 3-methylhippuric acid (3-MHA), 4-methylhippuric acid (4-MHA), potassium ferrocyanide, and potassium ferricyanide were purchased from Sigma Aldrich (St. Louis, MO).

3.2.2 Molecular Diffusion Coefficient Measurements

Molecular diffusion coefficients (D_m) were measured for a number of analyte/mobile phase combinations using a dual-ultraviolet (UV) detector setup that has been described previously.[13] A diagram of the experimental setup can be found in the Figure 3-1. Briefly, the polyimide was removed from two spots, roughly 2.5 m apart, on a piece of fused silica capillary, 360 μm outer

diameter (o.d.) with a nominal inner diameter (i.d.) of 50 μm (Polymicro Technologies, Phoenix, AZ). This capillary was threaded through two Linear Ultraviolet-Visible (UV-Vis) 200 spectrophotometers (Thermo Scientific, Waltham, MA) with the capillary windows each being centered in one of spectrophotometers. All measurements were made with a rise time of 0.1 s, while the sensitivity was adjusted for each analyte to maximize the signal-to-noise. The capillary inlet was inserted into a scintillation vial containing the desired solute (1-2 mg/mL) in mobile phase. The vial was placed in an in-house made pressure vessel. The outlet was also placed in a vial of mobile phase to prevent evaporation. Nitrogen pressure was applied to the vessel to force sample through the capillary. As the analyte traveled through the detection zones, sigmoidal signal curves were recorded. Data was then differentiated using Igor Pro (Wavemetrics, Inc, Lake Oswego, OR) to generate peaks. The peaks were then fit to Gaussians for the measurement of variance. The capillary's effective inner diameter was calculated using reference solutions of potassium ferrocyanide and potassium ferricyanide in 1 M KCl, which have known D_m, at a concentration of approximately 1 mg/mL.[14] All measurements were made at ambient lab temperature (22.5 ± 0.2 °C).

3.2.3 Peak parking Measurements

Peak parking methods have been used previously for the measurement of diffusion coefficients in chromatographic systems.[7,15,16] Peak parking experiments were carried out with the same Acquity UPLC that was used in Chapter 2. The columns used were: a Hypercarb column (4.6 mm x 100 mm, 3 μm) purchased from Thermo Fisher Scientific Inc. (Waltham, MA) and a C18 BEH column (2.1 mm x 50 mm, 1.7 μm) provided by Waters Corp. A four-port valve (Valco, Houston, TX) was placed between the injector and column to allow manual control of the flow stoppage. The columns were kept in the Acquity column heater at a temperature of 30 °C or 55 °C as denoted.

Runs were performed with no stop in order to get a baseline variance for the analyte under the specific mobile phase conditions. For a peak-parking run, the flow was diverted away from the column using the valve when the analyte band reached half way down the column length. The valve had a restrictor capillary to make sure the backpressure of the diverted flow was equal to that

generated by the column. After the stop time, the valve was turned to direct flow back to the column, where the analyte band was eluted off for detection. Measurements using a range of stop times were recorded for each set of conditions. As described previously, ascorbic acid washing of the Hypercarb column was performed each day before use.

Peak parking experiments were performed on both the Hypercarb and C18 BEH columns using the standard test metabolites and a variety of (v/v) water/MeOH + 0.1% FA mobile phases at 30 °C. Measurements were also made for Hypercarb at 55 °C in order to see if significant variation occurred due to use of an elevated temperature. The mobile phase and analyte used were both varied to obtain measurements over a range of retention factors (k'~ 0.75-40). Measurements were taken in at least triplicate for all conditions and stop times.

3.3 Results and Discussion

3.3.1 Experimental Molecular Diffusion Coefficient Measurement

In order to determine the stationary phase surface diffusion properties of these materials, it was first necessary to determine D_m for a number of analyte/mobile phase combinations. This was accomplished by measuring Taylor-Aris dispersion of the analytes in a capillary with two UV detectors spaced approximately 2.5 m apart along the capillary. Due to the low pressures associated with peak parking experiments (< 500 bar), viscosity changes due to pressure do not need to be accounted for in D_m measurements.[13] The raw UV signal was differentiated to generate peaks (Figure 3-2). These were then fit with Gaussians, whose variance can be used to find the temporal variance accumulated between the detectors ($\sigma_{t\_net}^2$):

$$\sigma_{t\_net}^2 = \sigma_{t2}^2 - \sigma_{t1}^2 \qquad \text{Equation 3-16}$$

where σ_{t1}^2 and σ_{t2}^2 are the temporal variances of the peaks measured at the first and second detectors, respectively. D_m is then calculated from Equation 3-17.

$$D_m = \frac{d_c^2 \Delta t}{96\sigma_{t\_net}^2} \qquad \text{Equation 3-17}$$

Here, d_c is the capillary i.d. and Δt is the time between the detected peaks.

Accurate knowledge of d_c over the length between detectors is vital for determination of D_m because it depends on the square of d_c. For this reason, a calibration of d_c was needed. In order to calibrate d_c between the detectors, D_m of potassium ferrocyanide and ferricyanide were measured. D_m of these species in 1 M KCl has been studied using a number of methods at 25 °C.[14] By comparing the experimental D_m to the literature values, the diameter of the capillary between the detectors can be determined. Since the experiments were done at room temperature (22.5 ± 0.2 °C) it was necessary to account for the temperature difference between the literature and experimental measurements. This was done using the Stokes-Einstein equation:

$$D_m = \frac{k_B T}{6\pi\eta r_H} \qquad \text{Equation 3-18}$$

where r_H is the hydrodynamic radius of the analyte. After calibration, d_c was found to be 46.4 μm, which is slightly outside of the manufacturer's claim that the diameter should be 50 $\pm$ 3 μm. To see if this calibrated diameter was realistic, a short region of the end of the capillary was clipped and imaged using a Hitachi S-4700 cold cathode field emission scanning electron microscope (SEM, Tokyo, Japan). An example image with measured diameters can be seen in Figure 3-3. Measuring on the vertical and horizontal axes, the diameters were measured as 47.18 μm and 46.58 μm. Although these values are not from the region between detectors, these values make the calibration diameter plausible. This calibrated value (46.4 μm) was then used, in conjunction with dual-UV measurements, to calculate D_m for a number of standard metabolite and mobile phase combinations. All measurements were taken at ambient lab temperature (22.5 ± 0.2 °C). Values were adjusted using Equation 3-18 for temperatures under which peak parking measurements were conducted (30 °C and 55 °C). The viscosities of water/methanol mobile phases at various temperatures have been previously reported.[17] Tables 3-1, 3-2, and 3-3 show the measured D_m for all analyte and mobile phase combinations used for C18 BEH at 30 °C, Hypercarb at 30 °C, and Hypercarb at 55 °C. At least triplicate measurements were made for each analyte/mobile phase pair, each with a different applied pressure to assure no variation with pressure occurred. These values have some error inherent

to them from the estimations made for temperature and viscosity, but this is likely less than the 10-15% error often associated with the Wilke-Chang method for calculating D_m based on solute structure and experimental conditions (temperature and viscosity).[18,19]

3.3.2 Peak Parking Experiments to Study PGC Surface Diffusion

Peak parking measurements were performed under a variety of retention conditions for both C18 BEH and Hypercarb columns in order to measure the stationary phase surface diffusion of various solutes. Figure 3-4, shows an example peak-parking chromatogram using Hypercarb. Peak tailing was observed throughout the peak parking experiments and made it difficult to accurately measure peak variance with the commonly used methods of iterative statistical moments (ISM) or by fitting Gaussians. The most accurate way to fit these peaks was with the Foley-Dorsey model of the Exponentially-Modified Gaussian (EMG) function:[20,21]

$$f(t) = A_{peak}\frac{\sigma_{fit}}{\tau_{fit}}\sqrt{\frac{\pi}{2}}\exp\left(\frac{\sigma_{fit}^2}{2\tau_{fit}^2} - \frac{t - t_R}{\tau_{fit}}\right)\left(1 - erf\left[\frac{2}{\sqrt{2}}\left(\frac{\sigma_{fit}}{\tau_{fit}} - \frac{t - t_R}{\sigma_{fit}}\right)\right]\right) \qquad \text{Equation 3-19}$$

where $f(t)$ is the measured signal, t is the time, A_{peak} is the peak amplitude, σ_{fit} is used to describe the Gaussian, "sigma-type" broadening contribution, and τ_{fit} is used to describe the exponential decay, "tau-type" broadening. Traditionally when fitting peaks using the EMG, the temporal variance of the fit peak ($\sigma_{t,EMG}^2$) is calculated using Equation 3-20.

$$\sigma_{t,EMG}^2 = \sigma_{fit}^2 + \tau_{fit}^2 \qquad \text{Equation 3-20}$$

When using this equation on the measured analyte peaks for the Hypercarb column, $\sigma_{t,EMG}^2$ was dominated by τ_{fit}^2 due to the strong tailing observed, masking any sigma-type broadening. Tau-type broadening can originate from several sources such as poorly swept volumes in the injector, connecting tubing and also slow kinetics of adsorption/desorption.[6,22,23] In the peak parking experiments, there is no convective flow. This lack of flow means that the only broadening processes that can affect peak width during flow stoppage are axial diffusion in the mobile and stationary phases. Since molecular diffusion has no directionality (it is equally probable toward the inlet or

outlet of the column) it will only contribute toward increasing the sigma component of the total variance.[6] As the purpose of peak parking experiments is to solely measure the effect of these diffusional processes on an injected band over a range of stop-flow times, it was thought that simply using σ_{fit}^2 alone as the "variance" of the peak would be a more accurate descriptor of the diffusional broadening.[6] For consistency, this method of peak fitting was also used for measurements made with the C18 BEH column, even though far less tailing was seen on this column. The variance has been taken from the temporal domain in which it was measured, to the spatial domain ($\sigma_{ax,L}^2$) by use of the analyte band velocity (u_a).

$$\sigma_{ax,L}^2 = \sigma_{fit}^2 u_a^2 \qquad \text{Equation 3-21}$$

By plotting the spatial variance versus the stop time for an analyte/mobile phase combination, it is possible to calculate the effective diffusion coefficient that an analyte experiences while stopped using:

$$\sigma_{ax,L}^2 = 2D_{eff}t_{stop} \qquad \text{Equation 3-22}$$

where t_{stop} is the stop time. Figures 3-5 illustrates the linearity between $\sigma_{ax,L}^2$ and t_{stop} for the analytes on C18 BEH at 30 °C (A), Hypercarb at 30 °C (B), and Hypercarb at 55 °C (C). Tables 3-4, 3-5, and 3-6 show the data for the fit trend lines for the plots of $\sigma_{ax,L}^2$ vs t_{stop} for C18 BEH at 30 °C, Hypercarb at 30 °C, and Hypercarb at 55 °C, respectively. The fit of all these trend lines had $R^2 \geq$ 0.98 for BEH and Hypercarb at 30 °C and $R^2 \geq 0.96$ for Hypercarb at 55 °C. As mentioned previously, D_{eff} (Equation 3-6) is the sum of the contributions from both mobile phase (D_m) and the stationary phase diffusion (D_s) to the overall band broadening in the stopped state. Values for D_{eff} and k' for all analyte/mobile phase compositions are presented in Tables 3-1, 3-2, and 3-3 for C18 BEH at 30 °C, Hypercarb at 30 °C, and Hypercarb at 55 °C, respectively.

In order to separate the contributions of mobile phase and stationary phase diffusion to D_{eff}, it is necessary to know γ_m for each column. This value is calculated by performing a peak parking measurement using an analyte that is unretained. This simplifies Equation 3-6 so that mobile phase

diffusion is the only contributor to D_{eff}. For these experiments the unretained species and conditions were ascorbic acid (in 50/50 (v/v) water/MeOH + 0.1% FA) for the C18 BEH column and acetone (in 5/95 (v/v) water/MeOH + 0.1% FA) for the Hypercarb column, both at 30 °C. Using the measured values for D_m and D_{eff} for the unretained species, it was found that γ_m was 0.43 for the C18 BEH and 0.46 for the Hypercarb column. As it is not expected for γ_m to change with temperature for Hypercarb, we assume the same value for γ_m at 55 °C. Using Equation 3-6, the determination of the contribution of stationary diffusion ($\gamma_s D_s$) to D_{eff} for the retained analytes could now be made (values for $\gamma_s D_s$ can be found in Tables 3-1, 3-2, and 3-3 for C18 BEH at 30 °C, Hypercarb at 30 °C, and Hypercarb at 55 °C). It should be noted that since γ_s is not known for the columns, the contributions of stationary phase and mobile phase diffusion will be discussed including their respective obstruction factors ($\gamma_s D_s$ and $\gamma_m D_m$). Figure 3-6 shows how the contributions of $\gamma_s D_s$ change as a function of retention for the C18 BEH (30 °C) and Hypercarb columns (30 °C and 55 °C), with error bars. More information on the calculation and propagation of error throughout these measurements can be found in the Appendix. At low k', C18 BEH shows a high level of stationary phase diffusion (4 x 10^{-6} cm^2/s) which quickly drops off as k' increases. Hypercarb shows a different trend in that $\gamma_s D_s$ was relatively flat across the whole range of k' at a low value (< 1 x 10^{-6} cm^2/s for 30 °C and < 1.5 x 10^{-6} cm^2/s for 55 °C).

In order to give a better picture of the contribution of $\gamma_s D_s$, it is useful to ratio it to $\gamma_m D_m$. Figure 3-7 shows $\gamma_s D_s / \gamma_m D_m$ as a function of k' for both columns at 30 °C as well as Hypercarb at 55 °C. Values for $\gamma_s D_s / \gamma_m D_m$ for C18 BEH at 30 °C, Hypercarb at 30 °C, and Hypercarb at 55 °C can be found in Tables 3-1, 3-2, and 3-3. Detailed information on the calculation of error bars can be found in the Appendix. The C18 BEH column shows a trend consistent with the surface-restricted diffusion model, in that stationary phase diffusion decreases as k' increases. This was expected for a traditional C18 bonded reversed phase stationary phase. At low k', $\gamma_s D_s / \gamma_m D_m > 1$ was observed, suggesting that surface diffusion dominated. Due to the low retention, it would be expected that the

analytes spend their time at the interface of the C18 chains and the bulk mobile phase. It has been suggested that this interfacial region at the end of the alkyl chains contains an elevated local concentration of organic modifier.[24–26] Solutes in this "organic modifier ditch" should experience faster diffusion since it is expected that the viscosity in this region would be lower than in the bulk mobile phase. Analytes that are more retained penetrate the C18 chains to a greater extent and experience corresponding lower rates of diffusion.[26] The Hypercarb column at 30 °C, however, shows a relatively constant $\gamma_s D_s/\gamma_m D_m \approx 0.2$ over the whole range of k'. Although the exact mechanism is currently unknown, we hypothesize that the difference in trend between Hypercarb and BEH could be due to the difference in surface chemistry. Without a bonded layer, interactions with the solute occur directly at the surface of the PGC particles. This also means that the local (interfacial) mobile phase composition could be more reflective of the bulk, leading to the absence of the "organic modifier ditch" seen with C18 bonded particles. This would lead to more constant surface diffusion as analytes with varying retention aren't experiencing different diffusive environments, as they do with C18 bonded particles. It was seen that even at the elevated temperature of 55 °C, $\gamma_s D_s/\gamma_m D_m$ is still centered around 0.2. This is significant since elevated temperatures are often used in capillary separations to promote rapid diffusion as well as reduce backpressure and analysis time.[27] The C18 BEH column reaches a similar value of $\gamma_s D_s/\gamma_m D_m \approx 0.2$ at the highest k' used.

It is important to see the bigger picture as it applies to gradient separations. We know from experience that C18 BEH particles provide low enough surface diffusion to allow for minimal contribution to peak broadening under conditions of high k' prior to elution by the mobile phase gradient. The data for Hypercarb suggests that it too will provide minimal contributions to broadening of focused bands prior to elution, since both surface diffusion ($\gamma_s D_s$) and diffusion ratios ($\gamma_s D_s/\gamma_m D_m$) exhibit even lower values on Hypercarb over the whole range of k' at both 30 °C and 55 °C. This factor is critical since long capillary columns packed with Hypercarb will require long run times at the flow rates and gradient rates needed for coupling to electrospray ionization-mass

spectrometry (ESI-MS) systems.

3.4 Conclusions

The surface diffusion characteristics of Hypercarb were studied for a mixture of model metabolites. This was done in order to determine whether long capillary columns packed with Hypercarb would be applicable to the separation of these types of samples. Data suggests that $\gamma_s D_s/\gamma_m D_m$ is relatively constant across the range of k' measured, staying centered at ~0.2 even at the elevated temperatures often used to speed up analysis time of capillary separations. This differs from the surface restricted diffusion seen for the C18 BEH column, where $\gamma_s D_s/\gamma_m D_m$ decreases as k' increases. It is important to note that the C18 BEH column levels off around $\gamma_s D_s/\gamma_m D_m = 0.2$ at high k', the same as Hypercarb across its whole range of k'. Although the exact mechanism is not known at this time, the fact that the PGC surface diffusion stays low across the range of k' suggests that the impact of stationary diffusion on gradient separations using Hypercarb columns should be minimal, even under the long runtimes (> 2 hours) associated with long capillary columns. The data shown here suggests that Hypercarb should be amenable to long capillary column separations of polar metabolites based on the improved retention of these compounds (Chapter 2) and the low level of stationary phase diffusion that would occur during these runs.

3.5 TABLES

Analyte	Mobile phase	k'	D_m (cm^2/s)	D_{eff} (cm^2/s)	$\gamma_s D_s$ (cm^2/s)	$\frac{\gamma_s D_s}{\gamma_m D_m}$
Ascorbic acid	50/50 water/MeOH	0	4.43 ± 0.08 x 10^{-6}	2.0 x 10^{-6}	-	-
Mandelic Acid	60/40 water/MeOH	0.75	5.07 ± 0.09 x 10^{-6}	2.95 x 10^{-6}	3.8 x 10^{-6}	1.6
4-MHA	75/25 water/MeOH	5.50	5.07 ± 0.09 x 10^{-6}	1.43 x 10^{-6}	1.3 x 10^{-6}	0.55
4-MHA	85/15 water/MeOH	13.7	5.96 ± 0.11 x 10^{-6}	1.12 x 10^{-6}	1.0 x 10^{-6}	0.37
4-MHA	92.5/7.5 water/MeOH	34.8	6.49 ± 0.12 x 10^{-6}	8.42 x 10^{-7}	7.8 x 10^{-7}	0.27

Table 3-1. Measured values for k', D_m, D_{eff}, $\gamma_s D_s$, and $\frac{\gamma_s D_s}{\gamma_m D_m}$ along with the conditions used for the C18 BEH column (2.1 mm x 50 mm, 1.7 µm) at 30 °C. D_m values determined by dual-UV measurements and adjusted to 30 °C. D_{eff} determined from plots of the change in spatial variance of all analytes as a function of stop time. Mobile phase compositions were (v/v) mixtures of water/MeOH + 0.1% FA.

Analyte	Mobile phase	k'	D_m (cm^2/s)	D_{eff} (cm^2/s)	$\gamma_s D_s$ (cm^2/s)	$\frac{\gamma_s D_s}{\gamma_m D_m}$
Acetone	5/95 Water/MeOH	0	2.61 ± 0.05 x 10^{-5}	1.3 x 10^{-5}	-	-
2-MHA	5/95 Water/MeOH	0.87	9.62 ± 0.17 x 10^{-6}	2.9 x 10^{-6}	9.9 x 10^{-7}	0.22
Hippuric acid	5/95 Water/MeOH	1.95	9.51 ± 0.17 x 10^{-6}	2.0 x 10^{-6}	7.0 x 10^{-7}	0.15
3-MHA	5/95 Water/MeOH	4.72	9.45 ± 0.17 x 10^{-6}	1.5 x 10^{-6}	8.7 x 10^{-7}	0.19
4-MHA	5/95 Water/MeOH	6.40	9.25 ± 0.16 x 10^{-6}	1.4 x 10^{-6}	8.7 x 10^{-7}	0.20
4-MHA	25/75 Water/MeOH	16.3	5.82 ± 0.10 x 10^{-6}	7.2 x 10^{-7}	5.9 x 10^{-7}	0.21
4-MHA	40/60 Water/MeOH	41.2	4.81 ± 0.09 x 10^{-6}	4.7 x 10^{-7}	4.3 x 10^{-7}	0.19

Table 3-2. Measured values for k', D_m, D_{eff}, $\gamma_s D_s$, and $\frac{\gamma_s D_s}{\gamma_m D_m}$ along with the conditions used for the Hypercarb column (4.6 mm x 100 mm, 3 μm) at 30 °C. D_m values determined by dual-UV measurements and adjusted to 30 °C. D_{eff} determined from plots of the change in spatial variance of all analytes as a function of stop-flow time. Mobile phase compositions were (v/v) mixtures of water/MeOH + 0.1% FA.

Analyte	Mobile phase	k'	D_m (cm^2/s)	D_{eff} (cm^2/s)	$\gamma_s D_s$ (cm^2/s)	$\frac{\gamma_s D_s}{\gamma_m D_m}$
2-MHA	5/95 Water/MeOH	0.81	$1.54 \pm 0.03 \times 10^{-5}$	4.7×10^{-6}	1.5×10^{-6}	0.20
Hippuric acid	5/95 Water/MeOH	1.66	$1.52 \pm 0.03 \times 10^{-5}$	3.25×10^{-6}	8×10^{-7}	0.11
3-MHA	5/95 Water/MeOH	3.75	$1.51 \pm 0.03 \times 10^{-5}$	2.7×10^{-6}	1.5×10^{-6}	0.21
4-MHA	5/95 Water/MeOH	4.81	$1.48 \pm 0.03 \times 10^{-5}$	2.3×10^{-6}	1.3×10^{-6}	0.19
4-MHA	25/75 Water/MeOH	11.1	$9.92 \pm 0.18 \times 10^{-6}$	1.20×10^{-6}	8.8×10^{-7}	0.19
4-MHA	40/60 Water/MeOH	28	$8.42 \pm 0.15 \times 10^{-6}$	1.02×10^{-6}	9.1×10^{-7}	0.23

Table 3-3. Measured values for k', D_m, D_{eff}, $\gamma_s D_s$, and $\frac{\gamma_s D_s}{\gamma_m D_m}$ along with the conditions used for the Hypercarb column (4.6 mm x 100 mm, 3 µm) at 55 °C. D_m values determined by dual-UV measurements and adjusted to 55 °C. D_{eff} determined from plots of the change in spatial variance of all analytes as a function of stop-flow time. Mobile phase compositions were (v/v) mixtures of water/MeOH + 0.1% FA.

Analyte	Mobile phase	R^2	Slope (cm^2/s)	Intercept (cm^2)
Ascorbic acid	50/50 water/MeOH	0.98	4.0×10^{-6}	6.6×10^{-6}
Mandelic Acid	60/40 water/MeOH	0.99	5.9×10^{-6}	6.1×10^{-3}
4-MHA	75/25 water/MeOH	0.99	2.85×10^{-6}	2.5×10^{-3}
4-MHA	85/15 water/MeOH	0.99	2.25×10^{-6}	2.3×10^{-3}
4-MHA	92.5/7.5 water/MeOH	0.99	1.68×10^{-6}	2.7×10^{-3}

Table 3-4. Values for slope, intercept and R^2 for the linear fit of $\sigma_{ax,L}^2$ vs t_{stop} for the peak parking experiments using the C18 BEH column (2.1 mm x 50 mm, 1.7 μm) at 30 °C. Analyte and mobile phase conditions are included. Slope values were changed to units of cm^2/s. Based on Equation 3-21, the slope of these trend lines are equal to $2D_{eff}$. Mobile phase compositions were (v/v) mixtures of water/MeOH + 0.1% FA.

Analyte	Mobile phase	R^2	Slope (cm^2/s)	Intercept (cm^2)
Acetone	5/95 Water/MeOH	0.99	2.5×10^{-5}	1.1×10^{-2}
2-MHA	5/95 Water/MeOH	0.99	5.8×10^{-6}	5.7×10^{-3}
Hippuric acid	5/95 Water/MeOH	0.99	4.0×10^{-6}	7.1×10^{-3}
3-MHA	5/95 Water/MeOH	0.99	3.0×10^{-6}	7.1×10^{-3}
4-MHA	5/95 Water/MeOH	0.99	4.7×10^{-6}	7.3×10^{-3}
4-MHA	25/75 Water/MeOH	0.99	1.4×10^{-6}	7.7×10^{-3}
4-MHA	40/60 Water/MeOH	0.98	9.4×10^{-7}	8.5×10^{-3}

Table 3-5. Values for slope, intercept and R^2 for the linear fit of $\sigma_{ax,L}^2$ vs t_{stop} for the peak parking experiments using the Hypercarb column (4.6 mm x 100 mm, 3 μm) at 30 °C. Analyte and mobile phase conditions are included. Slope values were changed to units of cm^2/s. Based on Equation 3-21, the slope of these trend lines are equal to $2D_{eff}$. Mobile phase compositions were (v/v) mixtures of water/MeOH + 0.1% FA.

Analyte	Mobile phase	R^2	Slope (cm^2/s)	Intercept (cm^2)
2-MHA	5/95 Water/MeOH	0.99	9.5×10^{-6}	6.2×10^{-3}
Hippuric acid	5/95 Water/MeOH	0.99	6.5×10^{-6}	8.1×10^{-3}
3-MHA	5/95 Water/MeOH	0.96	5.4×10^{-6}	1×10^{-2}
4-MHA	5/95 Water/MeOH	0.98	4.6×10^{-6}	1×10^{-2}
4-MHA	25/75 Water/MeOH	0.99	2.4×10^{-6}	7.2×10^{-3}
4-MHA	40/60 Water/MeOH	0.99	2.0×10^{-7}	9.2×10^{-3}

Table 3-6. Values for slope, intercept and R^2 for the linear fit of $\sigma_{ax,L}^2$ vs t_{stop} for the peak parking experiments using the Hypercarb column (4.6 mm x 100 mm, 3 μm) at 55 °C. Analyte and mobile phase conditions are included. Slope values were changed to units of cm^2/s. Based on Equation 3-21, the slope of these trend lines are equal to $2D_{eff}$. Mobile phase compositions were (v/v) mixtures of water/MeOH + 0.1% FA.

3.6 FIGURES

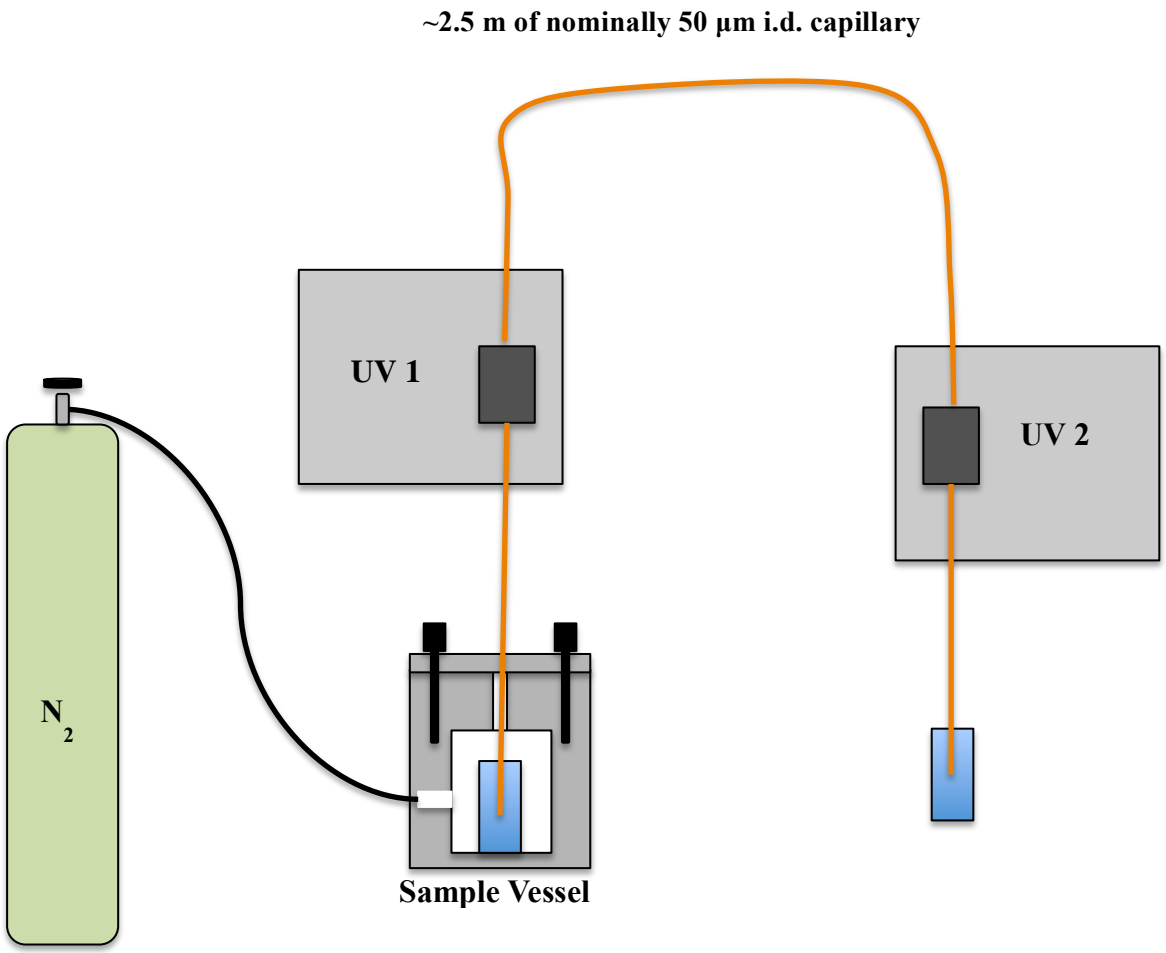

Figure 3-1. Dual UV setup for D_m determination studies. Pressure is applied to the sample vessel, forcing dilute sample in mobile phase through the capillary. D_m calculated using Equations 3-16, 3-17, and 3-18.

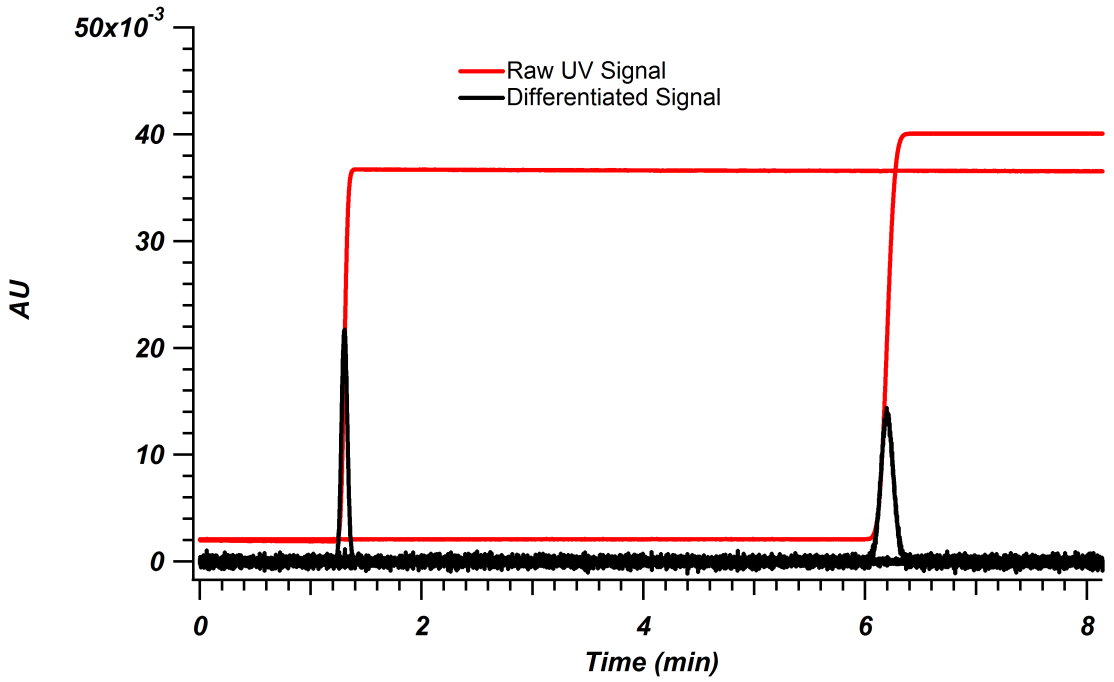

Figure 3-2. Mobile phase diffusion coefficient measurement for 4-methylhippuric acid in 5/95 (v/v) water/MeOH + 0.1% FA performed using a capillary, dual-UV setup. Raw signal (red) is sigmoidal due to analyte fronts passing by the two detectors. These sigmoidal curves are differentiated into Gaussian peaks (black) in order to calculate D_m from the change in variance between the peaks using Equations 3-16, 3-17, and 3-18. UV settings: 240 nm, 0.1 s rise time.

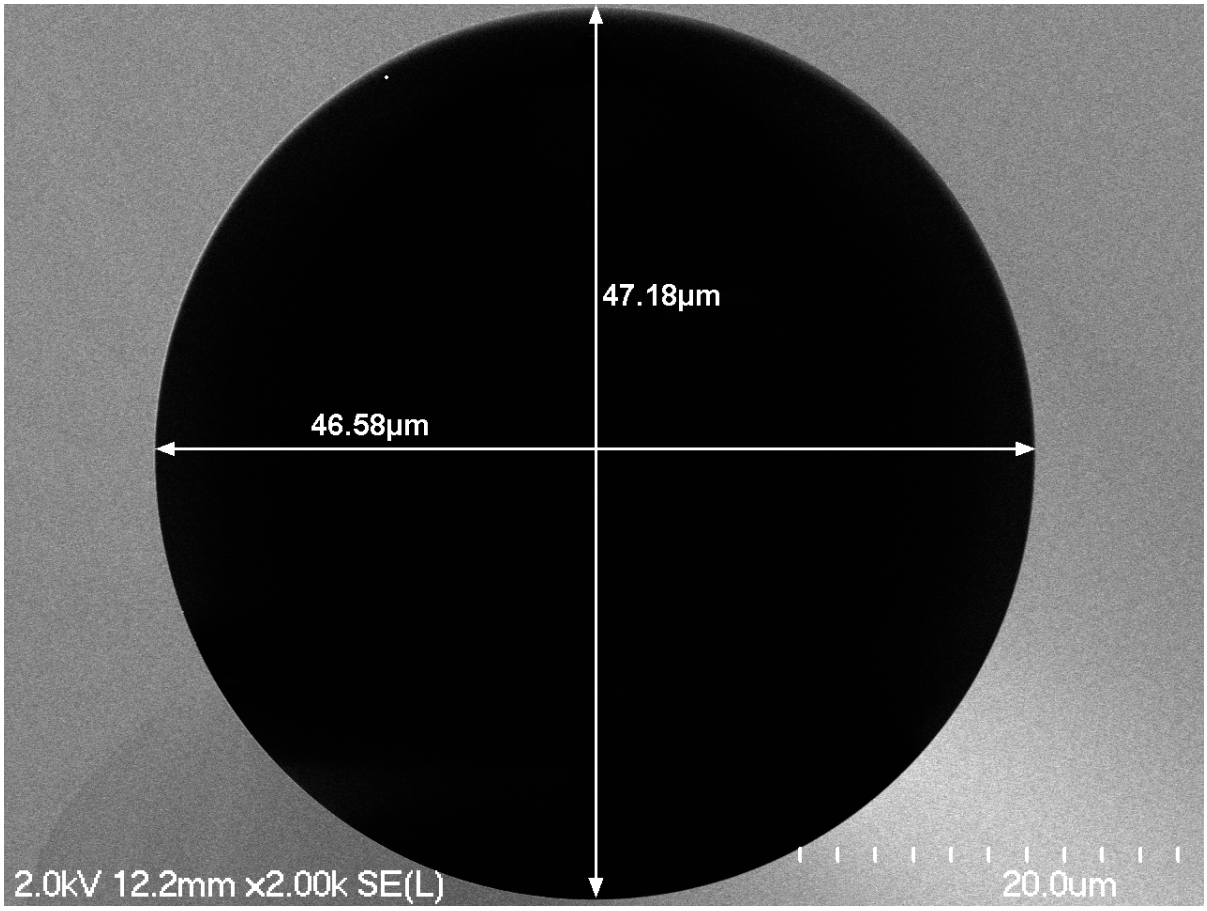

Figure 3-3. SEM image of a section of the nominally 50 µm capillary used for D_m measurements with measured diameter marked for the vertical and horizontal axes. Section was clipped from the end of the capillary, so may not be representative of the diameter between detectors, but allows for comparison to the d_c found via calibration with ferricyanide and ferrocyanide.

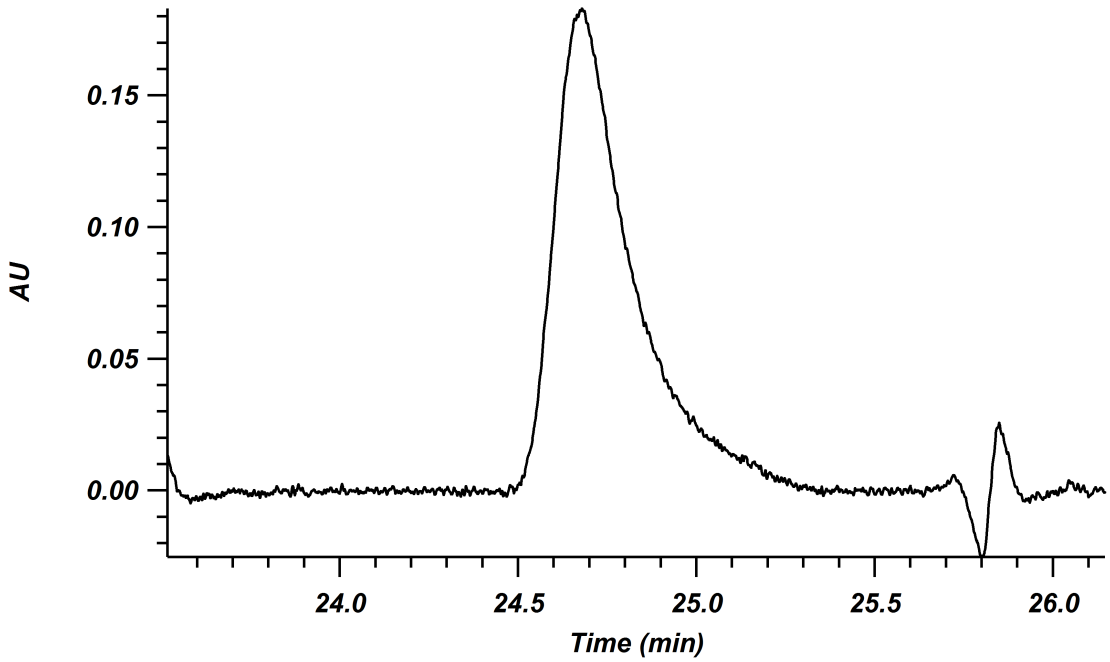

Figure 3-4. Example peak after a peak-parking time of 20 minutes for 2-MHA in 5/95 water/MeOH + 0.1% FA on the Hypercarb column (4.6 mm x 100 mm, 3 µm) at 30 °C. Peak shows significant tailing that could not be accurately fit using the traditional method of ISM.

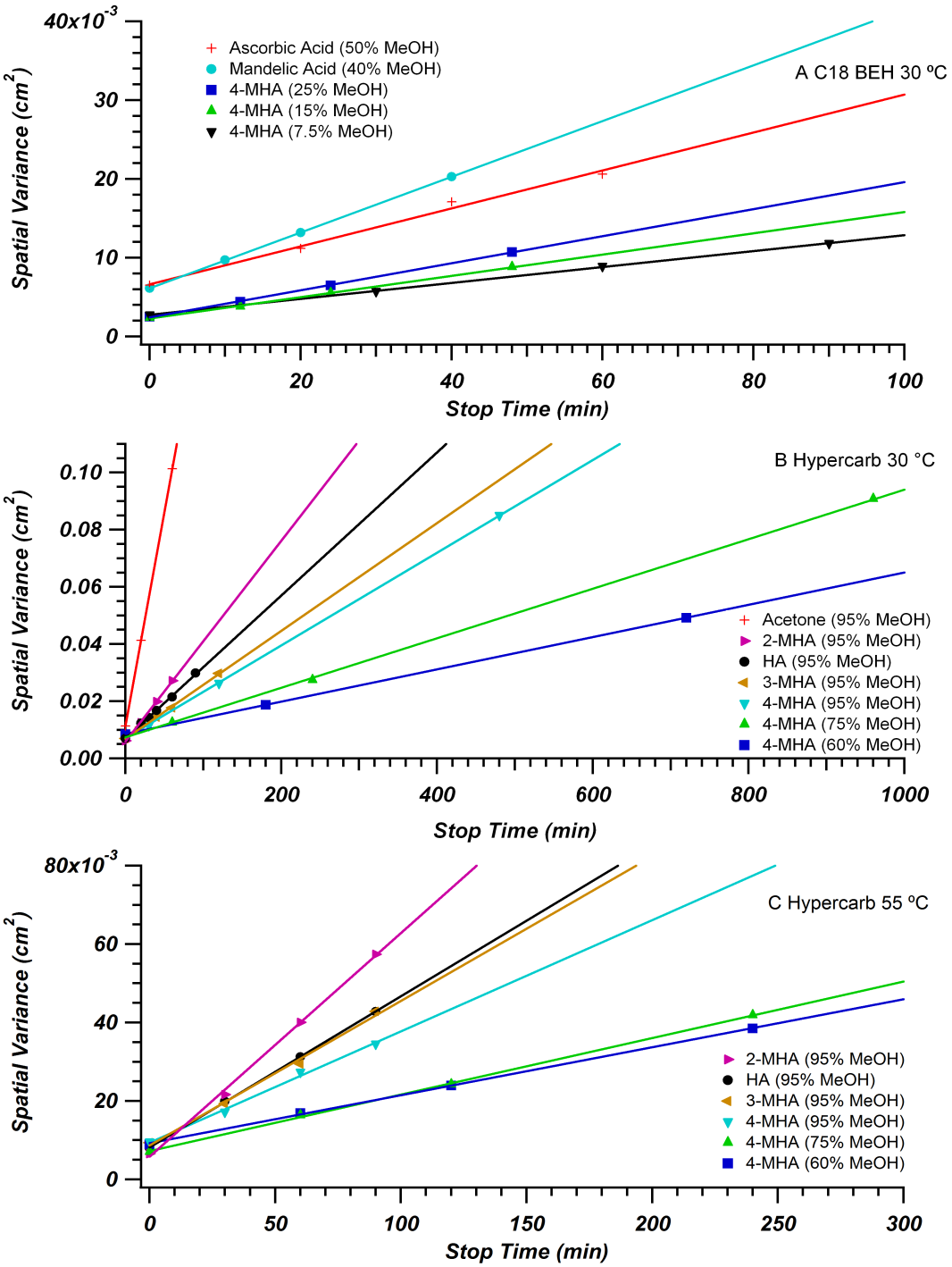

Figure 3-5. Change in spatial variance of all analytes as a function of stop time for C18 BEH at 30 °C (A), Hypercarb at 30 °C (B) and Hypercarb at 55 °C (C). Based on Equation 3-22, the slope of these trend lines are equal to $2D_{eff}$. In order to cover a range of retention factors, different analytes and mobile phase conditions were used.

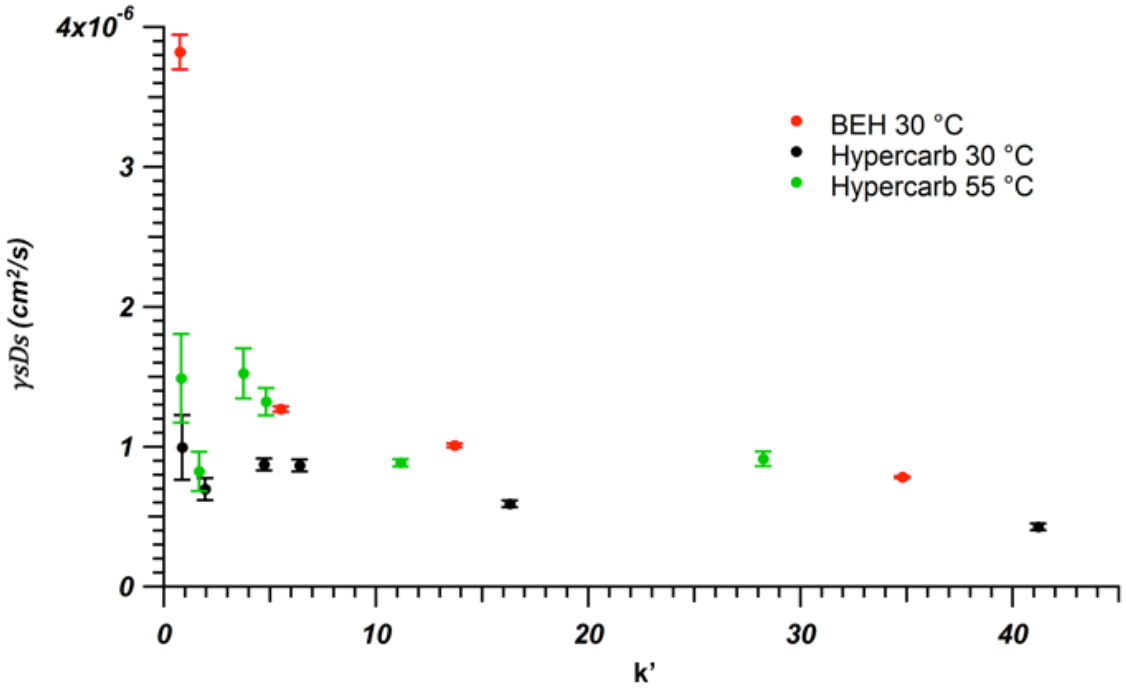

Figure 3-6. Comparison of $\gamma_s D_s$ for C18 BEH at 30 °C (red), Hypercarb at 30 °C (black), and Hypercarb at 55 °C (green) as a function of analyte retention factor. The choice of analyte and mobile phase composition were varied in order to cover a wide range of retention factors for each column. Error bars are shown for each data point. In-depth discussion of error calculation can be found in the Appendix.

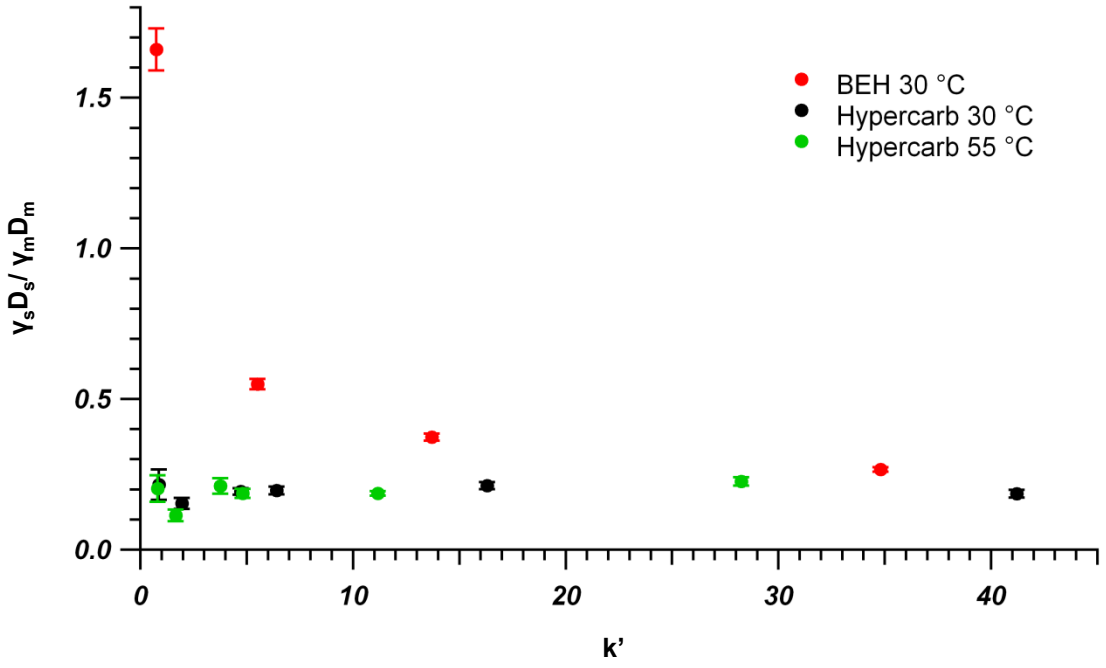

Figure 3-7. Comparison of $\gamma_s D_s / \gamma_m D_m$ as a function of retention factor for C18 BEH (red) at 30 °C, Hypercarb at 30 °C (black) and Hypercarb at 55 °C (green). The choice of analyte and mobile phase composition were varied in order to cover a wide range of retention factors for each column. Error bars are shown for each data point. In-depth discussion of error calculation can be found in the Appendix**.**

REFERENCES

(1) Neue, U. D.; Marchand, D. H.; Snyder, L. R. J. Chromatogr. A **2006**, 1111, 32–39.

(2) Neue, U. D. J. Chromatogr. A **2005**, 1079, 153–161.

(3) Hearn, M. T. W.; Hodder, A. N.; Aguilar, M. I. J. Chromatogr. A **1985**, 327, 47–66.

(4) Neue, U. D. HPLC Columns: Theory, Technology, and Practice; Wiley-VCH, Inc: New York, 1997.

(5) Neue, U. D. Journal of Chromatography A. 2008, 107–130.

(6) Giddings, J. C. Dynamics of Chromatography; Marcel Dekker: New York, 1965.

(7) Miyabe, K.; Matsumoto, Y.; Guiochon, G. Anal. Chem. **2007**, 79, 1970–1982.

(8) Miyabe, K.; Guiochon, G. J. Chromatogr. A **2010**, 1217, 1713–1734.

(9) Miyabe, K.; Guiochon, G. Anal. Chem. **2000**, 72, 1475–1489.

(10) Glasstone, S.; Laidler, K. J.; Eyring, H. The theory of rate processes; 1941.

(11) Miyabe, K. J. Chromatogr. A **2008**, 1194, 184–191.

(12) Miyabe, K. J. Chromatogr. Sci. **2009**, 47, 452–458.

(13) Kaiser, T. J.; Thompson, J. W.; Mellors, J. S.; Jorgenson, J. W. Anal. Chem. **2009**, 81, 2860–2868.

(14) Gerhardt, G.; Adams, R. N. Anal. Chem. **1982**, 54, 2618–2620.

(15) Miyabe, K.; Kobayashi, H.; Tokuda, D.; Tanaka, N. J. Sep. Sci. **2006**, 29, 2452–2462.

(16) Miyabe, K.; Matsumoto, Y.; Ando, N. Anal. Sci. **2009**, 25, 211–218.

(17) Snyder, L. R.; Kirkland, J. J.; Dolan, J. W. Introduction to Modern Liquid Chromatography, 3rd ed.; John Wiley & Sons, Inc.: Hoboken, 2010.

(18) Wilke, C. R.; Chang, P. AIChE **1955**, 1, 264–270.

(19) Li, J.; Carr, P. W. Anal. Chem. **1997**, 69, 2530–2536.

(20) Foley, J. P.; Dorsey, J. G. **1983**, 55, 730–737.

(21) Foley, J. P.; Dorsey, J. G. J. Chromatogr. Sci. **1984**, 22, 40–46.

(22) Stankovich, J. J.; Gritti, F.; Stevenson, P. G.; Guiochon, G. J. Sep. Sci. **2013**, 36, 2709–2717.

(23) Grinias, J. P.; Bunner, B.; Gilar, M.; Jorgenson, J. W. Chromatography **2015**, 2, 669–690.

(24) Rafferty, J. L.; Siepmann, J. I.; Schure, M. R. J. Chromatogr. A **2011**, 1218, 2203–2213.

(25) Jaroniec, M. In Journal of Chromatography A; **1996**, 722, 19–24.

(26) Rybka, J.; Holtzel, A.; Melnikov, S. M.; Seidel-Morgenstern, A.; Tallarek, U. Fluid Phase Equilib. **2016**, 407, 177–187.

(27) Grinias, K. M.; Godinho, J. M.; Franklin, E. G.; Stobaugh, J. T.; Jorgenson, J. W. J. Chromatogr. A **2016**, 1469, 60–67.

CHAPTER 4. USE OF ISOCRATIC RETENTION DATA AND SPREADSHEET MODELING TO PREDICT RETENTION IN GRADIENT ELUTION ON STANDARD BORE HYPERCARB COLUMNS

4.1 Introduction

4.1.1 Fundamentals of Gradient Prediction

As discussed in Chapter 3, gradient separations are a powerful tool for the analysis of complex mixtures. They allow for solutes covering a wide range of k' to be separated in a reasonable timeframe, while maintaining similar peak widths due to gradient compression.[1,2] This improvement comes at the cost of added complexity compared to isocratic methods. Variables such as gradient initial and final conditions as well as gradient slope have a large impact on the separation.[3–5] This added complexity can make the optimization of a gradient separation for a particular sample a time consuming task. Early during the development of the basic principles of gradient theory, the value of the ability to predict gradient elution based on isocratic retention data was clear. Based on the linear solvation strength model, researchers initially thought that $\log k'$ varied linearly with organic content in the mobile phase.[6,7]

$$\log k' = \log k'_{00} - S\varphi \qquad \text{Equation 4-1}$$

Here, S is a term that is specific for the solute and is related to it molecular weight. As discussed previously, this assumption has been shown, using a variety of organic modifiers, to be untrue and that curvature will occur over wide ranges of φ. Multiple empirical equations have been developed over the years, allowing for better fit with experimental retention data.[8–10]

Having a quality fit of isocratic retention data is important, as this allows determination of k' at any mobile phase composition. As the mobile phase composition is changing throughout the gradient, so is the k' of a solute.[7] In order to calculate t_R, it is necessary to relate k' to the time (t) in

the gradient. This allows for the retention at any point in the gradient to be known. By solving the integral form of the fundamental gradient equation, this is possible.[11]

$$\int_0^{t_R} \frac{dt}{k'(t)} = t_m \qquad \text{Equation 4-2}$$

Put simply, this integral describes the condition that once an analyte spends an amount of time in the mobile phase equal to the column deadtime (t_m), it will be eluted off the column. The solutions to this integral allow for incorporation of values associated with retention, initial mobile phase composition, final mobile phase composition, and gradient slope into the calculation of t_R as well as the width of the peak upon elution.[1] The ease by which it is now possible to model gradient separations has allowed for significant improvements in the rate at which optimal chromatographic conditions may be found.

There are several commercially available programs that offer gradient prediction models in order to allow for "dry" experiments, which have the ability the optimize gradients based on either experimental isocratic or gradient data.[12] After a series of baseline experimental separations are performed to define the experimental space, the software allows parameters (pH, temperature, and gradient conditions depending on input separations) to be manipulated via modeling, allowing rapid determination of optimal conditions. Although these programs offer a wide range of functionalities to study the effect of experimental parameters individually, or in combination, they can be quite expensive. Recently, a study by Gilar *et al*. demonstrated a model for the prediction and visualization of retention times and peak widths for gradient separations using large volume injections on microfluidic devices.[4,13] Although this approach it not capable of the comprehensive optimization like commercial software, it had the benefits of only requiring isocratic retention data and also being widely available as a downloadable spreadsheet.

4.1.2 Gradient Separations using Porous Graphitic Carbon

Gradient separations with PGC columns have been used successfully in a number of methods analyzing for polar solutes.[14–18] These separations are based on change of organic content in aqueous

mobile phases, similar to reversed phase gradients. Although these studies assume that PGC acts as a traditional reversed phase system, a comparison to models under gradient conditions has not been shown to date. Confirmation of Hypercarb acting within the limits of traditional gradient models would open up the door to rapid optimization of gradient parameters for the analysis of complex mixtures.

Gradient elution has also presented some difficulties with PGC columns. Several publications have suggested that column "aging" occurs, in which retention gradually decreases as the column is used more.[16,19] Due to the high level of retentivity of PGC, this has often been attributed to the susceptibility of PGC to contamination, thus reducing the ability for solutes to interact with the PGC surface. In order to counteract contamination, washing steps involving strong organic solvents, acids/bases and column backflushing have been used.[16,17,19] Other studies have claimed that this loss of retention is due to slow re-equilibration of the column after a gradient run.[14,20] It is believed that the redox properties are to blame for the observed slow re-equilibration of PGC columns after gradient separations, ultimately leading to repeatability problems from run-to-run. As we have seen, any changes in redox state between runs can lead to varying retention times. A number of treatment methods have been developed based upon reaching a repeatable redox state before subsequent runs are performed.[16,20,21] These processes require additional steps that are otherwise unnecessary for traditional reversed phase columns, adding significantly to the total analysis time for a series of samples, while variability has still been seen to occur.

4.2 Experimental Methods

4.2.1 Chemicals

For gradient separations, HPLC grade methanol (MeOH) and acetone were used as received from Fisher Scientific (Waltham, MA). Deionized water was obtained using a Barnstead Nanopure ultrapure water system (Dubuque, IA). For the purpose of mobile phase modification, formic acid (LC-MS grade), L-ascorbic acid and sodium sulfite were used as received from Sigma Aldrich (St. Louis, MO). The model metabolite test mixture, discussed previously, was used here and contained

mandelic acid (MA), hippuric acid (HA), 2-methylhippuric acid (2-MHA), 3-methylhippuric acid (3-MHA), and 4-methylhippuric acid (4-MHA), all of which were used as received from Sigma Aldrich

4.2.2 Instrumentation, Chromatographic Columns and Gradient Conditions

The Acquity UPLC system used to perform gradient separations on Hypercarb and C18 BEH columns was described previously in Chapter 2, but will be summarized here in short. A 4.6 mm x 100 mm column packed with 3 µm Hypercarb from Thermo Fisher Scientific (Waltham, MA), along with a 2.1 mm x 50 mm column packed with 1.7 µm BEH particles (Waters Corp, Milford, MA) were used to study the gradient separations of model metabolites. A Waters Acquity UPLC with photodiode array (PDA) detection was used for all experiments. Columns were kept at 30 °C and 5 µL injections were used for all experiments. The Acquity Binary Solvent Manager was used to generate and deliver gradients using mobile phase A (water + 0.1% FA) and mobile phase B (MeOH + 0.1% B) unless otherwise noted. Going forward, gradient mobile phase methods will be solely referred to by their change in MeOH content, as this is the most important factor describing their design. C18 BEH separations were performed using two gradients: the first from 5-50% MeOH in 30 minutes, and the second being 5-30% MeOH in 30 minutes. Both of these were at a flow rate of 0.3 mL/min. Hypercarb gradient conditions were 5-95% MeOH in 90 minutes at 1 mL/min. Redox washing methods used for Hypercarb gradients will be discussed as necessary in the results. For gradients containing sodium sulfite or ascorbic acid, the additive was dissolved in both mobile phases A and B, although it was necessary to add a small amount of water to mobile phase B to allow for dissolution of the additives. In these cases, mobile phase B was 5/95 water/MeOH + 0.1% FA with the desired reducing agent added.

Before modeling of the gradient separations can be performed, it was vital to know the dwell volume of the Acquity system used. The dwell volume, or gradient delay volume, is the system volume between where the gradient is produced and the head of the column.[22] To measure the dwell volume, a gradient was programmed to go from 100% mobile phase A (water) to 100% mobile phase B (water + 0.1% acetone), in 5 minutes. The column was removed, and was replaced by a short length

of 50 μm i.d. open capillary tubing (Polymicro Technologies, Inc Phoenix, AZ) connecting the injector and detector in order to provide sufficient backpressure for the pumps. This capillary tubing contributes a negligible volume and will not throw off the measurement of the dwell volume. Using the PDA, acetone response was tracked over the course of the gradient at 265 nm. Measurements of dwell volume were made using two different flow rates, 50 μL/min and 25 μL/min, each in triplicate.

4.2.3 Modeling of Gradient Separations

In order to investigate the consistency of Hypercarb retention with gradient models, the prediction spreadsheet developed by Gilar *et al.* was used to compare predicted gradient chromatograms to experimental chromatograms using the same conditions.[4,13] Complementary models were also produced using C18 BEH data. This gradient prediction model was originally developed for studying the effect of gradient conditions on peak width in microfluidic separations. These separations normally involve injecting sample volumes that are much larger than the column volume, which can lead to volume overload for lightly retained analytes. Since the studies being done here are with standard bore columns and relatively small injection volumes, the spreadsheet is being used to solely predict retention times. The details associated with the development of the model and calculations used to predict chromatograms are beyond the scope of the work presented here, as our goal is only to compare the predicted and experimental gradient retention times to confirm the expected behavior of PGC columns under gradient conditions. A qualitative overview of the model workflow will be provided here, but if the reader is interested in a more detailed discussion of the predictive model, they are recommended to read a set of papers discussing its development and use.[4,13]

The model simulates an injected band using two infinitesimally small zones, which define the front and rear of an injected solute plug, traveling through the column. The modeling sheets require a set of variables for column parameters, chromatographic conditions, instrumental parameters and isocratic retention data for the species being separated (in this case the standard metabolite mixture) in order to calculate the elution times. These parameters are then used in an iterative calculation to

predict retention times according to the following procedure. First, the mobile phase strength is calculated at the initial band position (column inlet). This mobile phase strength is then used to calculate the k' of the analyte under those conditions, and the velocity of the analyte band. Using the set time between modeled points, a distance traveled can be found. This distance designates a new position on the column. The calculation cycle continues iteratively, until the zone position reaches the outlet of the column. This process is performed for both the front and rear zones, with the time between zones reaching the outlet defining the peak width, and the average of the times being the retention time. The modeled times for each analyte, were then used in a visualization spreadsheet, to produce the predicted chromatogram for the conditions used.[4,13]

4.3 Results and Discussion

4.3.1 Modeling of C18 BEH and Hypercarb Gradients

To gain better understanding of Hypercarb's use with traditional gradient separation models, as well as gauge the effect that the redox state of the surface has on gradients, comparative predicted separations were needed. Before modeling of gradients can be properly performed it is necessary to know the system dwell volume (V_{dwell}). This volume accounts for contributions from not only connecting tubing, but also any other in-line components such as valves or mixers that occur between the point of gradient generation and the column inlet. It is important to know this volume as it varies between commercial systems, and leads to time delays between gradient generation and when the solvent reaches the column itself, ultimately impacting the final retention times of solutes. This value is not required for isocratic separations, as the mobile phase composition is not changing over time. To determine V_{dwell}, a linear gradient from 100% mobile phase A (water) to 100% mobile phase B (water + 0.1% acetone) in 5 minutes was performed. Using the PDA on the Acquity, acetone response was tracked over the course of the gradient. By measuring the time it takes for the acetone intensity to reach 50% of its max height ($t_{1/2}$), it is possible to calculate the delay time (t_{delay}) by:[23]

$$t_{delay} = t_{1/2} - \frac{t_G}{2} \qquad \text{Equation 4-3}$$

where t_G is the length of the gradient (5 minutes in this case). When the signal is at 50% of its max intensity, the gradient is half way completed. As a linear gradient was used, the beginning of the gradient will have been first detected at $\frac{t_G}{2}$ earlier than $t_{1/2}$. t_{delay} can then be used to calculate the dwell volume using the flow rate (F).

$$V_{dwell} = t_{delay} * F \qquad \text{Equation 4-4}$$

Figure 4-1 shows an example gradient used to calculate this volume. By finding the point where the intensity is at half of its maximum and tracing down to the x-axis, $t_{1/2}$ is found. V_{dwell} is then calculated using Equations 4-3 and 4-4. Measurements made at both 25 µL/min and 50 µL/min were in agreement with a calculated V_{dwell} of 80 µL.

Modeling calculations are based on an extrapolation of isocratic retention data, allowing knowledge of the retention at any point in the gradient based the mobile phase conditions. For this reason, k' data for the standard metabolites in a variety of water/MeOH + 0.1% FA composition mobile phases was needed. This k' data, which was previously discussed in Chapter 2, is known to often deviate from linearity over large ranges of organic content. To account for this curvature, the model I will be using requires the data is fit with an alternative equation to that previously discussed in Chapter 2 (Equation 2-8).[4,13]

$$\log k' = \log k'_{00} - \frac{B_{sol}\varphi}{1 + a_{curve}\varphi} \qquad \text{Equation 4-5}$$

Although both Equations 2-8 and 4-5 allow for fit of non-linear retention data, Equation 4-5 was used here as the prediction model was developed using this form. Plots of this retention behavior for standard metabolites on Hypercarb and C18 BEH columns can be seen in Figure 4-2. The fit parameters for the model metabolites on Hypercarb and C18 BEH can be seen in Tables 4-1 and 4-2, respectively. As Equation 4-5 fits the curvature of the retention data differently than Equation 2-8, it led to differing values k'_{00} than were reported in Chapter 2.

As the prediction model was originally developed for large volume injections on low volume microfluidic columns, gradient separations with a C18 BEH column were modeled in order to prove

that the spreadsheet still accurately predicts retention times on larger bore columns. Using the metabolite retention parameters (Table 4-2), the column dimensions, instrument parameters, and gradient conditions for C18 BEH, the model simulates two zones, equivalent to the front and rear of the injected band for each analyte, traveling down the column as the gradient progresses. The model parameters used for the 5-50% and 5-30% MeOH gradients can be seen in Table 4-3. For all modeled chromatograms, the total porosity of the column (ε_t), or the fraction of the empty column volume that is filled with liquid, was set such that the predicted dead time was equal to the experimental deadtime for the column being used. Figure 4-3 shows the predicted gradient chromatograms for both the 5-50% MeOH (A) and 5-30% MeOH (B). The predicted retention times for C18 BEH gradients can be found in Table 4-4. It is important to note that the prediction shows a single peak for each compound even though the model simulates a zone for the front and rear of the peak, individually. This observation is due to injecting such a small volume (5 µL) in comparison to the column volumes (0.124 mL and 1.26 mL for BEH and Hypercarb, respectively). Also, as the model was designed to predict the compression of large volume injections, it assumes that no further band broadening processes occur, leading to the sharp peaks seen here when small injection volumes relative to the column volume are used. The predicted chromatograms show good resolution between the MA, HA and 2-MHA, but show the 4-MHA and 3-MHA peaks overlapping significantly. This co-elution is not surprising with how similar the isocratic retention data for these analytes are over the range of MeOH compositions (Figure 4-2 B). With little difference between retention at any mobile phase conditions, it is impossible to fully separate these compounds even with the shallower gradient that goes from 5-30% MeOH in 30 minutes.

By substituting in the Hypercarb column dimensions, retention data (Table 4-1), and gradient conditions, the modeled chromatogram in Figure 4-4 was produced for the 5-95% MeOH gradient in 90 minutes. The parameters used for the model can be seen in Table 4-5. The predicted retention times for Hypercarb gradients can be found in Table 4-6. It is important to note that since the isocratic retention data was obtained using AA treatment steps, the predicted retention times will reflect that of

a reduced PGC surface. With the significantly increased metabolite retention on Hypercarb, the gradient had to extend to much stronger mobile phase conditions than were needed for C18 BEH. The gradient also occurs over a much longer time than is normally used for a column of these dimensions. This change is due to the fact that, in our experience, standard bore Hypercarb columns were not very stable. Rapid changes or big jumps in water/MeOH + 0.1% FA composition caused the bed to destabilize and gap. Again, the predicted peaks look very narrow due to the small injection volume, and the spreadsheet assuming no further band spreading beyond the injection contribution. All of the peaks in the standard metabolite sample are fully resolved on the PGC column. Even though many different redox washing conditions will be discussed for the Hypercarb gradients, all of them are assuming identical retention data and gradient conditions, so only a single model was needed for comparison.

4.3.2 Gradient Separation of Standard Metabolites on C18 BEH and Hypercarb

Gradient separations on the C18 BEH column were performed using two different gradients: one going from 5-50% MeOH in 30 minutes and the other from 5-30% MeOH in 30 minutes. These experimental chromatograms are shown in Figure 4-5. All of the peaks come out in the first half of both gradients, in mobile phase with a high water content. As predicted, the last eluting solutes, 3-MHA and 4-MHA, overlap greatly. These two points display the problem that traditional C18 reversed phase have with separating analytes like these small metabolites as well as structurally similar compounds. The analytes do not interact strongly with the stationary phase, limiting the retention and in turn causing the analytes to elute in a very small separation window with regard to mobile phase strength. This lack of retention becomes a problem when separating complex, biologically relevant samples for metabolomics studies. The retention times for experimental chromatograms as well as percent difference with the predicted times can be seen in Table 4-4. Since the 4-MHA and 3-MHA peaks are not well resolved in the experimental data, only one of them was used for comparison to the model. Since the 4-MHA elutes earlier than 3-MHA, its retention time was chosen as the maximum of the latest eluting peak. 3-MHA was seen as a slight shoulder on the

trailing side of the peak, but its retention time could not be measured. The predicted and experimental retention times line up well for both sets of conditions, with the percent difference for all metabolites being below 6%. This agreement shows that the model has been successfully adapted for use to predict gradient separations on larger bore columns.

Hypercarb exhibits some unique retention properties that are not present with C18 bonded silica stationary phases, apparent based on the significantly increased retention of metabolites when compared to C18 BEH, as well as the redox properties of the surface that necessitated the use of a reducing agent to give consistent retention from day-to-day (Chapter 2). One thing that was not clear was how these particles would perform under gradient conditions and if they would be well modeled with the same prediction methods. Based on the retention of the metabolites on Hypercarb, it was clear that the gradients used would require going to high organic content when compared to the C18 BEH gradients. Since the isocratic retention data was obtained using AA treatments, it was necessary to use a reducing agent to treat with the Hypercarb particles before gradient separations were performed. Initially, the column was treated with the same procedure used previously. This treatment involved slowly flowing with 95/5 water/MeOH + 10 mM AA + 0.1% FA for 90 column volumes, before being flushed off with initial gradient conditions lacking AA (30 column volumes). Then three sequential gradients were run with a 90 minute gradient from 5-95% MeOH. These runs can be seen in Figure 4-6. A summary of the measured retention times and percent difference with the model for all redox treatments on Hypercarb can be seen in Tables 4-6 and 4-7, respectively. Similar to the isocratic data, the retention times tend to drift outwards as the run number increases. This drift, along with the significant difference between experimental and predicted retention times, suggest that the initial AA wash was not sufficient to keep the redox state of the particles stable over the course of the sequential runs. Also, even in the first run, where the surface was most recently treated with AA, the retention times are still significantly larger than predicted by the model. This could be due to either natural oxidation that occurred over the course of the gradient due to dissolved oxygen in the mobile phase (similar to what is seen isocratically) or possibly a sign that the change in mobile phase

compositions somehow impacts the extent/rate of oxidation.

With this in mind, it was thought that adding an AA treatment step between each gradient run would keep a more stable redox state and in turn stable, as well as shorter, retention times. Figure 4-7 shows two gradient separations, with identical gradient conditions as Figure 4-6, but now with a 20 column volume AA wash, and subsequent 20 column volume flush before each run, instead of a single treatment before a series of runs. The large signal seen at the beginning of the runs was due to residual AA being washed off the column since the flushing step was kept short in order to allow minimal oxidation to occur before the gradients were run. Due to the large baseline shifts produced by AA, many of the chromatograms going forward will be included without baseline subtraction in order to give the best picture of the overall retention times. This washing step should allow any of the particle surface that had been oxidized over the course of the previous gradient, to be reduced again for the following run. These chromatograms show more repeatable retention times compared to the sequential runs without AA treatment between, but the peaks were still far from the predicted retention times (all metabolites with ≥ 15 % difference) suggesting that surface oxidation is still occurring. This level of retention shift seems inconsistent with dissolved oxygen being the sole cause of surface oxidation over the course of the gradient. Previously, retention times of the later eluting peaks (3-MHA and 4-MHA) were seen to drift by ~15% over the course of 4 sequential isocratic runs (each 40 minutes long, totaling 160 minutes) (Figure 2-2 B) and this was believed to be due solely to oxidation by O_2 in the mobile phase. Since even larger changes in retention time shifts were seen over the course of a 90 minute gradient, this could possibly be a sign that the change in mobile phase compositions somehow impacts the extent/rate of oxidation in addition to the natural oxidation that occurs with flowing mobile phase, but there was no clear way to distinguish between these possible causes.

Since it was still suspected that oxidation occurring over the course of the gradient runs was leading to the large difference between experimental and predicted retention times, a way to mitigate that effect was needed. It was thought that using a gradient with AA in the mobile phase would give

the best results. Since there would be AA present at all times throughout the gradient, any sites that become oxidized over the course of the gradient will hopefully be reduced immediately by AA. As AA absorbs strongly in the UV region, it was necessary to use much lower concentrations than previously used for treatment steps in order to allow for detection of the metabolites. Figure 4-8 shows a 90 minute gradient separation of metabolites from 5-95% MeOH with 100 uM AA in the mobile phase. One thing to notice is the large peak seen in the early part of the run. This is due to AA buildup on the column when flushing with the initial conditions of the gradient. Since the AA is lightly retained, a large concentration of it elutes as higher organic content starts to reach the column, leading to this peak. This peak also obscured detection of the MA peak. The retention times are repeatable and match the predicted gradient much better than the previous methods, with differences less than 8% for the detected compounds, suggesting that the addition of some amount of AA to the mobile phases was successful in stabilizing the surface redox state over the course of the run.

In order to investigate the effect that background AA concentration has on retention, gradient separations were performed with AA concentrations of 50 μM and 1 μM in the mobile phase. The chromatograms can be seen in Figures 4-9 and 4-10 for the 50 μM and 1 μM conditions, respectively. By reducing the AA concentration to 50 μM the AA peak in the beginning of the run is small enough to allow detection of the MA peak. Similar to the 100 μM AA runs, these retention times are generally in good agreement with the predicted retention times, with the exception of MA. It is unclear as to why this significant difference was seen. The isocratic retention data for MA is known across the full range of MeOH content, so the model should be accurate, but the peak is still off by 16%. When using 1 μM AA in the mobile phase, the retention times were significantly further out in time, and increased from run-to-run. This observed retention shift suggests that such a small level of AA could not keep up with the rate of PGC surface oxidation. It should also be noted that AA is unstable and will react while just sitting in the mobile phase container with the presence of oxygen. With such a small concentration of AA it is possible that a significant amount of the AA was consumed by oxidation in the reservoir, which would also limit the ability to reduce the surface.

The inherent drawback of using high levels of AA in the mobile phase for the gradient separations is that a large background peak was consistently seen in the first 20 minutes of each run. Another compound that has previously been used as a reducing agent for PGC is sodium sulfite.[24] Sodium sulfite also has the benefit of being UV transparent at the wavelengths used for detection. Similar to the runs with AA in the mobile phase, 90-minute gradient runs from 5-95% MeOH were performed, now with 500 μM sodium sulfite in both mobile phases. These chromatogram can be seen in Figure 4-11. The sodium sulfite provides clearer chromatograms in the early portion due to its UV transparency. When looking at the retention times, they are at slightly longer times than the gradients with high concentrations of AA in the mobile phases. This shift to longer retention times, along with the fact that the concentration of sodium sulfite was significantly higher than that of the AA comparisons, suggest that sodium sulfite is less effective as a reducing agent than AA for the redox sites on Hypercarb.

A summary of the comparisons of all experimental and modeled Hypercarb gradient retention times can be seen in Tables 4-6 and 4-7. It should be noted again that the modeled retention times are based off of isocratic k' data, where redox treatment was used. This data, once again, makes clear how important it is to control the redox properties of the particles. As the reducing agent treatment process gets more rigorous, leading up to it being present in the mobile phase at high levels, the experimental times become closer to the predicted times. Under those conditions, the experimental retention times of all metabolites, except for MA, line up relatively well with the modeled times.

4.4 Conclusions

Now that it is known that Hypercarb will provide sufficient retention to allow for injection focusing and a low enough level of surface diffusion for long gradient separations, we needed to investigate how it performs under gradient conditions, and if it could be modeled with traditional methods. With knowledge of the retention of standard metabolites over a range of mobile phase compositions, it was possible to use a gradient prediction model to allow comparison to experimental gradients. The gradient model used was adapted from a model for large volume injections on

microfluidic columns. Although the chromatographic conditions used here are significantly different, the model still was able to accurately predict the model metabolite retention times on an analytical bore C18 BEH column.

Due to the significantly higher retention of metabolites on PGC, gradients needed to go to much higher levels of MeOH to elute the solutes compared to C18 BEH. The gradient method used here was 5-95% MeOH in 90 minutes. It was found that the surface redox state played a large role in the overall retention times found using gradient separations. This is to be expected as the same observation was seen using isocratic separations. Also, as the predicted retention times were based on k' data using AA treatment, it was expected that any shift in the surface redox state would manifest as changes in retention time from the predicted. When AA washing steps are only performed before the separations, the experimental retention times are significantly longer than predicted. This is in line with the trend seen previously where surface oxidation occurred over time when flowing mobile phase through the column. In order to counteract the surface oxidation occurring over the course of the gradient, reducing agent was added to the gradient mobile phases so that it was present at some level throughout the whole run. It was thought that the reducing agent could prevent oxidation or quickly reduce any sites being oxidized over the course of the runs. Conditions using 100 μM and 50 μM AA in the mobile phase showed retention times that were, with the exception of MA, in good agreement with the predicted retention times. This confirmed that PGC operates as expected under gradient conditions, but with the added complication of redox variability. This study reinforces the assertion that the redox properties of Hypercarb play a major role in the quality and repeatability of the separations in both isocratic and gradient modes. The ability to successfully model Hypercarb gradients accurately means that optimum conditions for gradient separations could be quickly developed, assuming that the isocratic k' data for the analytes in question are known.

4.5 TABLES

	MA	2-MHA	HA	3-MHA	4-MHA
$log\ k'_{00}$	1.68	3.57	4.49	5.50	5.84
a_{curve}	0.69	1.21	2.14	1.91	2.15
B_{sol}	4.30	8.46	13.68	14.53	16.42

Table 4-1. Fit parameters for retention of standard metabolites when data from Figure 4-2 (A) was fit with Equation 4-5 for Hypercarb column (4.6 mm x 100 mm, 3 μm). Retention data measured over a range of water/MeOH + 0.1% FA mobile phases. This data is used for modeling of gradient separations. Column temperature: 30 °C. Flow rate: 1 mL/min.

	MA	HA	2-MHA	3-MHA	4-MHA
$log\ k'_{00}$	1.10	1.35	1.49	1.92	1.92
a_{curve}	0.11	0.52	0.12	0.26	0.31
B_{sol}	3.43	4.89	4.09	4.88	5.03

Table 4-2. Fit parameters for retention of standard metabolites when data from Figure 4-2 (B) was fit with Equation 4-5 for C18 BEH column (2.1 mm x 50 mm, 1.7 μm). Retention data measured over a range of water/MeOH + 0.1% FA mobile phases. This data is used for modeling of gradient separations. Column temperature: 30 °C. Flow rate: 0.3 mL/min.

	Gradient	
	5-50% MeOH	5-30% MeOH
Column i.d. (mm)	2.1	2.1
Column Length (mm)	50	50
Column Total Porosity (ε_t)	0.715	0.715
Initial Grad Conditions (%MeOH)	5	5
Gradient Span (%MeOH)	45	25
Gradient Time (min)	30	30
Injection Volume (µL)	5	5
Sample Solvent (%MeOH)	5	5
V_{dwell} (µL)	80	80

Table 4-3. Column dimensions, gradient conditions, and instrumental parameters used to model C18 BEH gradients. The gradients being modeled were 5-50% MeOH and 5-30% MeOH, both in 30 minutes. Total column porosity was set such that the predicted deadtime was equal to the experimental deadtime. Data was used in conjunction with standard metabolite retention parameters from Table 4-2 to model C18 BEH gradients.

Solute	5-50% MeOH Gradient			5-30% MeOH Gradient		
	Predicted t_R (min)	Measured t_R (min)	% Difference	Predicted t_R (min)	Measured t_R (min)	% Difference
MA	3.43	3.59	+4.7	3.63	3.84	+5.8
HA	4.41	4.47	+1.4	4.88	5.04	+3.3
2-MHA	5.93	6.00	+1.2	6.74	7.03	+4.3
4-MHA	9.35	9.21	-1.5	11.74	11.73	-0.1
3-MHA	9.51	Not measured	Not measured	11.93	Not measured	Not measured

Table 4-4. Comparison of predicted and experimentally measured retention times for C18 BEH gradient separations. Model chromatogram can be seen in Figure 4-3. Experimental separations (Figure 4-5) were collected using a C18 BEH column (2.1 mm x 50 mm, 1.7 µm) and gradient conditions of 5-50% MeOH as well as 5-30% MeOH, both in 30 minutes. Due to the overlapping retention times of 4-MHA and 3-MHA, only a single retention time was used for the peak. As 4-MHA elutes earlier than 3-MHA, its retention time was chosen as the maxima of the latest eluting peak. Column temperature: 30 °C. Flow rate: 0.3 mL/min. Retention times used for calculating % difference were the average of multiple identical runs. % difference $= \frac{t_{expt}-t_{pred}}{t_{pred}}$, where t_{expt} is the experimentally measured retention time and t_{pred} is the predicted retention time.

	5-95% MeOH Gradient
Column i.d. (mm)	4.6
Column Length (mm)	100
Column total porosity (ε_t)	0.76
Initial Grad Conditions (%MeOH)	5
Gradient Span (%MeOH)	90
Gradient Time (min)	90
Injection Volume (µL)	5
Sample Solvent (%MeOH)	5
V_{dwell} (µL)	80

Table 4-5. Column dimensions, gradient conditions, and instrumental parameters used to model the Hypercarb gradient. The gradients being modeled were 5-95% MeOH in 90 minutes. Total column porosity was set such that the predicted deadtime was equal to the experimental deadtime. Data was used in conjunction with standard metabolite retention parameters from Table 4-1 to model Hypercarb gradients.

Solute	Predicted t_R (min)	Average Experimentally Measured t_R (min)					
		Sequential Injections	AA treatment between runs	100 µM AA in MP	50 µM AA in MP	1 µM AA in MP	500 µM sulfite in MP
MA	18.11	23.4	22.2	Not measured	21.0	24.9	22.0
2-MHA	46.06	54.3	52.8	49.7	50.1	55.4	51.2
HA	53.02	64.4	61.2	55.4	55.7	65.7	58.6
3-MHA	70.40	85.1	81.1	72.5	72.7	85.6	76.0
4-MHA	73.81	89.5	85.1	75.6	75.9	89.9	79.3

Table 4-6. Predicted and experimentally measured retention times for Hypercarb gradient separations. Model chromatogram can be seen in Figure 4-4. Parameters used for modeling can be found in Table 4-5. Experimental separations were collected using a Hypercarb column (4.6 mm x 100 mm, 3 µm) and a gradient of 5-95% MeOH in 90 minutes at 30 °C and 1 mL/min. Redox washing conditions are labeled within the table. Retention times were the average of multiple identical runs.

Solute	% difference between predicted and measured retention times					
	Sequential Injections	AA treatment between runs	100 μM AA in MP	50 μM AA in MP	1 μM AA in MP	500 μM sulfite in MP
MA	+29.5	+22.6	Not measured	+16.0	+37.2	+21.8
2-MHA	+18.0	+14.6	+7.8	+8.7	+20.2	+11.1
HA	+21.6	+15.5	+4.6	+5.1	+24.0	+10.5
3-MHA	+21.0	+15.2	+3.0	+3.3	+21.7	+8.0
4-MHA	+21.3	+15.3	+2.5	+2.9	+21.9	+7.4

Table 4-7. Percent difference of predicted and experimentally measured retention times for Hypercarb gradient separations. Model chromatogram can be seen in Figure 4-4. Experimental separations were collected using a Hypercarb column (4.6 mm x 100 mm, 3 μm) and a gradient of 5-95% MeOH in 90 minutes at 30 °C and 1 mL/min. Redox washing conditions are labeled within the table. Retention times used for calculating percent difference were the average of multiple identical runs. % difference $= \frac{t_{expt} - t_{pred}}{t_{pred}}$, where t_{expt} is the experimentally measured retention time and t_{pred} is the predicted retention time

4.6 FIGURES

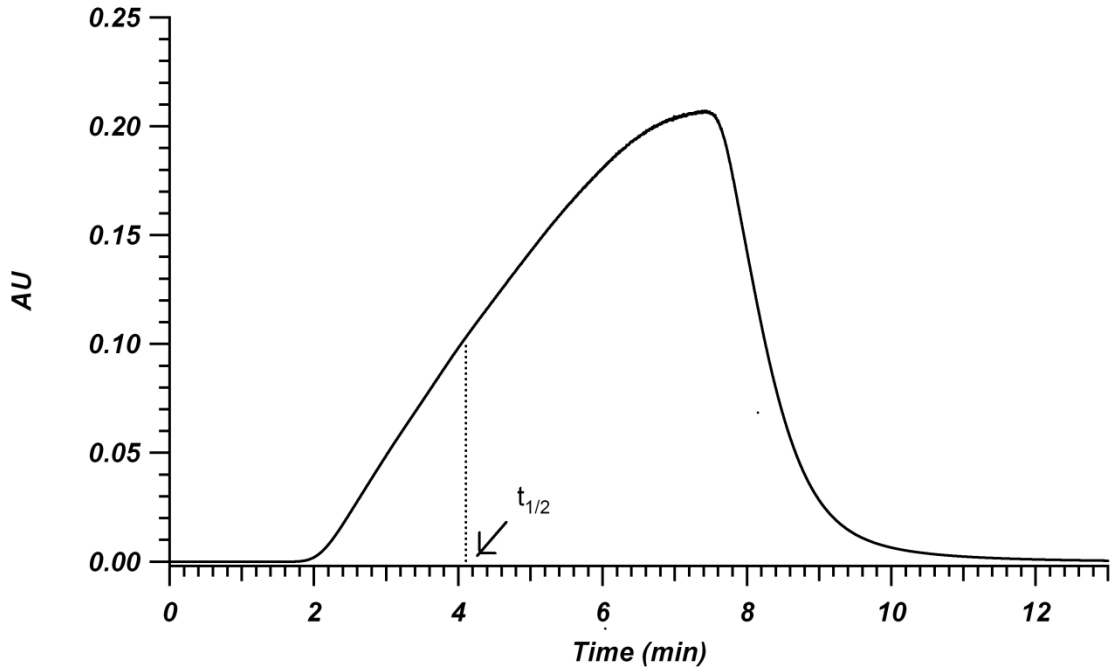

Figure 4-1. Gradient chromatogram used to determine the system dwell volume. Gradient went from 100% mobile phase A (water) to 100% mobile phase B (water + 0.1% acetone) in five minutes. A short length of capillary was used to connect the injector and detector to minimize any extra volume contributions. Flow rate was 50 µL/min. To calculate V_{dwell}, it was necessary to find the time at which the acetone intensity reached 50% of its maximum ($t_{1/2}$) for use with Equations 4-3 and 4-4. $t_{1/2}$ is marked on the plot (4.09 minutes).

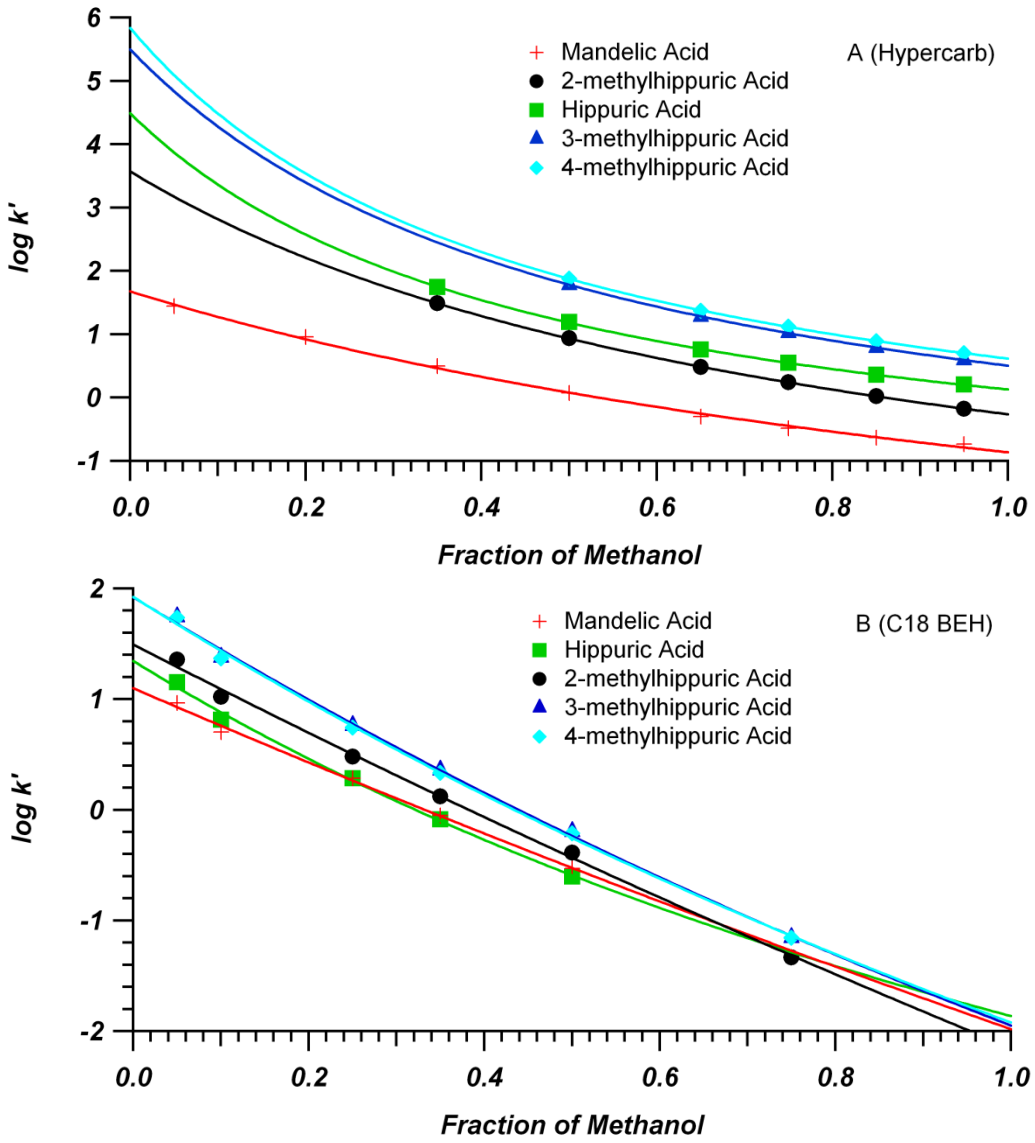

Figure 4-2. Plot of log of retention factors of the model metabolites as a function of methanol volume fraction in the mobile phase on the Hypercarb (A, 4.6 mm x 100 mm, 3 µm) and C18 BEH (B, 2.1 mm x 50 mm, 1.7 µm) columns. Measurements made in water/MeOH + 0.1% FA mobile phases at 30 °C, Experimental data, which was discussed in Chapter 2, was fit with Equation 4-5.

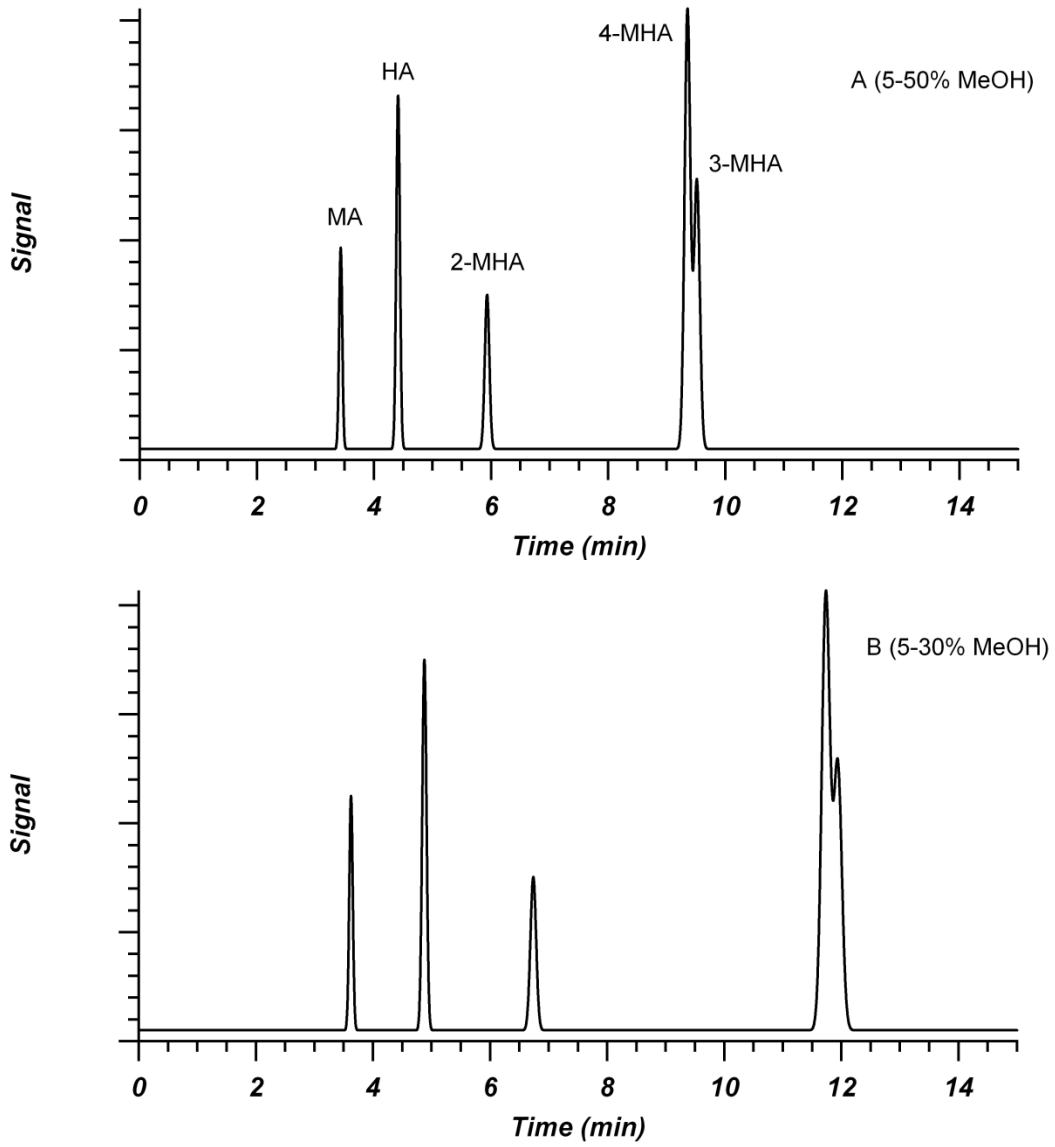

Figure 4-3. Predicted gradient chromatograms for metabolites on C18 BEH. Prediction based on isocratic retention data (Table 4-2) and gradient parameters (Table 4-3). Two different gradient conditions were use: 5-50% methanol in 30 minutes (A) and 5-30% methanol in 30 minutes (B). Column: 2.1 mm x 50 mm, 1.7 µm C18 BEH. Assumed flow rate: 0.3 mL/min. Predicted retention times can be found in Table 4-4

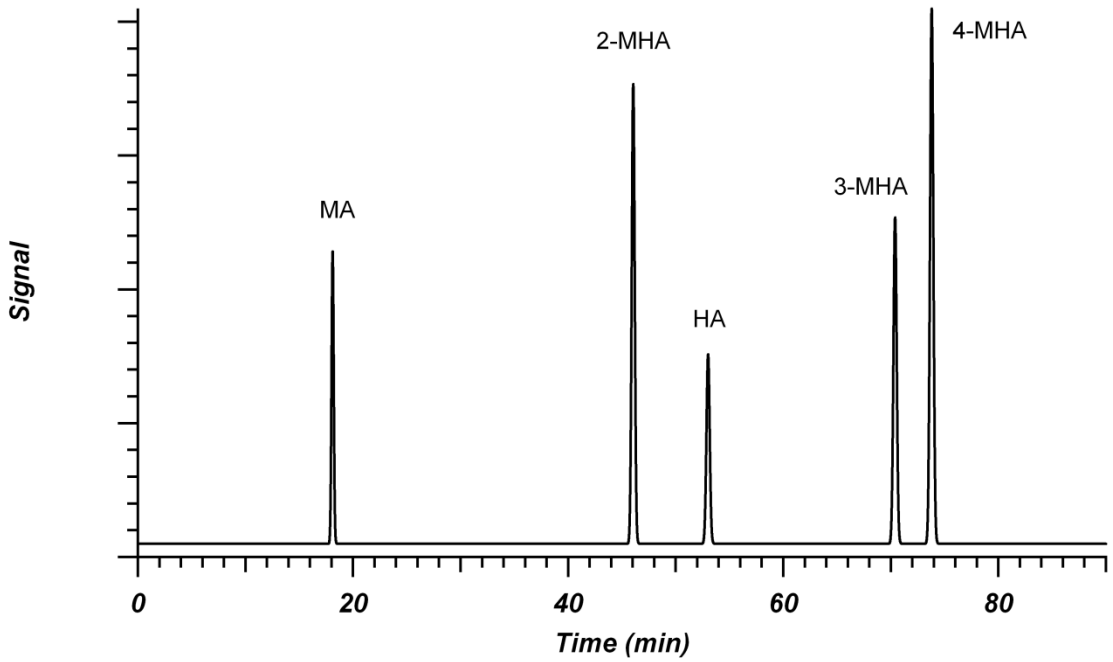

Figure 4-4. Predicted gradient chromatogram for metabolites on Hypercarb. Prediction based on isocratic retention data (Table 4-1) and gradient parameters (Table 4-5). Gradient conditions: 5-95% MeOH in 90 minutes. Column: 4.6 mm x 100 mm, 3 μm Hypercarb. Assumed flow rate: 1 mL/min. Predicted retention times can be found in Table 4-6.

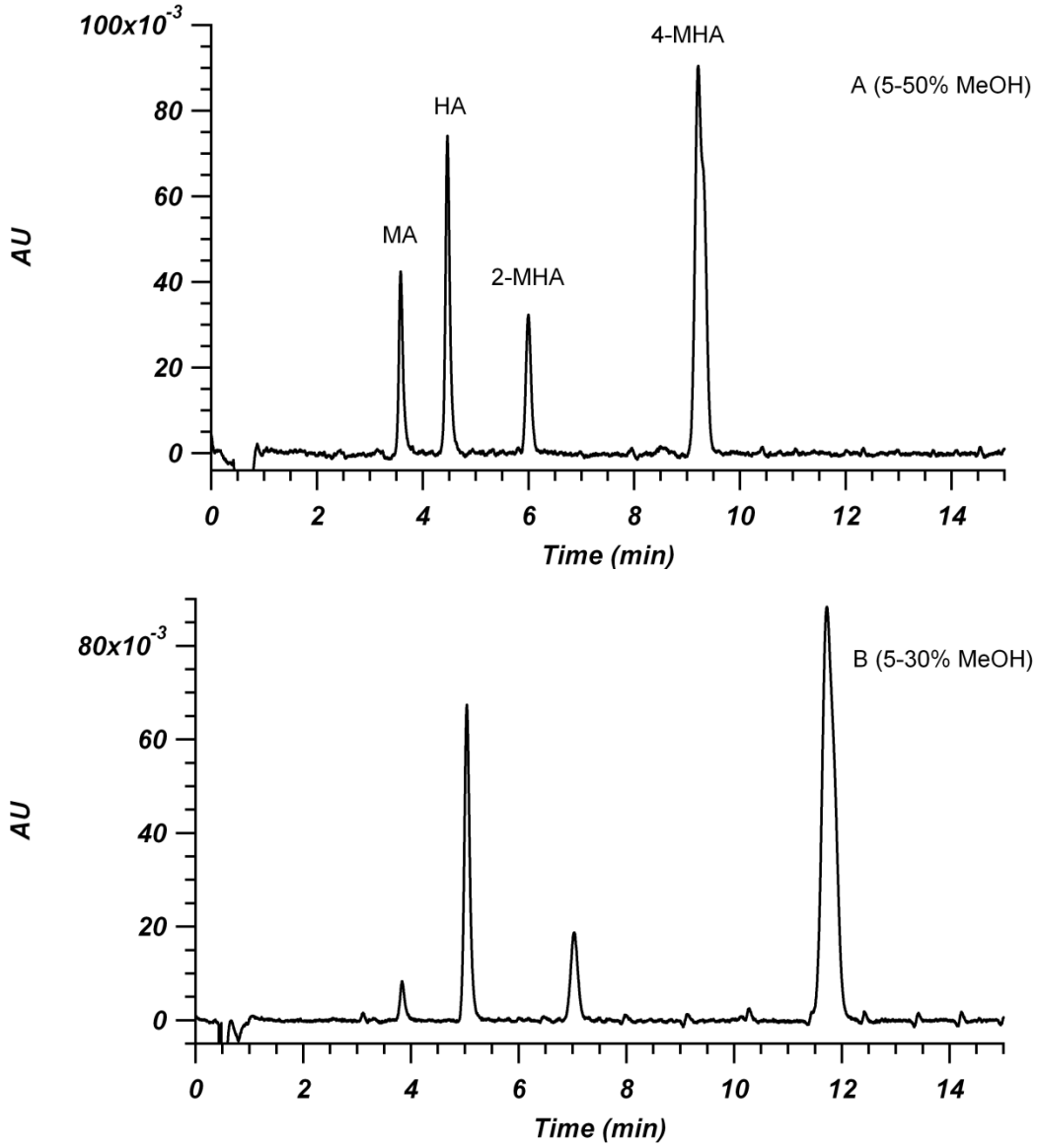

Figure 4-5. Gradient separations of model metabolites on C18 BEH using gradients of 5-50% MeOH (A) and 5-30% MeOH (B), both in 30 minutes. Column: 2.1 mm x 50 mm, 1.7 µm C18 BEH. Wavelength: 240 nm. Column temperature: 30 °C. Flow rate: 0.3 mL/min. Retention times can be seen in Table 4-4.

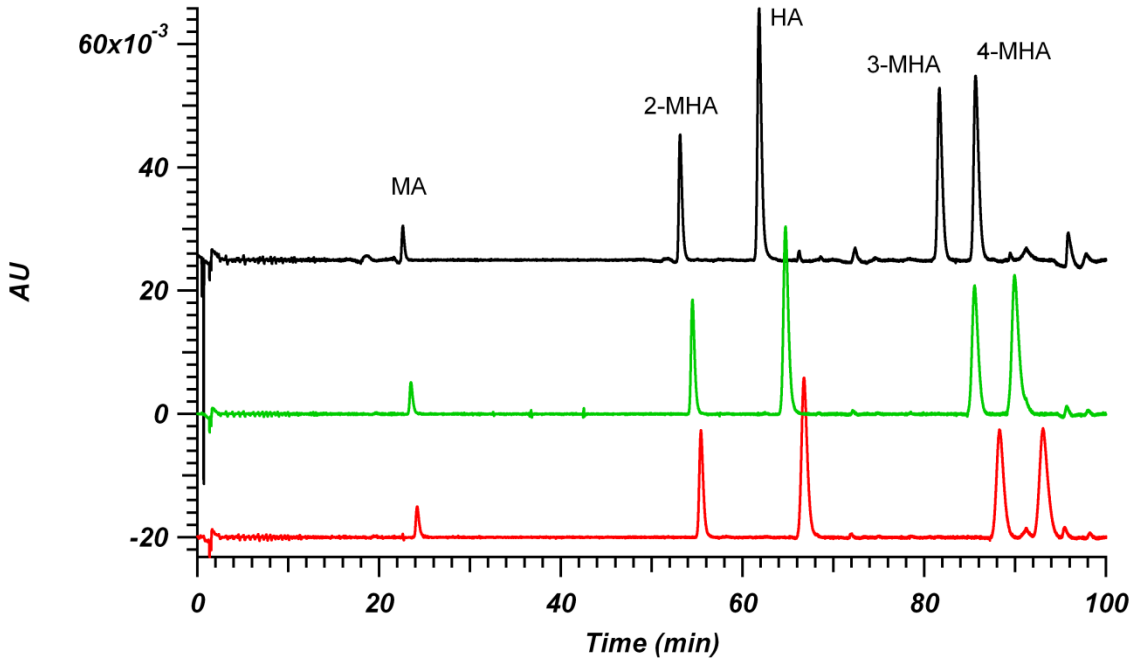

Figure 4-6. Sequential gradient separations of model metabolites on Hypercarb with 10 mM ascorbic acid treatment only before the first run. Gradient conditions: 5-95% methanol in 90 minutes. Column: 4.6 mm x 100 mm, 3 µm Hypercarb. Wavelength: 240 nm. Column temperature: 30 °C. Flow rate: 1 mL/min. The order of runs was black (first), green (second) and then red (third). Retention times can be seen in Table 4-6.

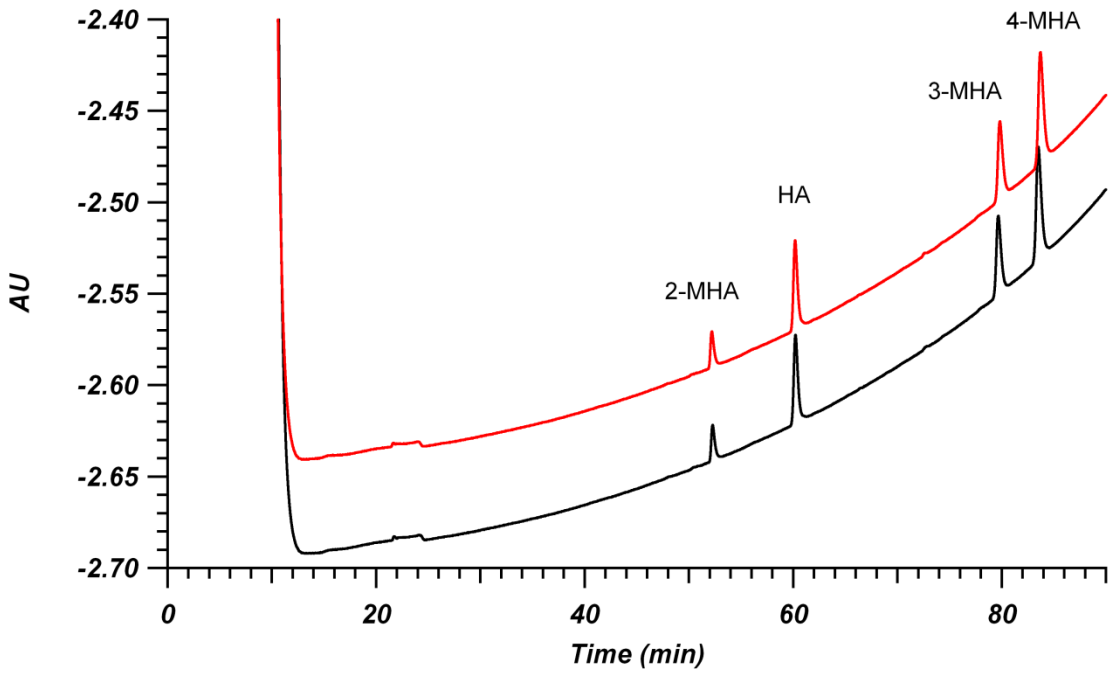

Figure 4-7. Replicate gradient separations of model metabolites on Hypercarb with 10 mM ascorbic acid treatment between runs. Gradient conditions: 5-95% methanol in 90 minutes. Column: 4.6 mm x 100 mm, 3 µm Hypercarb. Wavelength: 240 nm. Column temperature: 30 °C. Flow rate: 1 mL/min. The large signal at the beginning of the runs is due to ascorbic acid washing off of the column from the treatment step performed before the run started. Retention times can be seen in Table 4-6.

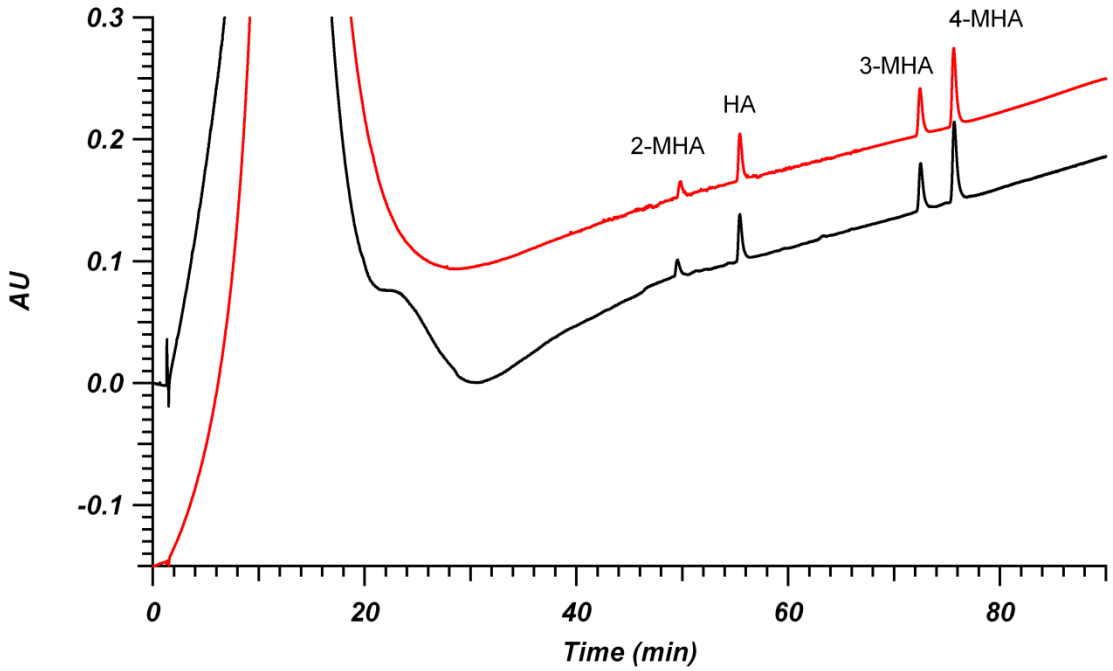

Figure 4-8. Replicate gradient separations of model metabolites on Hypercarb with 100 µM ascorbic acid in the mobile phase. Gradient conditions: 5-95% methanol with 100 µM ascorbic acid added, in 90 minutes. Column: 4.6 mm x 100 mm, 3 µm Hypercarb. Wavelength: 240 nm. Column temperature: 30 °C. Flow rate: 1 mL/min. The large peak at the beginning of the runs is due to ascorbic acid washing off of the column. Retention times can be seen in Table 4-6.

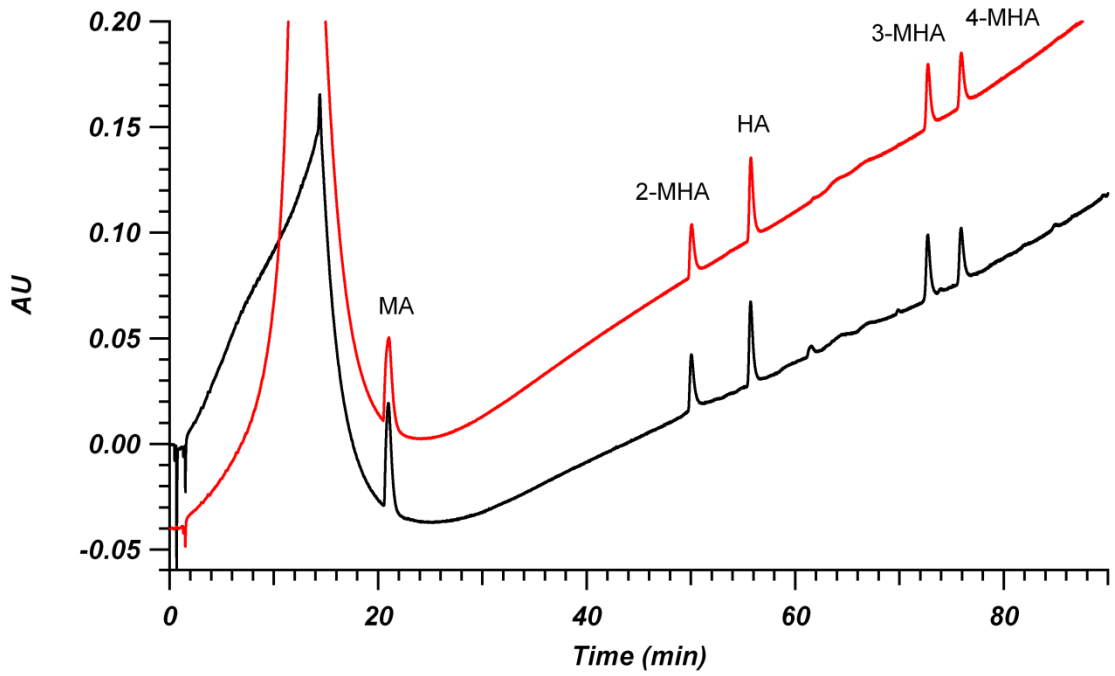

Figure 4-9. Replicate gradient separations of model metabolites on Hypercarb with 50 µM ascorbic acid in the mobile phase. Gradient conditions: 5-95% methanol with 50 µM ascorbic acid added, in 90 minutes. Column: 4.6 mm x 100 mm, 3 µm Hypercarb. Wavelength: 240 nm. Column temperature: 30 °C. Flow rate: 1 mL/min. The large peak at the beginning of the runs is due to ascorbic acid washing off of the column. Retention times can be seen in Table 4-6.

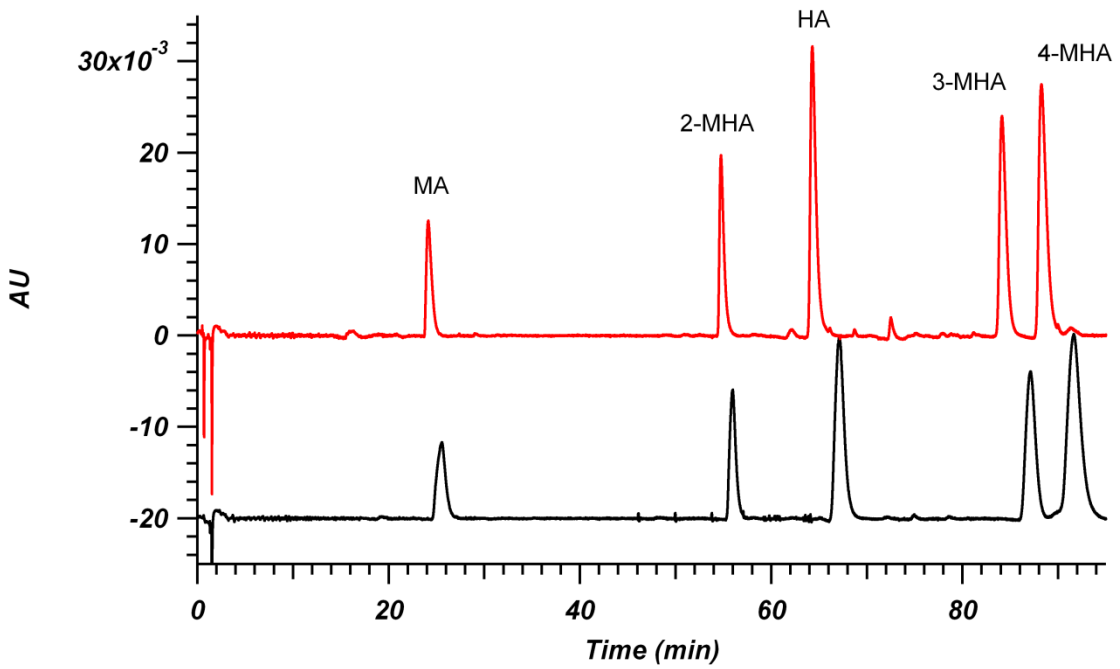

Figure 4-10. Replicate gradient separations of model metabolites on Hypercarb with 1 µM ascorbic acid in the mobile phase. Gradient conditions: 5-95% methanol with 1 µM ascorbic acid added, in 90 minutes. Column: 4.6 mm x 100 mm, 3 µm Hypercarb. Wavelength: 240 nm. Column temperature: 30 °C. Flow rate: 1 mL/min. Retention times can be seen in Table 4-6.

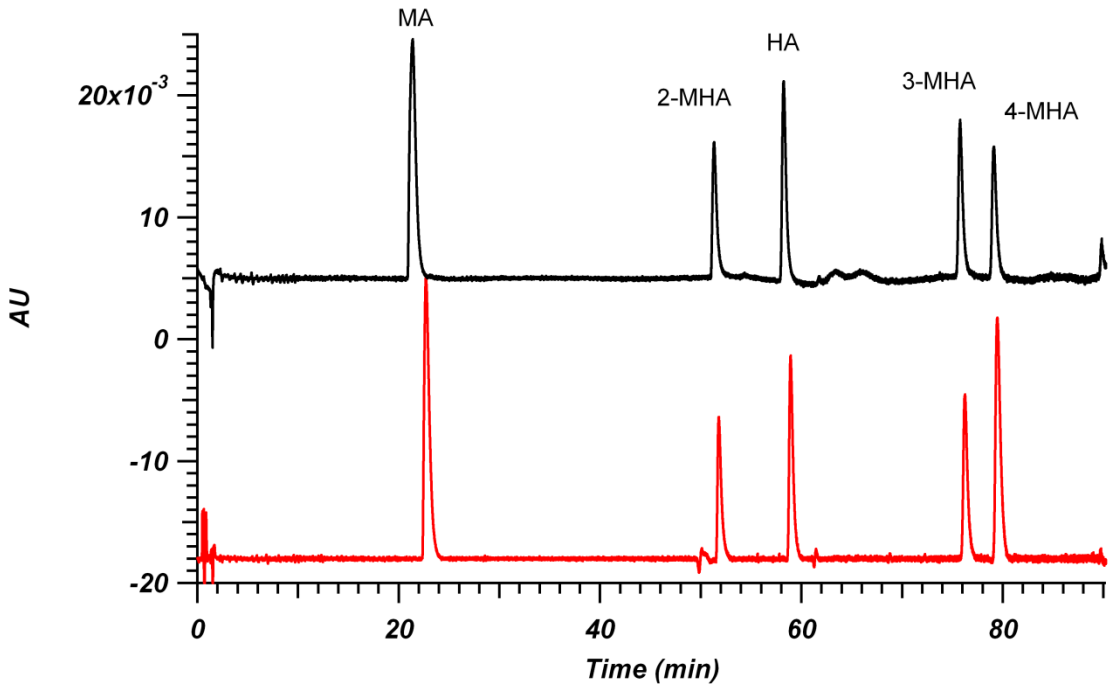

Figure 4-11. Replicate gradient separations of model metabolites on Hypercarb with 500 µM sodium sulfite in the mobile phase. Gradient conditions: 5-95% methanol with 500 µM sodium sulfite added, in 90 minutes. Column: 4.6 mm x 100 mm, 3 µm Hypercarb. Wavelength: 240 nm. Column temperature: 30 °C. Flow rate: 1 mL/min. Retention times can be seen in Table 4-6.

REFERENCES

(1) Neue, U. D. *J. Chromatogr. A* **2005**, *1079*, 153–161.

(2) Neue, U. D.; Marchand, D. H.; Snyder, L. R. *J. Chromatogr. A* **2006**, *1111*, 32–39.

(3) Nikitas, P.; Pappa-Louisi, A. *Journal of Chromatography A*. 2009, pp 1737–1755.

(4) Gilar, M.; McDonald, T. S.; Johnson, J. S.; Murphy, J. P.; Jorgenson, J. W. *J. Chromatogr. A* **2015**, *1390*, 86–94.

(5) Neue, U. D. *Journal of Chromatography A*. 2008, pp 107–130.

(6) Snyder, L. R.; Dolan, J. W. *High-Performance Gradient Elution: The Practical Application of the Linear-Solvent-Strength Model*; 2006.

(7) Snyder, L. R.; Dolan, J. W.; Gant, J. R. *Journal of Chromatography A*. 1979, pp 3–30.

(8) Neue, U. D. *Chromatographia* **2006**, *63*, S45–S53.

(9) Torres-Lapasio, J. R.; Garcia-Alvarez-Coque, M. C.; Roses, M.; Bosch, E. *J. Chromatogr. A* **2002**, *955*, 19–34.

(10) Nikitas, P.; Pappa-Louisi, A.; Agrafiotou, P. *J. Chromatogr. A* **2002**, *946*, 9–32.

(11) Neue, U. D.; Kuss, H. J. *J. Chromatogr. A* **2010**, *1217*, 3794–3803.

(12) Molnar, I. *Journal of Chromatography A*. 2002, pp 175–194.

(13) Gilar, M.; McDonald, T. S.; Roman, G.; Johnson, J. S.; Murphy, J. P.; Jorgenson, J. W. *J. Chromatogr. A* **2015**, *1381*, 110–117.

(14) Jansen, R. S.; Rosing, H.; Schellens, J. H. M.; Beijnen, J. H. *J. Chromatogr. A* **2009**, *1216*, 3168–3174.

(15) Hsieh, Y.; Duncan, C. J. G.; Brisson, J. *Rapid Commun. Mass Spectrom.* **2007**, *21*, 629–634.

(16) Pabst, M.; Altmann, F. *Anal. Chem.* **2008**, *80* (19), 7534–7542.

(17) Pabst, M.; Grass, J.; Fischl, R.; Le, R.; Jin, C.; Borth, N.; Altmann, F. *Anal. Chem.* **2010**, *82*, 9782–9788.

(18) Holmgren, E.; Carlsson, H.; Goede, P.; Crescenzi, C. *J. Chromatogr. A* **2005**, *1099*, 127–135.

(19) Reepmeyer, J. C.; Brower, J. F.; Ye, H. *J. Chromatogr. A* **2005**, *1083*, 42–51.

(20) Bapiro, T. E.; Richards, F. M.; Jodrell, D. I. *Anal. Chem.* **2016**, *88*, 6190–6194.

(21) Melmer, M.; Stangler, T.; Premstaller, A.; Lindner, W. *J. Chromatogr. A* **2010**, *1217* (39), 6097–6101.

(22) Neue, U. D. *HPLC Columns: Theory, Technology, and Practice*; Wiley-VCH, Inc: New York, 1997.

(23) Dolan, J. W. *LCGC North Am.* **2006**, *24*, 458.

(24) Shibukawa, M.; Terashima, H.; Nakajima, H.; Saitoh, K. *Analyst* **2004**, *129*, 623–628.

CHAPTER 5. CAPILLARY COLUMNS PACKED WITH POROUS GRAPHITIC CARBON FOR SEPARATIONS OF URINARY METABOLITES

5.1 Introduction

5.1.1 Analysis of Urinary Metabolites with LC-MS

Due to its ease of collection and large available sample volumes; urine has long been a useful biofluid for diagnostics. To date, over 3,000 metabolites have been detected from human urine.[1] As no one method has been able to detect every metabolite, identification of these compounds has required the use of a variety of complementary techniques, such as NMR, GC/MS and LC-MS. LC-MS separations of metabolites have traditionally been performed using C18-bonded columns.[2–5] These columns provide repeatable separations and a satisfactory retention level for a broad range of analytes. Although urine does contain some amount of lipids and fatty acids, it is composed largely of very hydrophilic metabolites.[1] These hydrophilic metabolites present a challenge with C18-bonded columns, as they are lightly retained, causing a large number of species to elute early in a gradient separation.[6,7] HILIC has also been used for the analysis of urine metabolites as it provides increased retention of polar compounds.[7,8] One study by Kloos *et al.* used a series of polar urine metabolites to test a number of reversed phase and HILIC stationary phases to see which provided the best separation.[9] Based on a number of criteria like peak shape, retention, and signal-to-noise, it was found that a diol-bonded HILIC column outperformed all reversed phase columns. For metabolite profiling in urine, it has been suggested that HILIC and reversed phase columns would provide complementary data.[7,10] This need to run samples on two different columns would greatly increase total analysis time. PGC packed columns could potentially be useful for the global analysis of urine as they have the ability to retain both polar and non-polar analytes within a single run with the use of electrospray ionization (ESI) compatible solvents.[11]

5.1.2 Development of UHPLC Gradient System

When analyzing complex samples such as urine, high-resolution separations are needed. The most useful descriptor of the performance of a gradient separation is the peak capacity (n_c), which describes the number of peaks that could be fit side-by-side with a resolution of 1 within a gradient separation window.[12]

$$n_c = \frac{t_g}{w_p} + 1 \qquad \text{Equation 5-1}$$

Here t_g is the gradient separation window, or the time between the first and last peak, and w_p is the arithmetic mean 4σ width of the peaks throughout that separation window. As samples increase in complexity, a higher peak capacity is needed to separate them with desirable resolution.

One method of increasing peak capacity is the use of longer gradient separations, although improvements will diminish at some point as times are extended.[13] Another method of improving peak capacity is to improve the column performance as $n_c \propto \sqrt{N}$.[14] This led to interest in packing long capillary columns with sub-2 μm particles, which provide greatly increased efficiency.[13] Although a number of commercial instruments are capable of reaching up to 1,000 bar, even higher pressures were needed in order to use long capillary columns with sub-2 μm particles.

Several LC systems capable of gradient separations at > 1,000 bar have been previously developed. The Jorgenson group developed a system capable of performing gradient separations up to 50,000 psi (3,400 bar) using preloaded gradients.[15] This system had the drawback of requiring split-flow to deliver proper flow rates to the column, causing a loss of sample in the process. Shen *et al.* published an automated instrument capable of gradient separations up 20,000 psi.[16] When analyzing metabolites and peptides, this system provided peak capacities of >1,000 in 400-2,000 minutes using 40-200 cm columns packed with reversed phase particles.[16] More recently, our group developed a gradient system capable of performing gradient separations up to 45,000 psi (3,000 bar).[13] This system was built around a commercial nanoAcquity instrument, which was used to generate a gradient and inject a sample in reverse order onto a gradient storage loop. A series of mechanical pin

valves were manipulated to isolate the instrument from the loop, and a pneumatic amplifier pump was used to push the gradient, now in the correct order, onto the column for analysis. Using this system, peak capacities of greater than 800 were seen in 700 minutes using one-meter columns packed with 1.9 μm C18 BEH particles. Replacing a number of mechanical pin valves with liquid CO_2 freeze/thaw valves has led to further performance improvement.[17] These CO_2 valves made the system more robust by removing a number of connections as well as improved performance by the elimination of dead volumes that were present in the mechanical valves.

5.1.3 Slurry Packing of Reversed Phase Capillary Columns

At the heart of every separation is the column, making it vital to produce efficient and stable columns. Slurry packing of columns involves suspending the desired particles in a solvent and placing them inside of a reservoir. For reversed phase particles, low viscosity organic solvents are most often used.[18] Pressure is then applied with a pump, pushing particles into an attached column blank. The column blank has a frit at the outlet so the bed will progressively build over time until the desired length is achieved. Although this process may seem simple, in practice it can be challenging due to the number of parameters that affect the final column performance. Parameters like choice of slurry solvent, pushing solvent, slurry concentration, packing pressure, particle size distribution, and particle agglomeration are some of the many interrelated factors impacting the performance of the final column.[19–23] Due to the complexity of this process, it was long viewed that column packing was more of an art than a science.

Over the years, a number of column packing studies have started to illuminate the effects of some of these column preparation parameters on the column's performance. The impact of column packing on bed morphology and column performance is largely related to the A-term.[24] As the column is packed, heterogeneities are formed causing variable flow paths through the bed and ultimately band dispersion by eddy dispersion. Recently, the ability to image and reconstruct bed morphology has emerged as a very powerful tool allowing relation of column performance and preparation methods to the actual bed structure. Some of the methods available for imaging of bed

morphology include focused ion-beam scanning electron microscopy, confocal laser scanning microscopy (CLSM) and scanning transmission electron microscopy.[25,26] CLSM has proven to be particularly useful for the imaging of capillary columns as it is non-invasive and therefore has little chance of disturbing the original bed structure.[20] This method works by staining the C18 bonded stationary phase using a hydrophobic fluorescent dye. After excess dye is flushed from the column, it is filled with a refractive index matching solution. Fluorescence images are then taken, slice-by-slice, through the column bed. These images are then stacked, allowing for a reconstructed image of the three-dimensional bed to be produced.

CLSM experiments have allowed for morphological observations to be related to kinetic performance of the column and the column packing procedures. Previous studies have illustrated the impact that particle slurry concentration had on the column microstructure. It was observed that columns packed using low and high slurry concentration extremes performed worse than intermediate concentrations.[20,22,27] At low slurry concentrations, there was radial size segregation of particles across the column diameter, with an enrichment of smaller particles near the column wall.[20] Size segregation would lead to local velocity differences and higher transchannel dispersion, decreasing the efficiency of the column. At high slurry concentrations, a more homogenous bed was seen because of minimization of the wall effect and particle size segregation, but the column efficiency was degraded by the inclusion of larger and more frequent voids formed in the bed during packing.[22] These voids increase eddy diffusion because velocity differences occur for solutes traveling through a dense region compared to a void. It was found that an intermediate slurry concentration was optimal as it balanced the wall effects and size segregation with the inclusion of voids.[27] This informed further study by Godinho *et al.* wherein they combined the use of high slurry concentrations and sonication of the column as it is packing.[23] The thought was that it would allow for the minimization of the wall effect and bed heterogeneities due to the high slurry concentration, while also minimizing the formation of voids during the packing process with sonication. The combination of the high slurry concentrations and sonication resulted in the production of the most efficient packed capillary

columns to date, with minimum reduced plate height (h_{min}) values as low as 1.05.[23]

5.1.4 Use of Porous Graphitic Carbon Packed Capillary Columns

Capillary columns packed with PGC have been seen relatively limited use to date. Applications using capillary PGC columns include the analysis of phthalate metabolites, catecholamines, oligosaccharides, and glycans.[28–31] Since PGC is not a widely used packing material compared to C18-bonded reversed phase materials, there has been little demand for high performing capillary columns. The primary reason for use of PGC seems to be its alternative retention properties. Similar to standard bore columns, a number of complications have been observed when using PGC packed capillary columns, further limiting their appeal to researchers. When performing gradient separations of phthalate metabolites from human urine, retention times drifted outwards as the number of runs increased.[28] Although drifting retention times are not as much of an issue with LC-MS platforms due to the ability to easily assign peaks from mass-to-charge (m/z) ratios, it is still an inconvenience and can complicate data analysis due to necessitating alignment of runs with data processing software. Several studies have also highlighted the importance of grounding the PGC column when performing LC-MS with ESI.[32–34] The PGC particles are electrically conductive and have been shown to allow for a higher level of current to flow back through the column from the ESI emitter. With C18 bonded columns, current can only be carried through the column by mobile phase, but PGC particles allow current to also travel by electronic conduction in the particles. This will increase the overall flow of current through the system as a whole, potentially causing redox reactions. These redox reactions can lead to split peaks for analytes as well as reduced signal due to oxidation of species in the chromatographic system.[32] To minimize the current production and issues due to use of PGC columns with ESI, it is common practice to decouple the column from the ESI emitter using an open capillary pigtail as well as grounding the connecting metal union.

Although a number of researchers have demonstrated the packing and use of capillary PGC columns, there has been little research to study the packing process or characterize these columns isocratically to determine their performance. Packing procedures that are published in the literature

range in the slurry concentrations (15-100 mg/mL) and slurry solvents (carbon tetrachloride or MeCN) used.[35–37] Capillary columns packed with Hypercarb were previously commercially available, although they are no longer for sale in this format. Even more limited than packing procedures is the characterization of the packed column's performance before use with the desired application. Knox and Ross demonstrated the most efficient column to date, with a standard bore column packed with 5 μm Hypercarb producing a $h_{\min}$ of ~2.6.[38] Until very recently, capillary columns had been limited to 25 cm or less in length due to the limited pressures used for packing. Zou *et al.* has recently published the packing and use of a 90 cm column packed with nominally 3 μm Hypercarb for the separation of glycans from urinary exosomes.[39] To date, this is the longest and highest performing (N ~ 100,000 plates) packed capillary PGC column ever reported in the literature, although little information was provided on the packing or characterization conditions. As discussed previously, increasing the column performance allows for the analysis of more complex mixtures. This increase in performance, in combination with the unique retention properties of PGC, has led to our interest in packing even longer columns for use with separations of urinary metabolites.

5.2 Experimental Methods

5.2.1 Chemicals

For the purpose of the preparation and use of capillary columns, HPLC grade acetonitrile (MeCN), hydrogen peroxide (30%), and potassium chloride were purchased from Fisher Scientific (Fair Lawn, NJ). Deionized water was obtained using a Barnstead Nanopure ultrapure water system (Dubuque, IA). Formic acid (FA), ascorbic acid (AA), hydroquinone (HQ), 1,4-benzoquinone (BQ), and trifluoroacetic acid (TFA) were purchased from Sigma Aldrich (St. Louis, MO).

5.2.2 Packing and Characterization of Capillary Columns

Nominally 3 μm Hypercarb particles were obtained by unpacking a commercially available 4.6 mm x 100 mm column from Thermo Fisher Scientific Inc. (Waltham, MA). These particles were analyzed using a Hitachi S-4700 cold cathode field emission scanning electron microscope (Tokyo, Japan). The images were used to determine the average particle diameter for column characterization

calculations. 1.9 µm C18 BEH particles provided by Waters Corporation (Milford, MA) were used as a comparison to traditional reversed phase systems.

The method used to pack capillary columns has been reported previously in detail. 75 µm i.d. x 360 µm o.d fused silica capillary tubing was purchased from Polymicro Technologies (Phoenix, AZ). Column blanks were cut to 140 cm and 240 cm for the one-meter and two-meter Hypercarb columns, respectively. Excess length was needed to allow for the significant amount of bed compression that was observed (~10 cm/m of column length). Outlet Kasil frits were created on capillary column blanks by pressing the tubing onto a glass microfiber filter (Whatman, Buckinghamshire, UK) wetted with 1/1 (v/v) ratio of formamide (Sigma-Aldrich) and potassium silicate (PQ Corporation, Valley Forge, PA).[40] Frits were set by drying them overnight in the oven at 50 °C. Hypercarb slurries were prepared by suspending a known mass of particles in acetone and sonicating for 5 minutes with a Cole Parmer Ultrasonic Cleaner 8891 (Vernon Hills, IL). Due to the limited mass of particles available, slurry concentrations were limited to 25 mg/mL for Hypercarb columns.

In order to pack the column, the slurry was placed into an in-house made packing vessel and the column blank was tied into the vessel using a UHPLC fitting. A stir bar was placed in with the slurry and the vessel was on a stir plate to prevent the particles settling throughout the packing process. The capillary was oriented using a piece of foam so that length of capillary to be packed was submerged in the sonication bath.[23] Only the outlet frit and 2 cm of the outlet were kept out of the bath. A series of two, 2 meter long columns were packed with and without sonication to see which condition produced the best columns. Sonication was performed during packing with an Elmasonic P 60 H (Elma Schmidbauer GmbH, Singen, Germany) sonicator using sweep mode at 80 kHz. Packing was initiated at 5,000 psi (350 bar) using a DSHF-300 Haskel pneumatic amplifier pump (Burbank, CA) with acetone used as the pushing solvent. After roughly 2 cm of bed was formed, the pressure was immediately ramped to 30,000 psi (2,000 bar). The sonicator bath was kept at 30 °C by adding ice throughout the packing process. Once the column reached the desired length, packing was stopped

by slowly draining the pressure to atmosphere in order prevent bed movement. One-meter long Hypercarb columns were packed with the same procedure, only the pressure was limited to 20,000 psi (1,400 bar) during packing. A C18 BEH column was packed to 40 cm using a 25 mg/mL slurry in acetone and packing pressure of 30,000 psi (2,000 bar).

After packing, columns were connected to a DSXHF-903 Haskel Pump using a UHPLC injector that was built in lab and that has been previously published.[21] They were then flushed at 30,000 psi (2,000 bar) and 42,000 psi (2,900 bar) for 20 column volumes in 5/95 water/MeCN + 0.1% FA for the one and two-meter Hypercarb columns, respectively. Since the bed was made of graphitic carbon, the traditional method of making a temporary frit using a heated wire stripper while flowing slowly was not possible. To prevent bed movement, one of the injector valves was cracked open very slowly such that a very small amount of flow was observed out of the valve. The pressure to the pumps was then drained slowly, and the column was allowed to depressurize slowly over the course of several hours. By marking the location of the head of the bed before depressurization and after depressurization, it was seen that the bed had not moved. Columns were then clipped to the desired length and a Kasil frit was put on the inlet to hold the bed in place.

Hypercarb column performance was also tested using isocratic conditions with a test mixture containing hydrogen peroxide and 1,4-benzoquinone (~400 μM) while C18 BEH column performance was tested using a test mixture containing ascorbic acid and hydroquinone (~400 μM). Low-pressure injections were performed using the UHPLC injector mentioned previously along with a DSTV-100 Haskel pump. Mobile phase conditions were 50:50 (v/v) water/MeCN + 0.1% TFA and 5/95 water/MeCN + 0.1% FA for the C18 BEH and Hypercarb columns, respectively. Detection was performed using amperometric detection with an 8 μm carbon fiber electrode pushed directly up to the outlet frit.[41] This allowed for detection of electro active species with negligible dead volume. The electrode was held at -0.2 V vs. Ag/AgCl reference electrode for Hypercarb and +1.1 V vs. Ag/AgCl for C18 BEH. The signal was passed through an SR750 current amplifier (Stanford Research Systems, Sunnyvale, CA) with a 10^9 V/A gain. High frequency noise was filtered out with a 3 Hz, 3

dB low pass filter. Data was acquired at 21 Hz using a custom written LabView 6.0 program (National Instruments, Austin, TX) on an Intel Core 2 Duo desktop computer with a 16-bit A/D converter.

Reduced van Deemter plots ($h - v$) were generated by performing runs of the test mixture over a range of linear velocities. Low frequency baseline drift was removed with baseline subtraction. Measured peaks were fit with an iterative statistical moments algorithm (± 3σ limits) written in Igor Pro 6.0 (Wavemetrics, Inc., Lake Oswego, OR) in order to determine retention times and theoretical plates.[42]

5.2.3 Use of Capillary Columns for Gradient Separations of Human Urine

Gradient separations using the packed capillary columns were performed using a modified commercial LC-MS system that has been shown previously and that will be discussed briefly here. This system, which is built around a nanoAcquity, has been demonstrated by performing constant pressure gradient separations up to 45,000 psi and can be seen in Figure 5-1.[17] The nanoAcquity is used solely for sample handling and gradient generation. Through a series of fluidic connections, the gradient and sample are loaded in reverse order onto a gradient storage loop (50 meters of 50 μm i.d. x 360 μm o.d. capillary). Connecting capillary is threaded through a liquid CO_2 freeze-thaw valve that freezes the mobile phase in the capillary after loading. When the pneumatic amplifier pump (DSHF-300 Haskel pump) is activated, the sample and gradient are now pushed through the column and on to MS in the correct order.

Since the gradients are performed with constant pressure rather than constant flow, they are reported by volume. Mobile phases consisted of (v/v) mixtures of Optima LC-MS water + 0.1% FA and MeCN + 0.1% FA (Fischer Scientific). For C18 BEH columns and one-meter Hypercarb columns, a gradient from 5-90% MeCN is performed in 27 μL. An example trace of the gradient profile can be found in Figure 5-2. A 2.1 μL pre-gradient hold in initial conditions (95/5 water/MeCN + 0.1% FA) was used for all gradients, as well as a 2.5 μL wash at 90% MeCN upon completion of the gradient. For the two-meter column, the gradient volume was doubled (5-90% MeCN is

performed in 54 µL) while all other volumes were the same. The capillary columns were kept inside of a Temperature Control Module II (Waters Corp) at 55 °C. Applied pressure was adjusted such that a flow rate around 300 nL/min was measured as gradient initial conditions (95/5 water/MeCN + 0.1% FA) flowed through the column. Human urine samples were diluted with aqueous MeCN to match the composition of gradient initial conditions for use with the LC-MS system.

2 µL injections were performed for all separations shown here. The outlet of the column was coupled to a quadrupole time-of-flight (qToF) Premier (Waters Corp) MS via a 20 µm i.d. fused silica capillary and 10 µm i.d. fused silica emitters (New Objective, Woburn, MA). A metal union was used to couple the column outlet to the connecting pigtail. This metal union was grounded to the instrument to prevent current back flow through the columns. A spray voltage of 3.0 kV and sampling cone voltage of 35 V were used for positive ionization mode. The source was kept at 110 °C with a nanoflow gas pressure was 0.4 bar. Data was collected in continuum mode with a collision voltage of 5 V so as to minimize fragmentation in the collision cell. Scan time was 0.6 s with an interscan delay time of 0.1 s for all runs.

5.3 Results and Discussion

5.3.1 Packing and characterization of 1 m and 2 m Columns with PGC

Before any columns were packed, it was important to know the structure and size of the particles being used. Hypercarb particles were extruded from a commercial column and dried before being imaged using SEM. Figure 5-3 shows an example image of the particle batch used for packing capillary columns as well as the particle size distribution information. It can be seen that a large range of particle diameters exists in the batch. Although the particles are marketed as 3 µm, the number average particle diameter measured here was 3.48 µm (n = 783). A relative standard deviation (RSD) of 21.5% was found, which is high but not uncommon for fully porous chromatographic particles. The particles spanned a large range of sizes, with spherical particles being seen from 0.78 µm to 5.72 µm. There is also some population of either broken particles, or otherwise non-spherical PGC fines that are likely left over from the manufacturing process.

As there is little literature on the packing of PGC columns, we were interested in going more in depth in an attempt to determine conditions that would produce high efficiency columns. Recently, our lab has published a method for producing the high efficiency reversed phase packed capillary columns utilizing high slurry concentrations of C18 BEH particles in combination with sonication during the packing process.[23] Since this method produced such high performing columns, we were interested in adapting it to Hypercarb particles to see how the columns would perform. In order to see how the effect of sonication impacted the overall column performance, two, 2-meter long columns were packed with sonication and two were packed without sonication. All other conditions were identical. As Hypercarb particles were extruded from a commercial column and were available in a limited quantity, it was not possible to use the 200 mg/mL slurry that was used previously with this method. 25 mg/mL slurries were used for all work presented here. Acetone was used as the slurry solvent as it provided an intermediate amount of particle aggregation when studied using in-solution imaging, with agglomerates of 2-7 particles being seen most often. Due to the relatively low slurry concentration and the need to pack two-meter columns, the packing process took several hours, with neither packing method improving the speed at which the columns were packed.

After packing, the columns were flushed using 5/95 water/MeCN + 0.1% FA to compress the bed and flush out any acetone left from the packing process. Traditionally, a temporary frit is placed in the column after flushing in order to hold the bed in place while decreasing the pressure. This was not possible with Hypercarb, so it was necessary to release pressure over a couple of hours in order to prevent bed movement. The inlet of the bed was marked and was not seen to move, signifying the slow pressure release was successful. The original 220 cm of bed was usually compressed by ~20 cm during flushing, suggesting that a number of voids were being filled by compression or that the large particle size distribution led to a loosely packed structure. One important factor that was unknown for Hypercarb was if it possessed enough mechanical stability to withstand the pressures associated with UHPLC. It is cited that PGC is stable up to 1,000 bar (14,000 psi), but studies of its stability at higher pressures have not been performed.[11] To see if the Hypercarb column could withstand the UHPLC

conditions, one column was flushed up to 55,000 psi (3,800 bar) and the inlet region of the bed, which experienced the highest pressure and sheer, was extruded for imaging. Figure 5-4 shows a SEM image of the particles from the extruded bed. The extruded particles showed no observable difference when compared to the original particle batch, confirming that the Hypercarb particles do possess enough mechanical stability to withstand the forces of UHPLC separations.

Traditionally in our lab, capillary columns are characterized with electrochemical detection at the outlet using a mixture of dihydroxybenzene compounds such as hydroquinone.[20,22,41] When these compounds were run on the Hypercarb columns no signal was seen using an electrode potential of +1.1 V vs. Ag/AgCl, one that would normally oxidize them. When a Linear UV/Vis 200 (Thermo Scientific, Waltham, MA) detector was used to detect solutes flowing off the column, a peak was seen when HQ was injected. Since a peak was seen for Hydroquinone with UV but not electrochemical detection, we became suspicious that the PGC surface redox properties may, once again, be complicating the separations. In an attempt to troubleshoot the electrochemical detection problems, we first turned to the well behaved C18 BEH columns. These columns have been shown to have no redox properties. Figure 5-5 A, shows example runs of HQ and BQ in 50/50 water/MeCN + 0.1% TFA. As HQ is detected by oxidation and BQ by reduction, different potentials were applied to the electrode to allow for detection with +1.1 V vs. Ag/AgCl used for oxidation and -0.2 V vs. Ag/AgCl for reduction. The opposite direction of the peaks corresponds to the opposite direction of the flow of current for oxidation and reduction. Figure 5-5 B shows the same measurements on the Hypercarb column in 5/95 water/MeCN + 0.1% FA. As expected for BQ, a negative peak was seen with the electrode at -0.2 V vs. Ag/AgCl. Again, when HQ was injected and the electrode was at +1.1 V vs. Ag/AgCl, no peak was seen, but when the electrode was held at -0.2 V vs. Ag/AgCl, a current corresponding to reduction was observed. These peaks also eluted at essentially the same time (small amounts of drift are seen with regulators controlling the pressure). This suggests that the band that is injected as HQ, is being oxidized by the PGC particles and ultimately eluting as BQ, where it can then be detected as the reduction back to HQ. It was unclear whether this effect was a natural function

of the particles themselves or was due to the application of a potential at the column outlet with the carbon fiber electrode.

In order to further study this apparent oxidation process, HQ and BQ were run on a standard bore column (4.6 mm x 100 mm, 3 μm Hypercarb) with photodiode array detection (PDA). As HQ and BQ have significantly different UV spectra in 5/95 water/MeCN + 0.1% (Figure 5-6 A) this would allow confirmation of whether the oxidation process occurs naturally or only in the presence of the external potential of the electrode. Figure 5-6 summarizes the study using the Acquity with PDA detection. Similar to what was seen with electrochemical detection, Figure 5-6 B shows that the HQ and BQ peaks elute at the same time from the Hypercarb column. Plotting the PDA signal at the peaks maxima (Figure 5-6 C) makes it clear that the injected HQ is being oxidized to BQ by the column. The UV spectra are identical, with neither peak showing any UV features of HQ. Due to the lack of external potential, this shows that the Hypercarb column has a natural oxidative surface. This is line with previous studies showing that Hypercarb particles had a potential of +0.35 V vs. Ag/AgCl and were seen to oxidize catecholamines.[43,44] It is also noteworthy that the oxidation process seems to occur quickly once the HQ reaches the column. If the oxidation process took a significant amount of time, then the peaks would likely differ in retention time and peak width. With slow kinetics, HQ would be traveling down the column while undergoing the redox process, and existing as equilibrium between BQ and HQ, each with their own velocity and retention time. As the peaks elute at the same time and with similar width, it suggests that the kinetics of the oxidation reaction occur very quickly, likely immediately when the HQ reaches the inlet of the PGC column. This study shows that PGC columns could lead to undesired oxidation of redox labile compounds, which could lead to complications with data analysis if one is unaware of this possibility.

In order to characterize columns, a sufficient deadtime marker is needed. For PGC, the only reported unretained compound is acetone. Due to acetone not being electrochemically active, this limits the characterization to UV detection. This UV detector requires that a short capillary pigtail be attached to the PGC column with the open capillary acting as the UV "cell." This type of detection

makes it difficult to determine absolute column performance since there is some amount of dead volume associated with the attached capillary pigtail. The additional volume leads to extra-column band broadening and a lower observed performance than would be seen with electrochemical detection. C18 bonded columns have a number of deadtime markers, with AA being a known electrochemically active species. AA, however, is retained on PGC and also is irreversibly oxidized by the column, making it useless for the reduction potentials we will use. After a number of ionic species were investigated, we realized that hydrogen peroxide (H_2O_2) may be a suitable as it can be detected by reduction. Figure 5-7 shows example chromatograms using UV detection of two samples containing either acetone or H_2O_2 as deadtime markers along with BQ. This shows that H_2O_2 is unretained and should allow for characterization of Hypercarb columns with electrochemical detection. It should be noted that hydrogen peroxide is an oxidant, and could lead to oxidation of the column, which we saw previously increased the retention times of acids.[45,46] Here, it was not seen to affect the column or retention with the nL scale injections being performed. It is also possible that no impact was seen due to BQ being a neutral compound, as it has been reported that oxidation impacts charged species most significantly.

Now that a suitable electrochemical system has been found, the two-meter columns packed with and without sonication were characterized using mixtures of H_2O_2 and BQ in 5/95 water/MeCN + 0.1% FA. Figure 5-8 shows reduced van Deemter plots for these columns. Values for $h_{\min}$, a, b, and c can be found in Table 5-1. Contrary to the study using C18 BEH particles, the non-sonicated Hypercarb columns performed better than the sonicated Hypercarb columns with the slurry concentration used (200 mg/mL C18 BEH vs. 25 mg/mL Hypercarb).[23] The average $h_{\min}$ for the two sonicated columns was 4.28 while the non-sonicated column had an average $h_{\min}$ of 3.3. These columns produced values for the number of theoretical plates at the optimal conditions (N_{max}) of 134,000 and 174,000 on average for the two meter long sonicated and non-sonicated columns, respectively. The columns are twice as long as any Hypercarb column that has been reported in the literature. Looking at the reduced terms, it seems that the b and c-terms tend to be larger on the

sonicated columns, leading to the larger h_{min}. Another useful parameter for the columns is the flow resistance (Φ), which is determined using Equation 5-2.[47]

$$\Delta P = \frac{\Phi u \eta L}{d_p^2} \qquad \text{Equation 5-2}$$

By plotting the normalized $\frac{\Delta P}{\eta L}$ vs. $\frac{u}{d_p^2}$, a linear trend is seen with slope being Φ. Φ for the columns can be found in Table 5-1. The sonicated columns tend to have slightly higher Φ values than the non-sonicated columns, suggesting a more densely packed column. Higher Φ values also seem to line up with increased c-term. As it would not be expected that a more densely packed column would affect traditional mobile phase mass transfer, it could be that the densely packed column increases some velocity dependent a-term contribution in the column, resulting in the higher apparent c-term values.[48,49] Overall, this study shows that non-sonicated columns performed markedly better than sonicated columns, with the 25 mg/mL slurry concentration used here.

Once satisfactory conditions were found to pack the two-meter columns, we were interested in seeing how a one-meter column performed under the same conditions. Previous studies with C18 BEH have found that when short and long columns are packed with identical conditions, the longer column tends to yield larger reduced plate heights.[25] A set of non-sonicated, one meter columns were packed with 25 mg/mL slurries of Hypercarb particles and characterized using electrochemical detection in 5/95 water/MeCN + 0.1% FA. Figure 5-9 displays the reduced van Deemter curves for one and two-meter Hypercarb columns. The one-meter columns perform better than the two meter columns, reaching $h_{\min}$ of 2.6 on average compared to 3.3 for the two-meter columns. N_{max} of roughly 110,000 plates was achieved for the one-meter columns, which is slightly higher than was previously seen for a column of similar length.[39] In general it seems that the improved a and c-term values are a large cause of the better performance of the one-meter columns This shows that there is some phenomenon happening during the packing process that causes the length beyond one-meter, to decrease in performance, leading to the overall higher reduced plate heights. As the bed length

increases, the packing process slows significantly which may influence the overall bed morphology as the particles are no longer hitting the bed at the same velocity. In general, the one-meter columns had improved c-term values. The correlation between Φ and column performance that was previously seen with the two-meter columns does not seem to hold here as the one-meter column both perform better and tend to have higher Φ than the non-sonicated, two-meter columns.

As a comparison to the Hypercarb columns shown here, a 30.1 cm column packed with 1.9 μm C18 BEH was characterized and its performance can be found in Figure 5-9 as well. This clearly shows that the Hypercarb columns perform significantly worse than the traditional reversed phase column. When looking at the reduced terms in Table 5-1, it can be seen that the C18 BEH column has significantly lower c-term contributions than any of the Hypercarb columns. This increased c-term for PGC could due to several factors. It is possible that it is a sign that the mass transfer rates of C18 BEH may be faster than on Hypercarb, which would not be too surprising considering the complex interplay of retention mechanisms that PGC displays. There could also be a higher apparent c-term due to contributions of a velocity dependent a-term.[48,49] Inhomogeneous packing due to a wide particle size distribution could lead to a wide variety of flow paths, which disguise themselves as c-term contributions from the mobile phase. It is also important to keep in mind that our interest in PGC is not for its efficiency, but rather because these alternative mechanisms allow for increased retention of polar compounds that present a challenge for reversed phase columns.

5.3.2 Analysis of Single Donor Urine with C18 BEH and PGC Capillary Columns

Now that conditions have been set to produce high performing capillary columns packed with Hypercarb, these columns are ready for application with more complex samples. A single donor urine sample was purchased from Innovative Research (Novi, MI). This sample was shipped frozen in a plastic centrifuge tube. Upon arrival, the sample was thawed, centrifuged to remove any precipitant, and split into 1 mL aliquots before being frozen again in glass vials. The sample was split into aliquots because previous research on sample preparation and storage has highlighted that the number

of freeze/thaw cycles a sample experiences influences its composition. As urine samples are only recommended to be used for 48 hours while cooled to 10 °C in the nanoAcquity Sample Manager, this storage system allows for individual aliquots to be removed for use as needed, without influencing the others that are still frozen.[50]

As the modified UHPLC gradient system is a constant pressure system and not a constant flow system, gradients were constructed based on volume instead of time. Previous studies on the constant pressure and constant flow systems demonstrated that peak capacities were similar from both systems. Constant pressure systems have the benefit of always operating at the maximum pressure and flow rate, whereas constant flow systems are limited by the pressure limits of the instrument with the maximum viscosity mobile phase over the course of the gradient. An example gradient profile used for the C18 BEH and one-meter Hypercarb columns can be seen in Figure 5-2. Although the C18 BEH and Hypercarb columns have different column volumes, identical gradient conditions will be used to allow for direct comparison of retention. The columns were held at 55 °C in order to reduce the viscosity of the mobile phase and promote rapid mass transfer throughout the separation. The applied pressure to the amplifier pump was adjusted so that the volumetric flow rate in gradient initial conditions (95/5 water/MeCN + 0.1% FA) was 300 nL/min. For the 30.1 cm C18 BEH and one-meter Hypercarb columns, roughly 6,500 psi was needed to reach 300 nL/min.

8-times dilute single donor urine samples were run on both C18 BEH and one-meter Hypercarb columns. The chromatograms for these separations can be seen in Figure 5-10. An initial look at these chromatograms reveals several important factors. First, with the C18 BEH column, there are several intense and extremely broad peaks that elute early in the gradient. As discussed in Chapters 2 and 4, this is likely due to volume overload of very polar species that are not retained on the C18 BEH column. The PGC chromatogram shows significantly fewer ions in the early portion of the chromatogram, suggesting that the alternative retention mechanisms provide improved retention of these polar solutes, causing them to no longer be volume overloaded. Since the same gradient conditions are used for both columns, it is easy to see that Hypercarb provides significantly increased

retention of the compounds in the urine sample. The separation window, or time frame within which most of the solute peaks elute, is much smaller on the C18 BEH column (40-70 minutes) than the Hypercarb column (60-130 minutes). The separation of such a complex sample in a small time window makes it difficult to get good resolution between peaks, leading to more overlap. The resolution between peaks looks to be significantly improved on the PGC column. It should be noted that little drift in retention times was seen for the Hypercarb columns run here. As the system is constant pressure, it also is hard to determine any source of retention time drift as a small increase in flow resistance will also cause retention to drift outwards due to decreased flow rate.

One thing that was surprising was the regular pattern with which peaks were eluting in the middle of the gradient on the C18 BEH column. There seemed to be a series of triplet peaks that was repeating and had similar changes in mass between the series. In order to make visualization of this easier, the chromatograms can be plotted as two-dimensional plots of m/z vs. time. These plots can be found in Figure 5-11 for the C18 BEH and Hypercarb gradients. Using this alternative visualization, it can clearly be seen that there is a repeating pattern of peaks with even shifts in m/z in the C18 BEH column. These show up as a diagonal trend of ions in Figure 5-11 A, where they are circled. When looking at the Hypercarb column, an increasing m/z diagonal is also seen (circled in Figure 5-11 B), although it is not as obvious due to the differing selectivity of PGC causing the series of peaks to be more separated in time. This type of trend suggests that there may be potential contamination or leaching of polymer or plasticizer into the sample. The even shifts in m/z between the triplicate sets are indicative of a 44 m/z repeating unit being added to a polymer chain. This m/z shift is often associated with polyethylene glycol oligomers. Within each triplet, there are also repeating m/z shifts with the addition of 14 m/z to the second and third peaks. This is in agreement with the addition of a $–CH_2$ unit to a polymer chain. It was suspected that the source of these contaminants was the polymer centrifuge tube that the urine was shipped in. This stressed the importance of sample collection and storage, which are known to be vital for metabolomics studies. Since these samples were contaminated with leachate from polymers, a new, uncontaminated sample was needed.

5.3.3 LC-MS Analysis of Pooled Urine using One and Two-Meter Hypercarb Columns

Since the polymer centrifuge tube that was used for shipping contaminated the single donor urine sample, it was necessary to find a new urine sample. The urine of four males was collected and pooled for use. Samples were mixed with equal volumes and centrifuged. This pooled stock was then separated into 1 mL aliquots and subsequently frozen. Throughout the process of collection, centrifugation, and storage, the urine sample never came in contact with polymer of any kind. Glass centrifuge tubes were used for collection and centrifugation while glass vials were used for storing the frozen urine samples. This was done in hopes of preventing the leaching of any polymer contaminants into the sample. These urine samples were then run on 30.1 cm C18 BEH, one-meter Hypercarb, and two-meter Hypercarb columns at 55 °C. The pressures required to achieve the 300 nL/min flow rate in gradient initial conditions were roughly 6,500 psi for the 30.1 cm C18 BEH and one-meter Hypercarb columns and 13,000 psi for the two-meter Hypercarb column.

As discussed previously, identical 27 µL gradients from 5-90% MeCN were used for the C18 BEH and one meter Hypercarb columns, while a 54 µL gradient was used for the two-meter Hypercarb column. Figure 5-12 shows example chromatograms when an 8x dilute pooled urine sample was run on all three columns. Figures 5-13, 5-14, and 5-15 display the two-dimensional m/z vs. time plots that were previously used to detect the presence of contaminants for the C18 BEH, one-meter PGC and two-meter PGC, respectively. These m/z vs. time plots do not show any diagonal patterns like was seen previously, suggesting that the sample collection and preparation methods involving no polymer containers achieved the goal of preventing contamination. As the C18 BEH and one-meter Hypercarb columns were run using identical conditions, they allow direct comparison of retention. Figure 5-12 shows that PGC offers much more retention for these metabolite samples. The majority of the metabolite peaks elute within a 30 minute window on the C18 BEH column (A), meaning all of the analytes elute within a relatively narrow solvent window (a change in roughly 25% MeCN). The one-meter Hypercarb (B) has the peaks spread out across a ~55 minute window, allowing for better resolution of the peaks. Besides two peaks at 79 and 98 minutes, all of the peaks

are very are narrow across the separation window. These two peaks are likely mass overloaded due to being present in high concentrations in the pooled urine sample.

When looking at the two-meter Hypercarb column (Figure 5-12 (C)), the retention times are moved to longer times due to the use of a column twice as long and a gradient of two times the volume. This extra gradient volume was needed since the column has twice the column volume of the one-meter column. By doubling the gradient volume, the % change in MeCN per column volume is the same for both the one and two-meter gradients. Although the gradient volume was doubled, the retention times on the two-meter column are not twice as long as the one-meter column due to the fact that the pre-gradient hold was kept the same for both gradients. The two-meter column expands the separation window even more, allowing for better resolution between peaks. A unexpected observation was made in that the one-meter Hypercarb column seemed to provide a much less complex looking chromatogram than the C18 BEH and two-meter Hypercarb columns. This observation was tested with several different one-meter columns and with freshly prepared samples each time, all of which showed the same trend. It is unknown why this would occur, as it would be expected that moving to the longer gradient associated with the two-meter Hypercarb column would lead to broader and less intense peaks, with some possibly dropping below the detection limit. The difference in complexity is also seen when looking at the two-dimensional plots in Figures 5-14 and 5-15. Many more ions are detected across the gradient on the two-meter column than the one-meter column. Even at these long run times the peaks are sharp. This confirms our previous study showing that the surface diffusion properties would make PGC amenable to these very long gradient separations.

In traditional metabolomics studies, this LC-MS data would then be imported into a metabolomics data analysis program in an attempt to determine the identities of the detected compounds. In particular, an attempt was made to utilize Progenesis QI (Nonlinear Dynamics, Newcastle, UK) for identification of metabolites. Metabolites can be difficult to identify with confidence, especially in comparison to peptides and proteins. The confidence with which

identifications are made is based on retention time (compared to a database of know standards of the compound), isotope distribution, mass error, fragmentation score, and collisional cross section. As we did not have access to a database for retention times on PGC or the ability to determine collisional cross-section values since the MS system does not have ion mobility capabilities, it was impossible to identify compounds with any level of certainty from our chromatograms.

One method for comparing the quality of gradient separations it is to calculate the peak capacity. Peak capacity was calculated using Equation 5-1. The 4σ peak width was measured for the peaks in each gradient across the separation window. The separation window was selected as the time of the first and last peak that was clearly not volume overloaded. There were two peaks on the Hypercarb columns that were significantly overloaded, leading to extremely wide peaks. As these peaks skewed the average width significantly, they were left out of peak capacity calculations shown here. Table 5-2 shows the average separation window, peak width, and peak capacities measured for the C18 BEH, one-meter Hypercarb and two-meter Hypercarb columns as measured from triplicate separations. Both the one and two-meter Hypercarb columns produced higher peak capacity values than the C18 BEH column. These values for PGC can only be compared to one literature source, which reported a peak capacity of 63 in 30 minutes.[51] It is expected that $n_c \propto \sqrt{N}$.[14] The C18 BEH and one-meter Hypercarb column produced very similar N_{max} values, suggesting that they should produce similar peak capacities. However, the peak capacity was 48% higher on the one meter PGC column. As the peak width on C18 BEH was smaller than on the one-meter PGC, the improved peak capacity can be attributed to the increased retention window over which the metabolites are eluted (~28 minutes on C18 BEH vs. ~55 minutes on PGC). The two-meter Hypercarb column shows an even higher peak capacity of 235 in the ~105 minute separation window. It is possible to attempt to predict the peak capacity expected for the two-meter column based on the isocratic performance and peak capacity of the one-meter column.

$$\frac{\sqrt{N_{max,2m}}}{\sqrt{N_{max,1m}}} = \frac{n_{c,2m}}{n_{c,1m}} \qquad \text{Equation 5-3}$$

Here, $N_{max,2m}$ and $N_{max,1m}$ are the number of theoretical plates from the two and one-meter columns while $n_{c,2m}$ and $n_{c,1m}$ are the peak capacities of the two and one-meter columns. When the average values for $N_{max,2m}$, $N_{max,1m}$, and $n_{c,1m}$ are inserted, it is predicted that the resulting peak capacity for the two-meter columns should be 235, which is exactly what was measured. This shows that the performance of the columns is being retained by the gradient LC-MS system, rather than a large performance loss due to extra-column volumes. Improved gradient separations of urine with PGC prove this material's potential for use with the analysis of metabolite samples using very long capillary columns.

5.4 Conclusion

In order to fully realize the potential of porous graphitic carbon for use with chromatographic separations, it was necessary to pack, characterize and utilize capillary columns for the analysis of a complex mixture. There has been little information published on the packing and characterization of PGC columns when compared to C18 bonded stationary phases. Here, we studied the effect of sonication on the performance of two-meter capillary Hypercarb columns. Previous studies using high slurry concentrations and sonication with C18 BEH columns yielded the most efficient packed columns ever produced. For PGC, it was actually seen that sonication yielded worse performing columns than not using sonication. It is important to note that the slurry concentration used was low in comparison to the study using C18 BEH. When one-meter columns were packed without sonication, $h_{\min}$ values as low as 2.45 were observed. To the best of my knowledge, this marks the most efficient PGC column produced to date.

The appeal of PGC as a packing material is that its properties are unique in providing improved retention for polar compounds compared to C18 bonded columns. Here, urine samples were analyzed with a modified LC-MS system capable of pressures up to 45,000 psi. Originally, a single donor urine sample was analyzed with C18 BEH and PGC columns, but was discovered to contain a

number of polymer leachate contaminants. The contamination stressed the importance of sample collection and preparation steps in the process of metabolite analysis. A new-pooled urine sample was analyzed with a 30.1 cm C18 BEH column, a one-meter Hypercarb column, and a two-meter Hypercarb column. The pooled sample, which was prepared using all glass, contained no apparent polymer contaminants. Overall, the PGC columns provided significantly improved separations when compared to the C18 BEH column. The alternative retention mechanisms allows for increased retention of the metabolites, and caused them to elute over a much wider separation window. This ultimately culminated in significantly improved peak capacities of 187 and 235 for the one and two-meter Hypercarb columns, respectively. These improved peak capacity values show the potential utility of PGC as an alternative stationary phase choice when analyzing complex polar samples such as urine.

5.5 TABLES

Term	2 m PGC sonicated		2 m PGC non-sonicated		1 m PGC non-sonicated		30.1 cm C18 BEH
	Column 1	Column 2	Column 1	Column 2	Column 1	Column 2	
a	2.22	1.26	0.96	1.74	1.06	1.23	0.32
b	1.67	2.84	2.43	1.31	1.47	1.71	1.64
c	0.65	0.79	0.63	0.39	0.33	0.34	0.20
$h_{\min}$	4.3	4.26	3.43	3.17	2.45	2.75	1.45
N_{max}	134000	135000	168000	181000	117000	104000	109000
Φ	618	623	594	550	573	599	-

Table 5-1. $h_{\min}$, N_{max}, Φ, a, b, c terms from fitting the reduced van Deemter curves of all Hypercarb and BEH columns discusses. All Hypercarb columns were packed using 25 mg/mL slurries in acetone and characterized using electrochemical detection (-0.2 V vs. Ag/AgCl) of BQ in 5/95 water/MeCN + 0.1% FA. C18 BEH column shown for comparison to a traditional reversed phase material. C18 BEH column was characterized using electrochemical detection (+1.1 V vs. Ag/AgCl) of HQ in 50/50 water/MeCN + 0.1% TFA. Flow resistance was not reported for the C18 BEH column, as it is not a suitable comparison across particle types.

	30.1 cm C18 BEH	1 m Hypercarb	2 m Hypercarb
t_g (min)	27	58	105
w_p (min)	0.22	0.31	0.45
n_c	126 ± 4	187 ± 3	235 ± 4

Table 5-2. Separation window, peak width and peak capacities obtained for the gradient separation of pooled urine sample using C18 BEH, one-meter Hypercarb, and two-meter Hypercarb columns. Peak capacities were calculated using Equation 5-1. Reported values are an average of three runs for each column. C18 BEH column: 30.1 cm x 75 μm i.d. packed with 1.9 μm particles. Hypercarb columns: 100 or 200 cm x 75 μm i.d. packed with 3.48 μm particles. 27 μL gradient from 5-90% MeCN used for C18 BEH and one-meter Hypercarb columns. 54 μL gradient from 5-90% MeCN used for two-meter Hypercarb column.

5.6 FIGURES

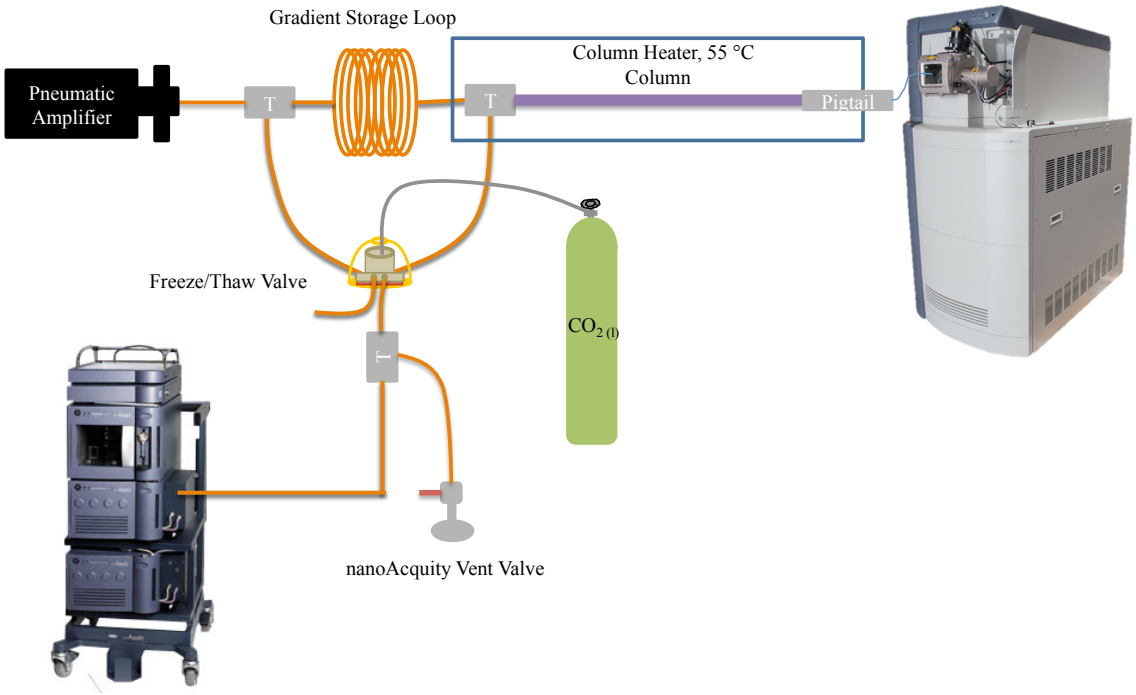

Figure 5-1. Schematic of the gradient UHPLC system used for capillary LC-MS analysis. This figure was used with permission of the author.[17]

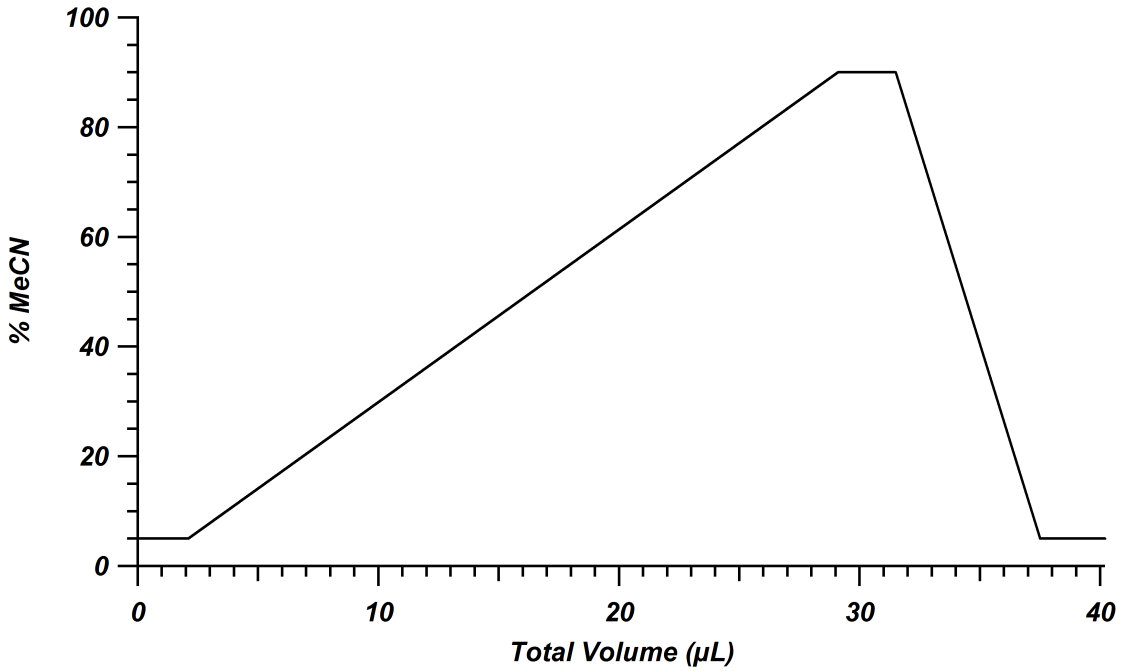

Figure 5-2. Gradient profile for the separation of human urine metabolites on the C18 BEH and one-meter Hypercarb columns. 27 µL gradient volume going from 5 to 90% MeCN. Note that this gradient is loaded in reverse so that it is pushed through the column in the correct order.

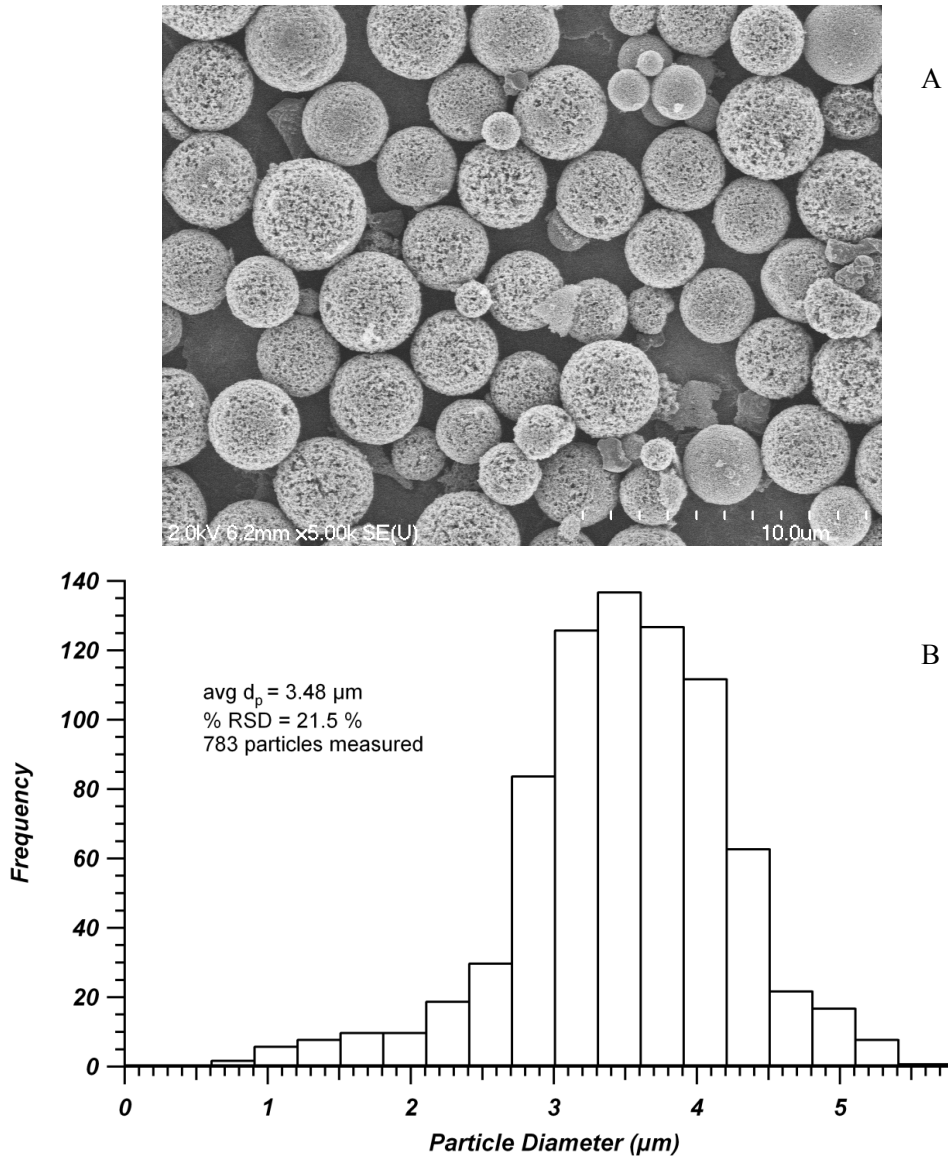

Figure 5-3. Example image of Hypercarb particle population used for capillary columns (A) and the histogram of particle distribution (B) with average and relative standard deviation in plot. Particles diameter was measured using ImageJ software. A total of 783 particles were measured for the population presented here.

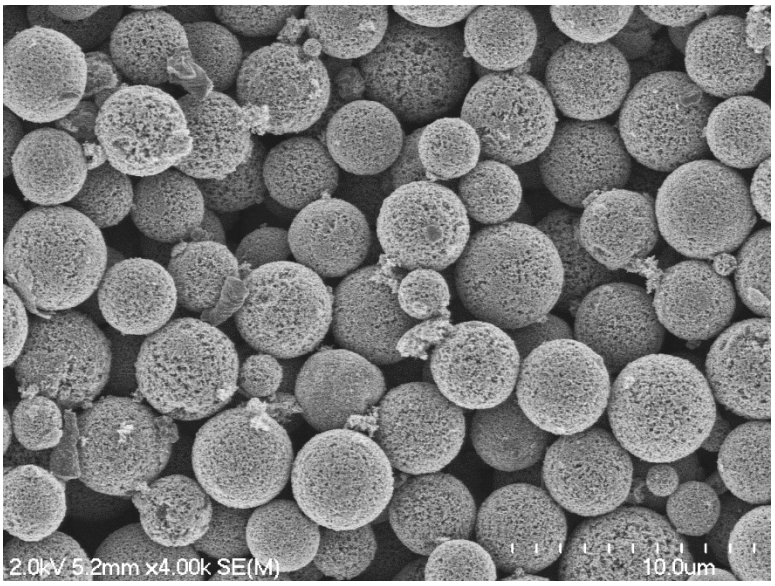

Figure 5-4. SEM image of extruded Hypercarb bed after flushing with 55,000 psi. The original column was packed with sonication, in order to expose the particles to the harshest conditions they may experience during the process. Column was flushed in 5/95 water/MeCN + 0.1% FA, after which the inlet region of the bed was extruded for imaging.

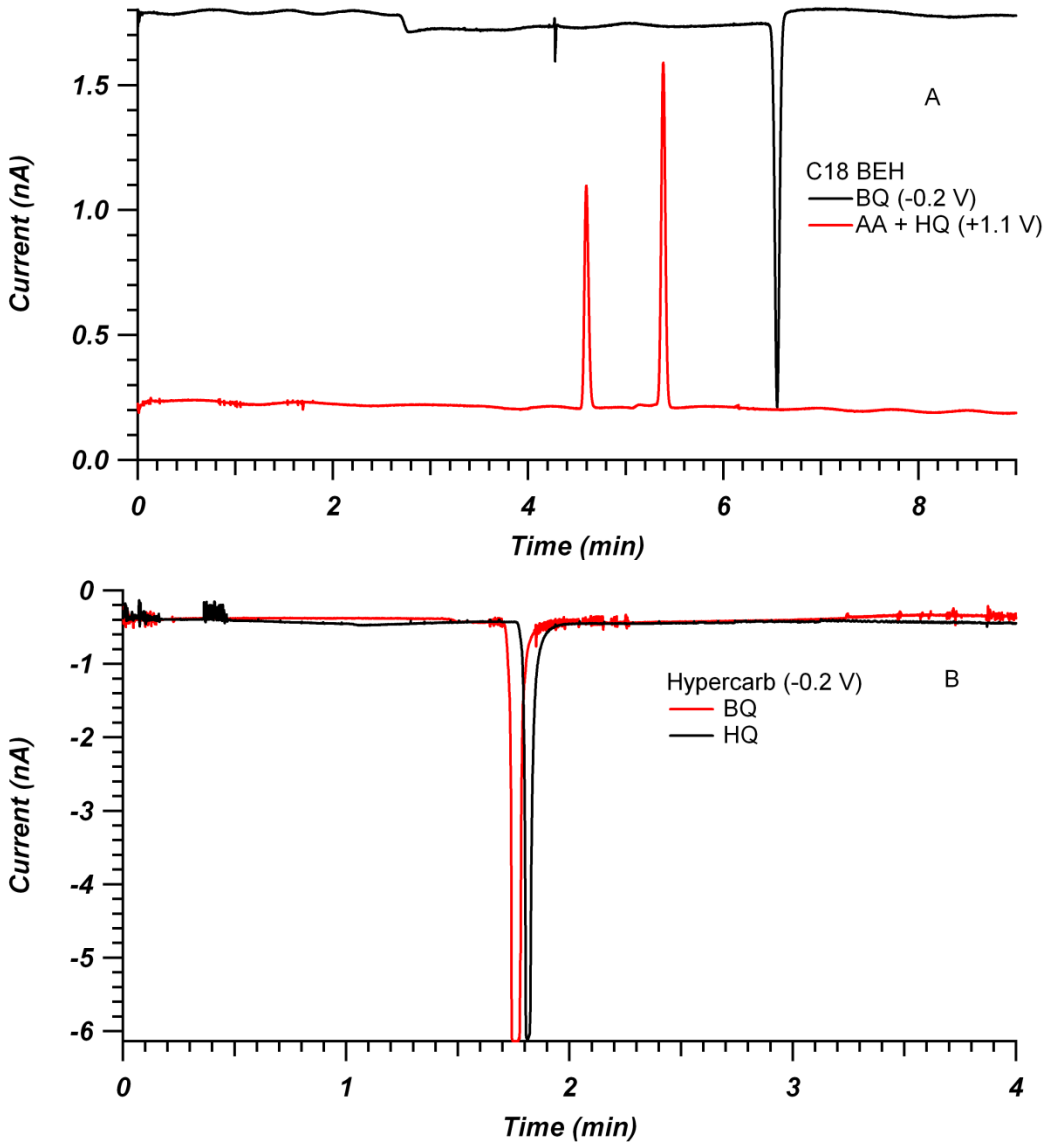

Figure 5-5. Chromatograms showing the detection of hydroquinone and 1,4-benzoquinone on C18 BEH (A) and Hypercarb (B) capillary columns using electrochemical detection. For the C18 BEH column, the oxidation of HQ was detected while the electrode was at +1.1 V (ascorbic acid also injected in sample). As BQ is the oxidized species of HQ, it was necessary to change the electrode potential to -0.2 V for detection (opposite signal directions due to oxidative vs. reductive current). For PGC, HQ was not detected at +1.1 V, but rather when either BQ or HQ was injected onto the Hypercarb column, an identical reduction current observed (electrode at -0.2 V). C18 BEH mobile phase: 50/50 water/MeCN + 0.1% TFA. Hypercarb mobile phase: 5/95 water/MeCN + 0.1% FA.

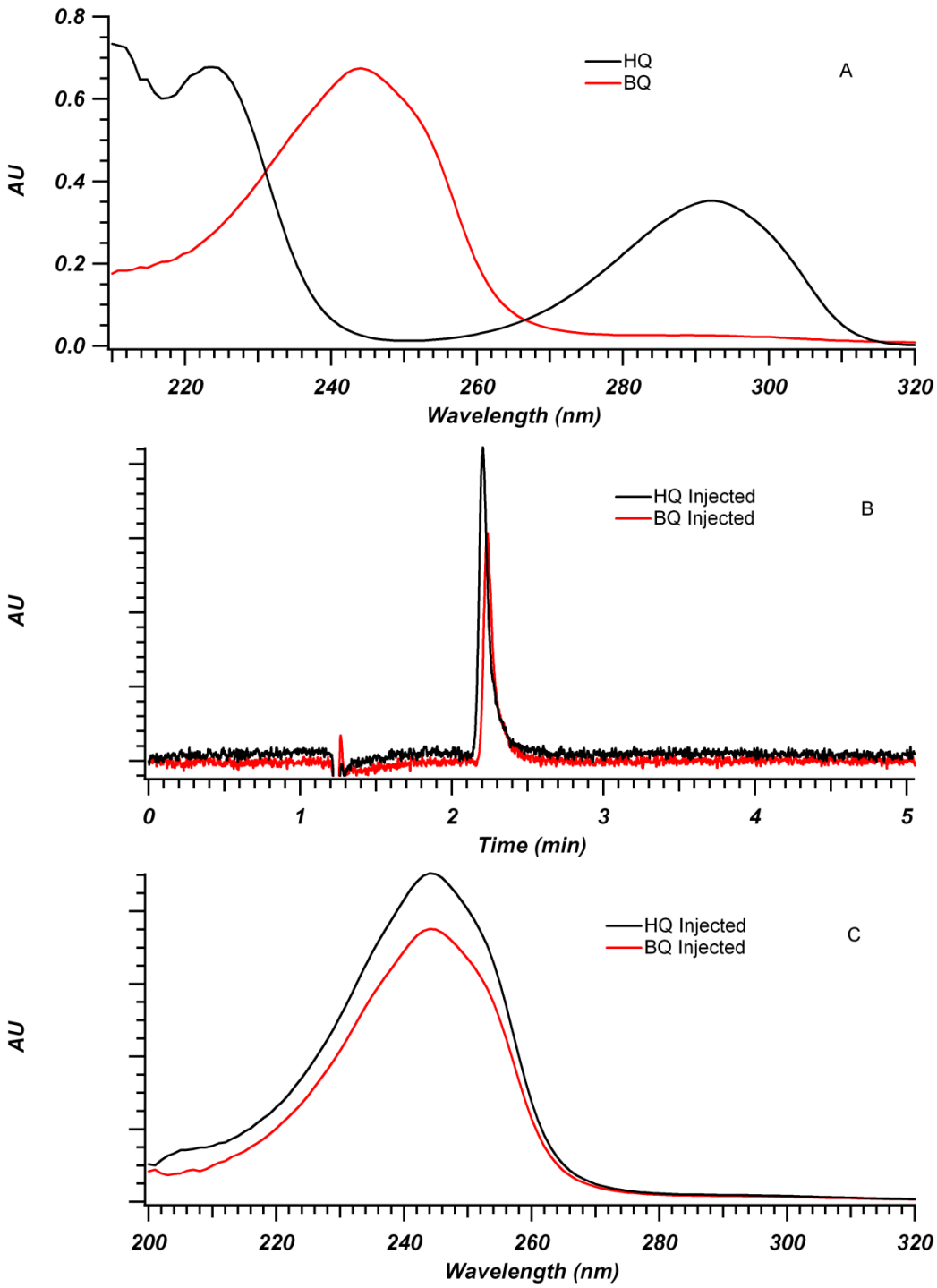

Figure 5-6. UV spectra measured for BQ and HQ in 5/95 water/MeCN + 0.1% FA (A), chromatogram showing BQ and HQ being injected separately onto a standard bore Hypercarb column (4.6 mm x 100 µm, 3 µm) with PDA detection (B) and corresponding UV spectra after being analyzed by Hypercarb column for each analyte (C). Flow rate: 1 mL/min. 30 °C.

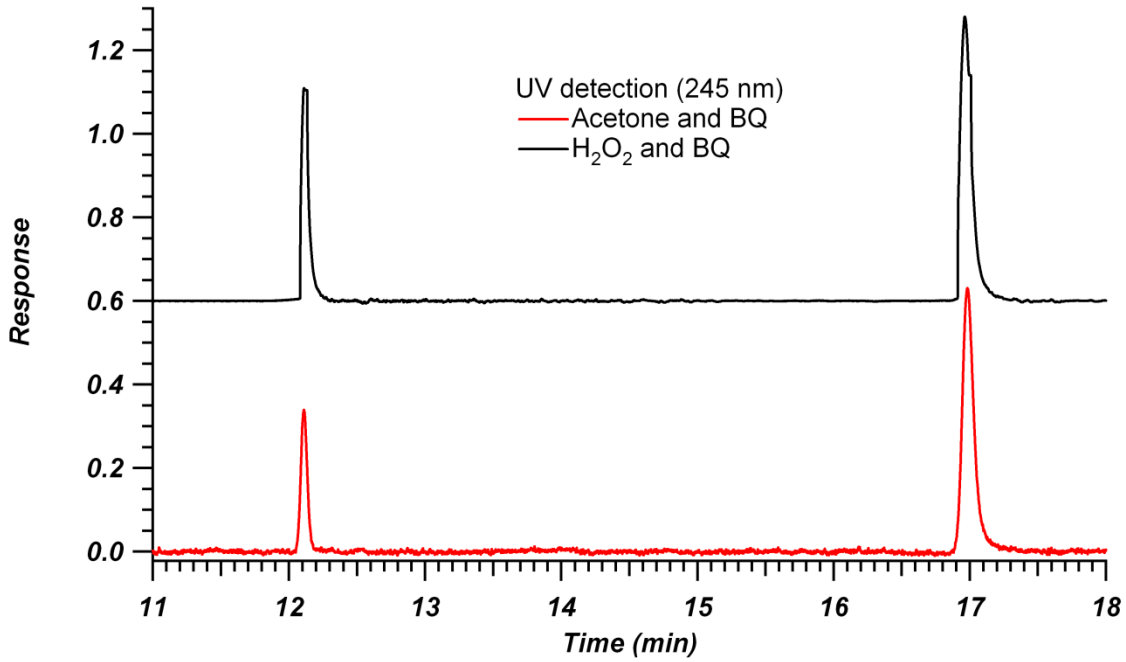

Figure 5-7. Chromatogram of samples containing acetone and hydrogen peroxide as potential deadtime markers using UV detection. Column was 100 cm x 75 µm i.d. packed with 3.48 µm Hypercarb. Mobile phase: 5/95 water/MeCN + 0.1% FA. Identical retention times of acetone and hydrogen peroxide suggest H_2O_2 acts as a deadtime marker. k' of BQ in 5/95 water/MeCN + 0.1% FA was 0.4.

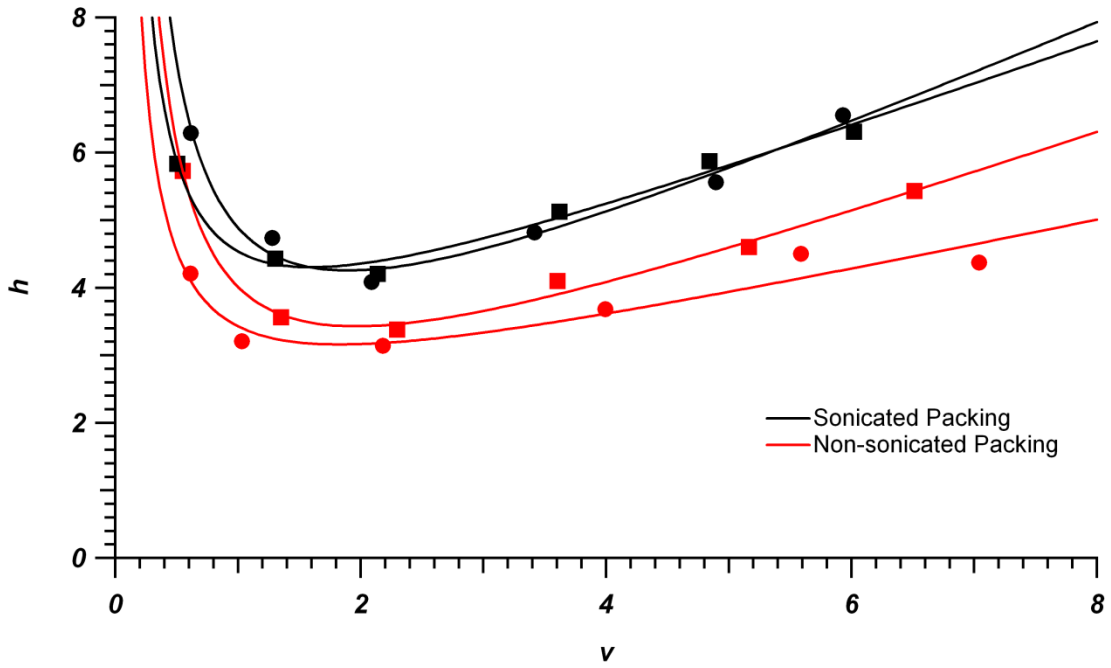

Figure 5-8. Reduced van Deemter plots of 1,4-benzoquinone for duplicate, 2 m packed Hypercarb columns when packed with (black) and without (red) sonication during the packing process. 25 mg/mL slurry in acetone used for all columns. Squares and circles are used to differentiate between the two columns from each condition. All columns were 200 cm x 75 µm i.d. packed with 3.48 µm Hypercarb and characterized using electrochemical detection (-0.2 V vs. Ag/AgCl) of BQ (k' ~0.4) at the outlet. Mobile phase: 5/95 water/MeCN + 0.1% FA.

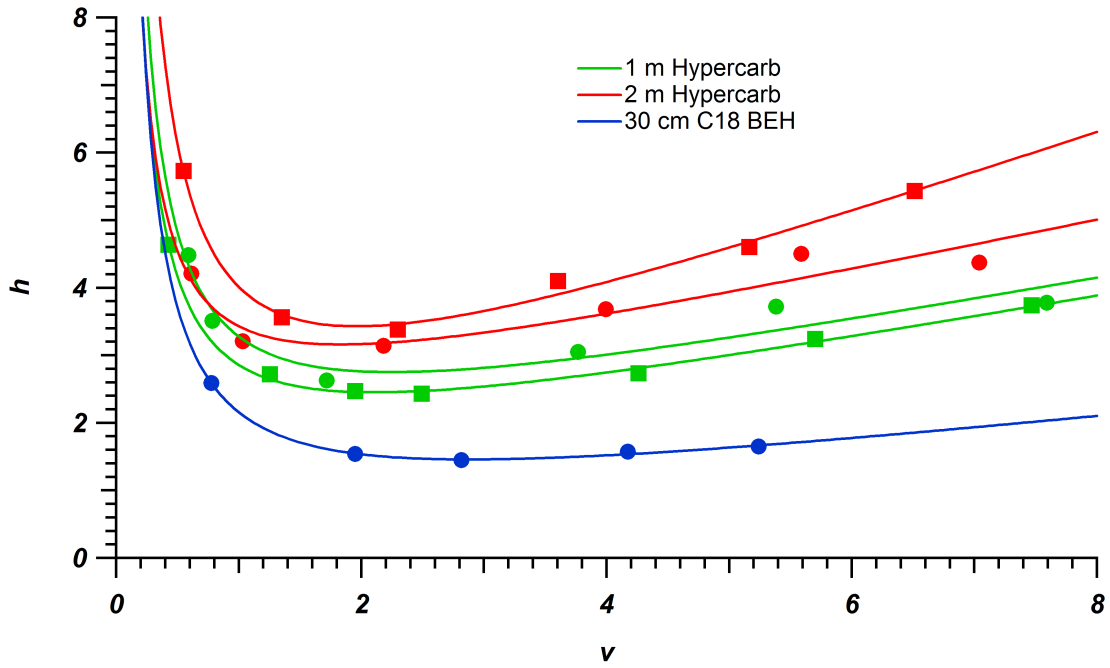

Figure 5-9. Reduced van Deemter plots of 1,4-benzoquinone for comparison of one (green) and two-meter (red) packed Hypercarb columns when packed without sonication during the packing process. A comparative C18 BEH column is shown in blue. 25 mg/mL slurry in acetone used for all Hypercarb columns. Squares and circles are used to differentiate between the two columns from each condition. Hypercarb columns were either 100 cm or 200 cm x 75 µm i.d. packed with 3.48 µm particles and characterized using electrochemical detection (-0.2 V vs. Ag/AgCl) of BQ (k' ~0.4) at the outlet with 5/95 water/MeCN + 0.1% FA. C18 BEH column was 30.1 cm x 75 µm i.d. packed with 1.9 µm particles and characterized using electrochemical detection (+1.1 V vs. Ag/AgCl) of HQ (k' ~0.2) at the outlet with 50/50 water/MeCN + 0.1% TFA.

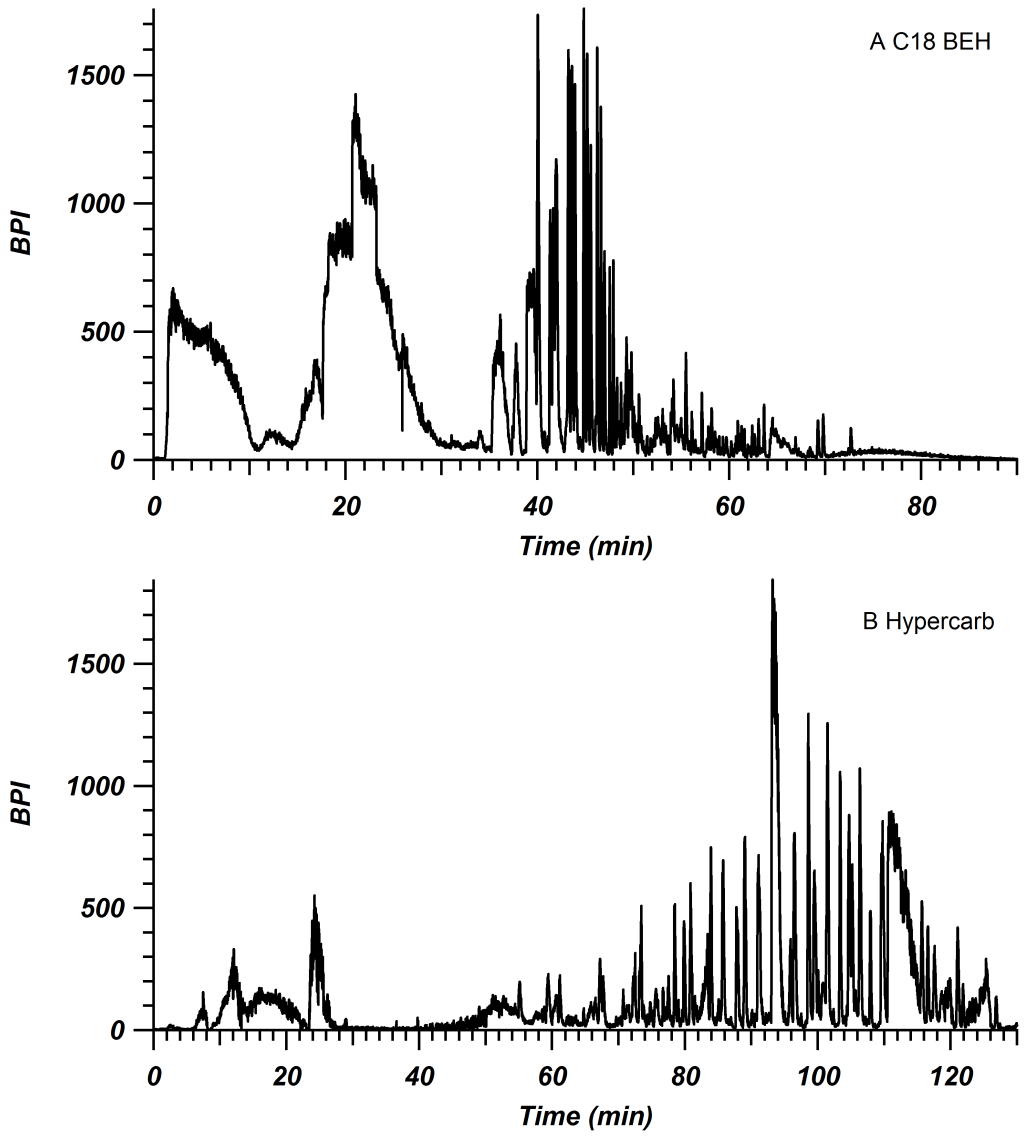

Figure 5-10. Gradient separations of single donor urine using C18 BEH (A) and Hypercarb (B) columns. Identical gradient conditions (27 µL from 5-90% MeCN) were used for both columns to allow direct comparison of retention times. Separations performed at 55 °C. Pressure was adjusted to make flow rate 300 nL/min for each column in gradient initial conditions. C18 BEH column: 30.1 cm x 75 µm i.d., 1.9 µm particles. Hypercarb column: 100 cm x 75 µm, 3.48 µm particles.

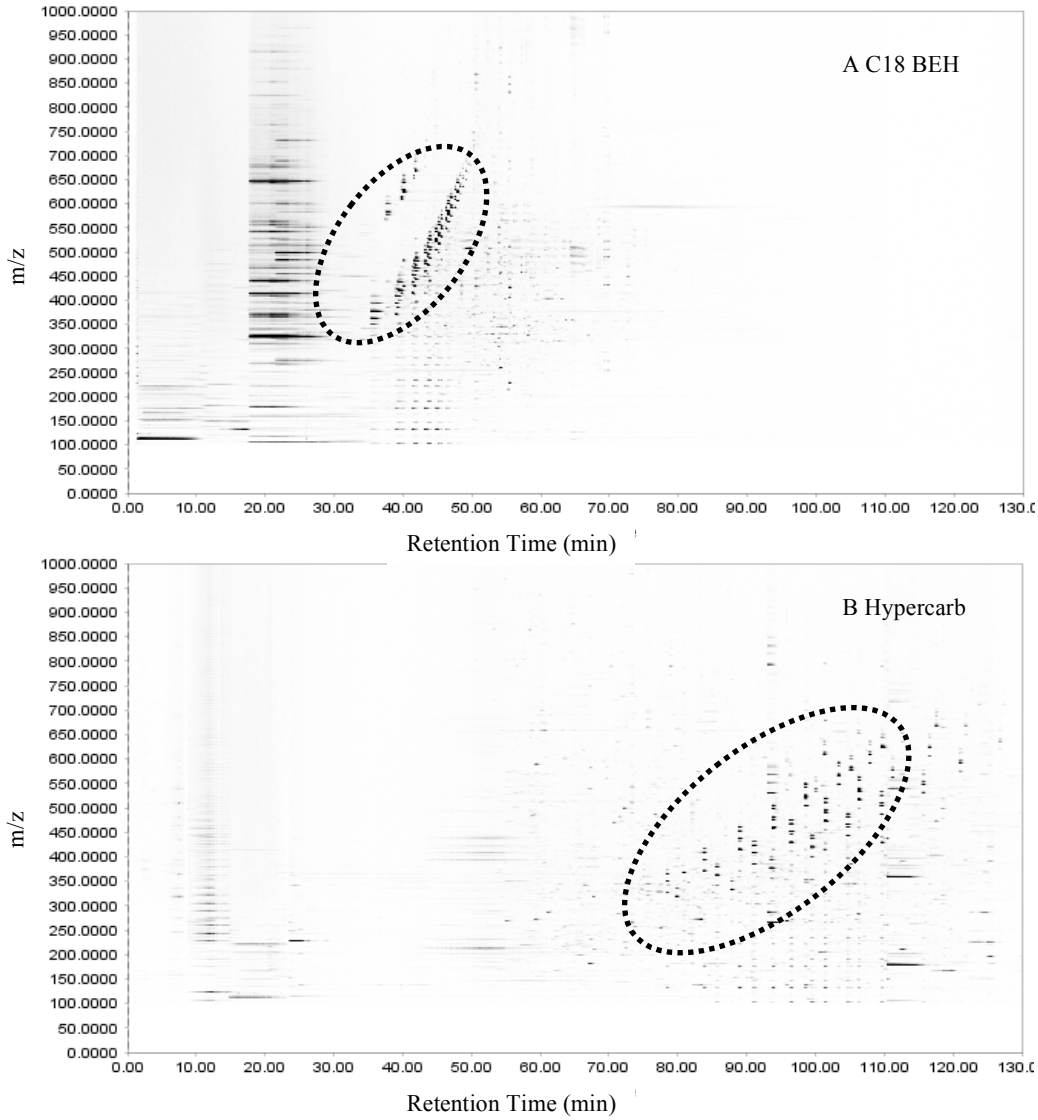

Figure 5-11. Two dimensional plots of the gradient separations of single donor urine using C18 BEH (A) and Hypercarb (B) columns, showing m/z vs. time. 27 µL gradient from 5-90% MeCN was used for C18 BEH and one-meter Hypercarb columns. Separations performed at 55 °C. Pressure was adjusted to make flow rate 300 nL/min for each column. C18 BEH column: 30.1 cm x 75 µm i.d., 1.9 µm particles. Hypercarb column: 100 cm x 75 µm, 3.48 µm particles. Circled regions show patterning of increase m/z, suggesting possible polymer contamination from sample preparation process.

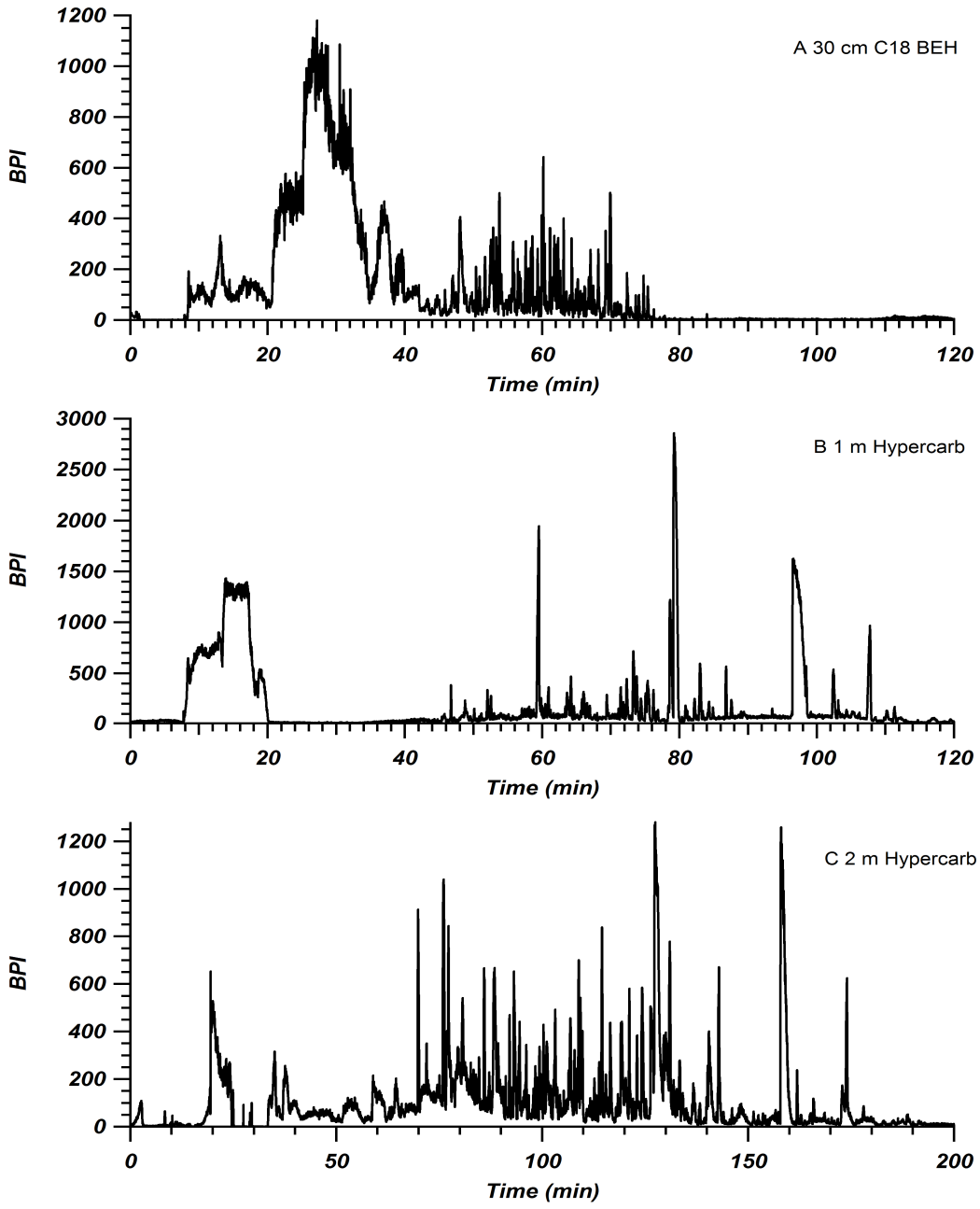

Figure 5-12. Gradient separations of pooled urine using C18 BEH (A), one-meter Hypercarb (B) and two-meter Hypercarb (C) columns. 27 µL gradient from 5-90% MeCN was used for C18 BEH and one-meter Hypercarb columns. 54 µL gradient used for two-meter Hypercarb column. Separations performed at 55 °C. Pressure was adjusted to make flow rate 300 nL/min for each column in gradient initial conditions. C18 BEH column: 30.1 cm x 75 µm i.d., 1.9 µm particles. Hypercarb column: 100 or 200 cm x 75 µm, 3.48 µm particles.

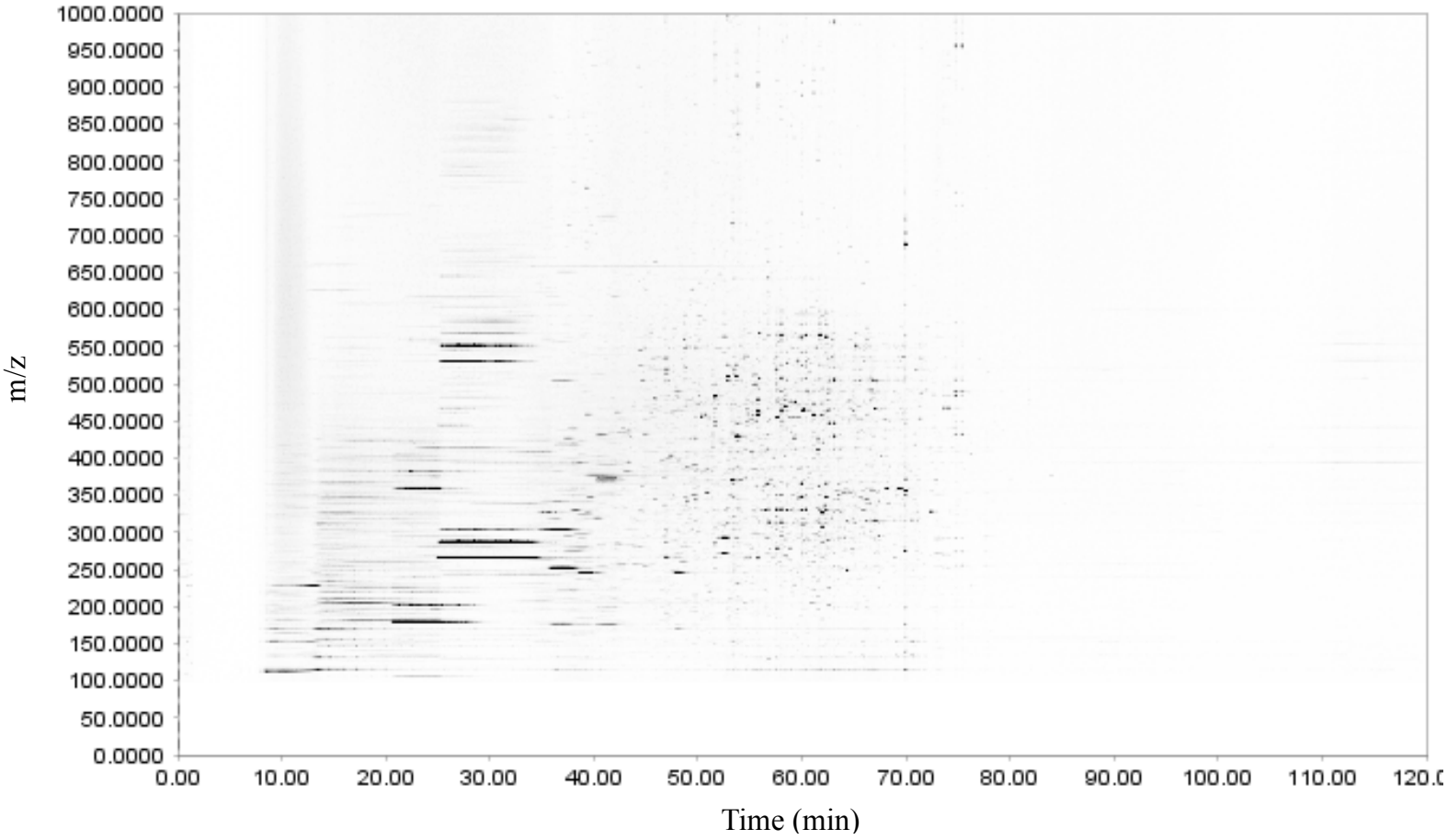

Figure 5-13. Two-dimensional plots of the gradient separations of pooled urine using C18 BEH showing m/z vs. time. Chromatogram can be seen in Figure 5-12 (A). C18 BEH column: 30.1 cm x 75 μm i.d., 1.9 μm particles.

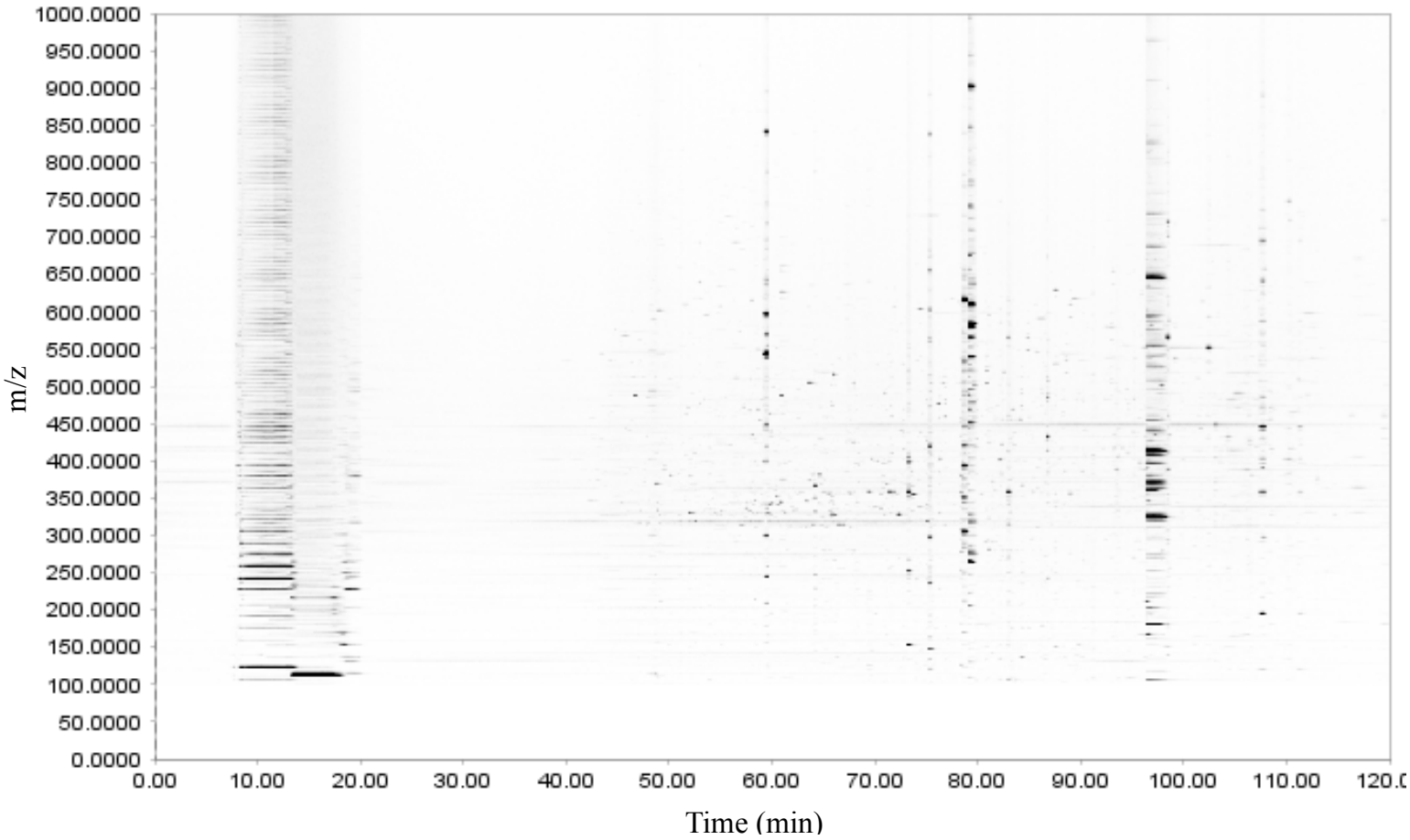

Figure 5-14. Two-dimensional plots of the gradient separations of pooled urine using one-meter Hypercarb showing m/z vs. time. Chromatogram can be seen in Figure 5-12 (B). Hypercarb column: 100 cm x 75 μm, 3.48 μm particles.

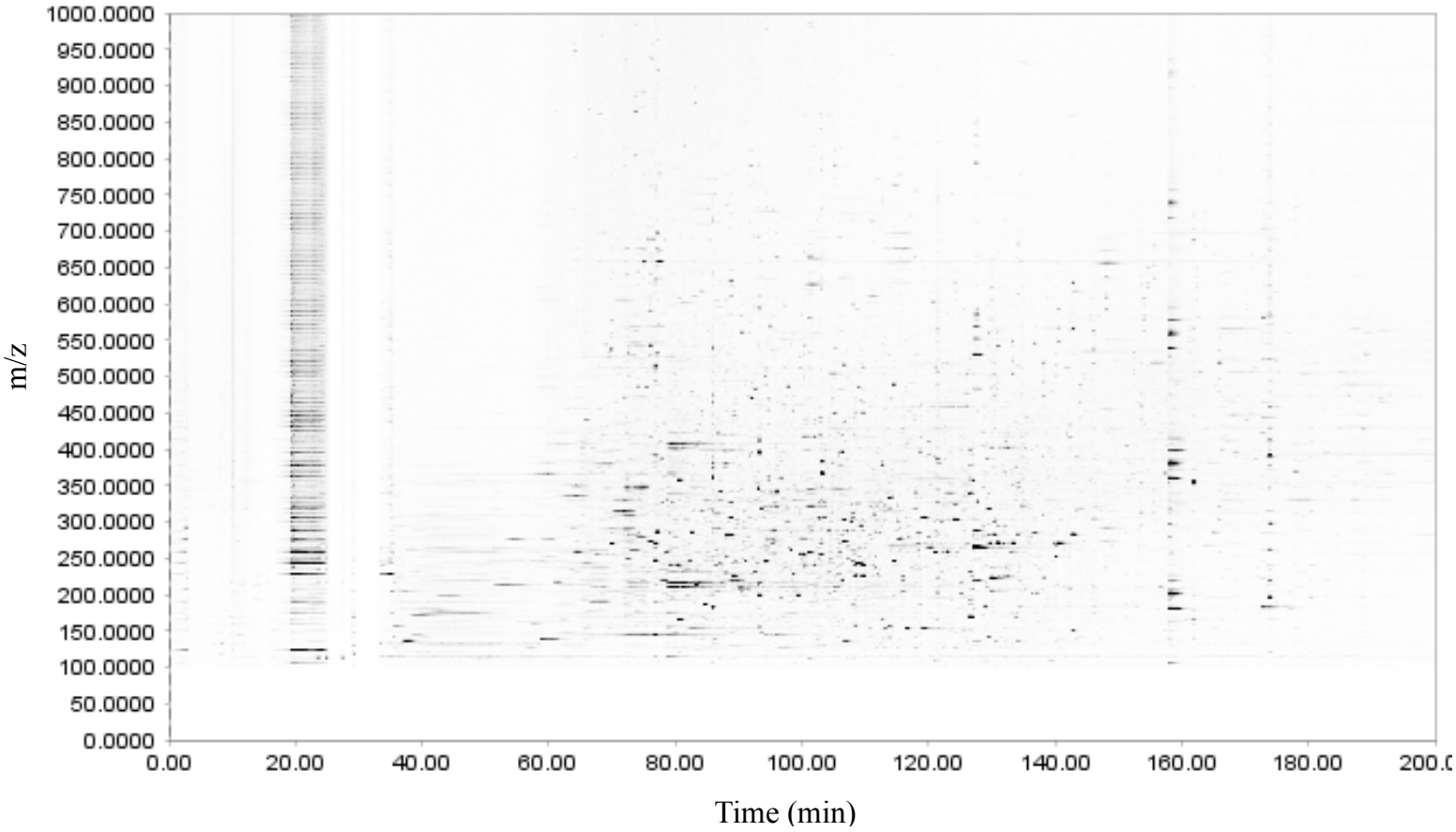

Figure 5-15. Two-dimensional plots of the gradient separations of pooled urine using two-meter Hypercarb column showing m/z vs. time. Chromatogram can be seen in Figure 5-12 (C). Hypercarb column: 200 cm x 75 μm, 3.48 μm particles.

REFERENCES

(1) Bouatra, S.; Aziat, F.; Mandal, R.; Guo, A. C.; Wilson, M. R.; Knox, C.; Bjorndahl, T. C.; Krishnamurthy, R.; Saleem, F.; Liu, P.; Dame, Z. T.; Poelzer, J.; Huynh, J.; Yallou, F. S.; Psychogios, N.; Dong, E.; Bogumil, R.; Roehring, C.; Wishart, D. S. *PLoS One* **2013**, *8* (9), 1–28.

(2) Gika, H. G.; Macpherson, E.; Theodoridis, G. A.; Wilson, I. D. *J. Chromatogr. B Anal. Technol. Biomed. Life Sci.* **2008**, *871* (2), 299–305.

(3) Roux, A.; Xu, Y.; Heilier, J.-F.; Olivier, M.-F.; Ezan, E.; Tabet, J.-C.; Junot, C. *Anal. Chem.* **2012**, *84* (15), 6429–6437.

(4) Want, E. J.; Wilson, I. D.; Gika, H.; Theodoridis, G.; Plumb, R. S.; Shockcor, J.; Holmes, E.; Nicholson, J. K. *Nat. Protoc.* **2010**, *5*, 1005–1018.

(5) Guy, P. A.; Tavazzi, I.; Bruce, S. J.; Ramadan, Z.; Kochhar, S. *J.Chromatogr.B* **2008**, *871*, 253–260.

(6) Matter, B.; Malejka-Giganti, D.; Csallany, A. S.; Tretyakova, N. *Nucleic Acids Res.* **2006**, *34* (19), 5449–5460.

(7) Cubbon, S.; Bradbury, T.; Wilson, J.; Thomas-Oates, J. *Anal. Chem.* **2007**, *79* (23), 8911–8918.

(8) Spagou, K.; Wilson, I. D.; Masson, P.; Theodoridis, G.; Raikos, N.; Coen, M.; Holmes, E.; Lindon, J. C.; Plumb, R. S.; Nicholson, J. K.; Want, E. J. *Anal. Chem.* **2011**, *83*, 382–390.

(9) Kloos, D. P.; Lingeman, H.; Niessen, W. M. A.; Deelder, A. M.; Giera, M.; Mayboroda, O. A. *J. Chromatogr. B Anal. Technol. Biomed. Life Sci.* **2013**, *927*, 90–96.

(10) Gika, H. G.; Theodoridis, G. A.; Wilson, I. D. *J. Sep. Sci.* **2008**, *31*, 1598–1608.

(11) West, C.; Elfakir, C.; Lafosse, M. *J. Chromatogr. A* **2010**, *1217*, 3201–3216.

(12) Neue, U. D. *J. Chromatogr. A* **2005**, *1079*, 153–161.

(13) Grinias, K. M.; Godinho, J. M.; Franklin, E. G.; Stobaugh, J. T.; Jorgenson, J. W. *J. Chromatogr. A* **2016**, *1469*, 60–67.

(14) Neue, U. D. *HPLC Columns: Theory, Technology, and Practice*; Wiley-VCH, Inc: New York, 1997.

(15) Link. Development and Application of Gradient Ultrahigh Pressure Liquid Chromatography for Separations of Complex Biological Mixtures, University of North Carolina, 2004.

(16) Shen, Y.; Zhang, R.; Moore, R. J.; Kim, J.; Metz, T. O.; Hixson, K. K.; Zhao, R.; Livesay, E. A.; Udseth, H. R.; Smith, R. D. *Anal. Chem.* **2005**, *77*, 3090–3100.

(17) Moore, S. M. Separation and Identification Techniques for Membrane Proteins Using Ultra-High Pressure Liquid Chromatography Coupled to Mass Spectrometry, University of North

Carolina at Chapel Hill, 2016.

(18) Snyder, L. R.; Kirkland, J. J.; Dolan, J. W. *Introduction to Modern Liquid Chromatography*, 3rd ed.; John Wiley & Sons, Inc.: Hoboken, 2010.

(19) Kirkland, J. J.; DeStefano, J. J. *J. Chromatogr. A* **2006**, *1126*, 50–57.

(20) Bruns, S.; Grinias, J. P.; Blue, L. E.; Jorgenson, J. W.; Tallarek, U. *Anal. Chem.* **2012**, *84*, 4496–4503.

(21) Treadway, J. W.; Wyndham, K. D.; Jorgenson, J. W. *J. Chromatogr. A* **2015**, *1422*, 345–349.

(22) Bruns, S.; Franklin, E. G.; Grinias, J. P.; Godinho, J. M.; Jorgenson, J. W.; Tallarek, U. *J. Chromatogr. A* **2013**, *1318*, 189–197.

(23) Godinho, J. M.; Reising, A. E.; Tallarek, U.; Jorgenson, J. W. *J. Chromatogr. A* **2016**, *1462*, 165–169.

(24) Gritti, F.; Guiochon, G. *Anal. Chem.* **2013**, *85*, 3017–3035.

(25) Blue, L. E.; Franklin, E. G.; Godinho, J. M.; Grinias, J. P.; Grinias, K. M.; Lunn, D. B.; Moore, S. M. *J. Chromatogr. A* **2017**, *In Press*.

(26) Bruns, S.; Tallarek, U. *J. Chromatogr. A* **2011**, *1218*, 1849–1860.

(27) Reising, A. E.; Godinho, J. M.; Hormann, K.; Jorgenson, J. W.; Tallarek, U. *J. Chromatogr. A* **2016**, *1436*, 118–132.

(28) Holm, A.; Solbu, K.; Molander, P.; Lundanes, E.; Greibrokk, T. *Anal. Bioanal. Chem.* **2004**, *378*, 1762–1768.

(29) Rinne, S.; Holm, A.; Lundanes, E.; Greibrokk, T. *J. Chromatogr. A* **2006**, *1119* (1–2), 285–293.

(30) Reid, C. W.; Stupak, J.; Szymanski, C. M.; Li, J. *Anal. Chem.* **2009**, *81*, 8472–8478.

(31) Dong, X.; Zhou, S.; Mechref, Y. *Electrophoresis* **2016**, *37* (11), 1532–1548.

(32) Törnkvist, A.; Nilsson, S.; Amirkhani, A.; Nyholm, L. L. M.; Nyholm, L. L. M. *J. Mass Spectrom.* **2004**, *39*, 216–222.

(33) Pabst, M.; Altmann, F. *Anal. Chem.* **2008**, *80* (19), 7534–7542.

(34) Törnkvist, A.; Sjöberg, P. J. R.; Markides, K. E.; Bergquist, J. *J. Chromatogr. B* **2004**, *801*, 323–329.

(35) Koivisto, P.; Stefansson, M. *Chromatographia* **2003**, *57*, 37–45.

(36) Al Rifafï, R.; Demesmay, C.; Rocca, J. L. *J. Chromatogr. A* **2002**, *973*, 177–186.

(37) Koivisto, P.; Törnkvist, A.; Heldin, E.; Markides, K. E. *Chromatographia* **2002**, *55* (1–2), 39

(38) Knox, J. H.; Ross, P. In *Advances in Chromatography, Vol 37*; Brown, P. R., Grushka, E., Eds.; Marcel Dekker: New York, 1997; pp 73–161.

(39) Zou, G.; Benktander, J. D.; Gizaw, S. T.; Gaunitz, S.; Novotny, M. V. *Anal. Chem.* **2017**, *89* (10), 5364–5372.

(40) Maiolica, A.; Borsotti, D.; Rappsilber, J. *Proteomics* **2005**, *5*, 3847–3850.

(41) Knecht, L. A.; Guthrie, E. J.; Jorgenson, J. W. *Anal. Chem.* **1984**, *56*, 479–482.

(42) Hsieh, S.; Jorgenson, J. W. *Anal. Chem.* **1996**, *68*, 1212–1217.

(43) Törnkvist, A.; Markides, K. E.; Nyholm, L. *Analyst* **2003**, *128*, 844–848.

(44) Rinne, S.; Holm, A.; Lundanes, E.; Greibrokk, T. *J. Chromatogr. A* **2006**, *1119*, 285–293.

(45) Shibukawa, M.; Terashima, H.; Nakajima, H.; Saitoh, K. *Analyst* **2004**, *129*, 623–628.

(46) Pabst, M.; Grass, J.; Fischl, R.; Le, R.; Jin, C.; Borth, N.; Altmann, F. *Anal. Chem.* **2010**, *82*, 9782–9788.

(47) Giddings JC. *John Wiley sons New York* **1991**, 97–101.

(48) Gritti, F.; Guiochon, G. *Journal of Chromatography A*. 2012, pp 2–40.

(49) Gritti, F.; Guiochon, G. *Journal of Chromatography A*. 2013, pp 1–13.

(50) Gika, H. G.; Theodoridis, G. A.; Wilson, I. D. *J. Chromatogr. A* **2008**, *1189*, 314–322.

(51) Melmer, M.; Stangler, T.; Premstaller, A.; Lindner, W. *J. Chromatogr. A* **2011**, *1218*, 118–123.

APPENDIX: CALCULATION OF ERROR IN SURFACE DIFFUSION

Due to the number of measurements and calculations needed to study stationary phase diffusion (Chapter 3), an in depth analysis of error was needed. This section will detail the calculation and propagation of error through the measurement of the surface diffusion properties of C18 BEH and Hypercarb materials. For discussion of the theory and principles surrounding the equations used here, the readers are directed to Chapter 3. The standard deviation of any value will be written as σ_x with the select term as the subscript. For example, the standard deviation in the retention factor (k') will be written as $\sigma_{k'}$.

The measurement of an analyte's diffusion coefficient in the mobile phase (D_m) was performed using frontal analysis with a capillary scale, dual-UV setup. The measured sigmoids were differentiated to form Gaussian peaks and calculate D_m using:

$$D_m = \frac{d_c^2\,\Delta t}{96\,\Delta\sigma_{net}^2} \qquad \text{A-1}$$

The standard deviation in d_c^2 can be calculated by:

$$\frac{\sigma_{d_c^2}}{d_c^2} = 2\left(\frac{\sigma_{d_c}}{d_c}\right) \qquad \text{A-2}$$

σ_{D_m} can then be calculated by accounting for the error in the measurements of the terms in Equation A-1. As measurements for a single solute were taken using a variety of pressures to assure no variability with pressure, Δt and $\Delta\sigma_{net}^2$ were assumed to be constants within any measurement.

$$\frac{\sigma_{D_m}}{D_m} = \sqrt{\left(\frac{\sigma_{d_c^2}}{d_c^2}\right)^2 + \left(\frac{\sigma_{\Delta t}}{\Delta t}\right)^2 + \left(\frac{\sigma_{\Delta\sigma_{net}^2}}{\Delta\sigma_{net}^2}\right)^2} = \frac{\sigma_{d_c^2}}{d_c^2} \qquad \text{A-3}$$

The peak parking experiments were then used to calculate D_{eff} of an analyte using Equation A-4:

$$\sigma_{ax,L}^2 = 2D_{eff}t_{stop} \qquad \text{A-4}$$

By plotting all of the measured $\sigma_{ax,L}^2$ and t_{stop} pairs, D_{eff} is calculated using the slope of a linear trend line and is equal to $\frac{slope}{2}$. $\sigma_{D_{eff}}$ can then be calculated using the following equation.

$$\frac{\sigma_{D_{eff}}}{D_{eff}} = \sqrt{(\frac{\sigma_{slope}}{slope})^2} = \frac{\sigma_{slope}}{slope} \quad \text{A-5}$$

$$\sigma_{D_{eff}} = \frac{\sigma_{slope}}{2} \quad \text{A-6}$$

D_{eff} represents the combination of the migration of an analyte through the mobile and stationary phases by:

$$D_{eff} = \frac{\gamma_m D_m}{1+k'} + \frac{k'\gamma_s D_s}{1+k'} \quad \text{A-7}$$

k' and $\sigma_{k'}$ are calculated as follows below. Since t_m is a constant, it is assumed that $\sigma_{t_m} = 0$.

$$k' = \frac{t_R - t_m}{t_m} \quad \text{A-8}$$

$$\sigma_{t_R - t_m} = \sqrt{\sigma_{t_R}^2 + \sigma_{t_m}^2} = \sigma_{t_R} \quad \text{A-9}$$

$$\frac{\sigma_{k'}}{k'} = \sqrt{(\frac{\sigma_{t_R - t_m}}{t_R - t_m})^2 + (\frac{\sigma_{t_m}}{t_m})^2} = \frac{\sigma_{t_R - t_m}}{t_R - t_m} \quad \text{A-10}$$

In order to find γ_m for the columns used, an unretained solute was studied with stopped-flow. Since $k' = 0$, A-7 can be rearranged and used to calculate the standard deviation of the mobile phase obstruction factor (σ_{γ_m}) as follows.

$$\gamma_m = \frac{D_{eff}(1+k')}{D_m} = \frac{D_{eff}}{D_m} \quad \text{A-11}$$

$$\frac{\sigma_{\gamma_m}}{\gamma_m} = \sqrt{(\frac{\sigma_{D_{eff}}}{D_{eff}})^2 + (\frac{\sigma_{D_m}}{D_m})^2} \quad \text{A-12}$$

With knowledge of γ_m, it becomes possible to calculate the contributions of stationary phase diffusion for retained species, by rearranging Equation A-7.

$$\gamma_s D_s = \left(D_{eff} - \frac{\gamma_m D_m}{1+k'}\right)\left(\frac{1+k'}{k'}\right) \quad \text{A-13}$$

In order to simplify the calculation of error in $\gamma_s D_s$, the equation can be broken down into individual terms. The contributions of mobile phase diffusion are simplified as follows.

$$\psi = \frac{\gamma_m D_m}{1+k'} \quad \text{A-14}$$

$$\sigma_{1+k'} = \sigma_{k'} \quad \text{A-15}$$

$$\frac{\sigma_\psi}{\psi} = \sqrt{(\frac{\sigma_{\gamma_m}}{\gamma_m})^2 + (\frac{\sigma_{D_m}}{D_m})^2 + (\frac{\sigma_{1+k'}}{1+k'})^2} \quad \text{A-16}$$

ψ can then be used to find the error in $D_{eff} - \psi$.

$$\sigma_{D_{eff}-\psi} = \sqrt{\sigma_{D_{eff}}^2 + \sigma_\psi^2} \quad \text{A-17}$$

The retention term due to interaction with stationary phase is simplified to k'_{total} as follows.

$$k'_{total} = \frac{1+k'}{k'} \quad \text{A-18}$$

$$\frac{\sigma_{k'_{total}}}{k'_{total}} = \sqrt{(\frac{\sigma_{1+k'}}{1+k'})^2 + (\frac{\sigma_{k'}}{k'})^2} \quad \text{A-19}$$

Ultimately $\sigma_{\gamma_s D_s}$ can be calculated by:

$$\frac{\sigma_{\gamma_s D_s}}{\gamma_s D_s} = \sqrt{(\frac{\sigma_{D_{eff}-\psi}}{D_{eff}-\psi})^2 + (\frac{\sigma_{k'_{total}}}{k'_{total}})^2} \quad \text{A-20}$$

In order to better compare analytes in different mobile phase conditions, leading to different D_m, it is useful to ratio the stationary and mobile phase contributions to diffusion. The error in $\frac{\gamma_s D_s}{\gamma_m D_m}$ can be calculated as follows.

$$\frac{\sigma_{\gamma_m D_m}}{\gamma_m D_m} = \sqrt{(\frac{\sigma_{\gamma_m}}{\gamma_m})^2 + (\frac{\sigma_{D_m}}{D_m})^2} \quad \text{A-21}$$

$$\frac{\sigma_{\frac{\gamma_s D_s}{\gamma_m D_m}}}{\frac{\gamma_s D_s}{\gamma_m D_m}} = \sqrt{(\frac{\sigma_{\gamma_s D_s}}{\gamma_s D_s})^2 + (\frac{\sigma_{\gamma_m D_m}}{\gamma_m D_m})^2} \quad \text{A-22}$$

In the following section an example calculation will be shown for the Hypercarb measurements using 2-methylhippuric acid in 5/95 water/MeOH + 0.1% FA at 30 °C. In this process, measurements for acetone, an unretained species, are also needed in order to calculate γ_m.

D_m measurements for both acetone and 2-MHA were taken in 5/95 water/MeOH + 0.1% FA using the capillary, dual-UV system. In order to find σ_{D_m}, it is first necessary to know $\sigma_{d_c^2}$.

$$\sigma_{d_c^2} = 2d_c^2\left(\frac{\sigma_{d_c}}{d_c}\right) = 2(2.15\ x\ 10^3\ \mu m^2)\left(\frac{0.41\ \mu m}{46.39\ \mu m}\right) = 38.4\ \mu m^2 \qquad \text{A-23}$$

This is then used to find σ_{D_m} for both acetone and 2-MHA based on their own measured values of D_m.

$$\sigma_{D_m,2MHA} = D_{m,2MHA}\left(\frac{\sigma_{d_c^2}}{d_c^2}\right) = \left(9.6\ x\ 10^{-6}\ \frac{cm^2}{s}\right)\left(\frac{38.4\ \mu m^2}{2.15\ x\ 10^3\ \mu m^2}\right) \qquad \text{A-24}$$

$$\sigma_{D_m,2MHA} = 1.7\ x\ 10^{-7}\frac{cm^2}{s} \qquad \text{A-25}$$

$$\sigma_{D_m,acetone} = D_{m,acetone}\left(\frac{\sigma_{d_c^2}}{d_c^2}\right) = \left(2.61\ x\ 10^{-5}\ \frac{cm^2}{s}\right)\left(\frac{38.4\ \mu m^2}{2.15\ x\ 10^3\ \mu m^2}\right) \qquad \text{A-26}$$

$$\sigma_{D_m,acetone} = 4.7\ x\ 10^{-7}\frac{cm^2}{s} \qquad \text{A-27}$$

It is now necessary to calculate $\sigma_{D_{eff}}$ for the two species based on the plots of σ_L^2 and t_{stop} created using stopped-flow experiments.

$$\sigma_{D_{eff,2MHA}} = \frac{\sigma_{slope,2MHA}}{2} = \frac{1.58\ x\ 10^{-7}\ \frac{cm^2}{s}}{2} = 7.9\ x\ 10^{-8}\ \frac{cm^2}{s} \qquad \text{A-28}$$

$$\sigma_{D_{eff,acetone}} = \frac{\sigma_{slope,acetone}}{2} = \frac{3.84\ x\ 10^{-7}\ \frac{cm^2}{s}}{2} \qquad \text{A-29}$$

$$\sigma_{D_{eff,acetone}} = 1.9\ x\ 10^{-7}\ \frac{cm^2}{s} \qquad \text{A-30}$$

Now that D_{eff} for acetone has been calculated it is necessary to calculate γ_m and σ_{γ_m} as well as $\gamma_m\ D_m$ and $\sigma_{\gamma_m D_m}$ for 2-MHA on the Hypercarb column.

$$\sigma_{\gamma_m} = \gamma_m\sqrt{(\frac{\sigma_{D_{eff,acetone}}}{D_{eff,acetone}})^2 + (\frac{\sigma_{D_m,acetone}}{D_{m,acetone}})^2} \qquad \text{A-31}$$

$$\sigma_{\gamma_m} = 0.478\sqrt{(\frac{1.9\ x\ 10^{-7}\ \frac{cm^2}{s}}{1.25\ x\ 10^{-5}\ \frac{cm^2}{s}})^2 + (\frac{4.7\ x\ 10^{-7}\frac{cm^2}{s}}{2.61\ x\ 10^{-5}\ \frac{cm^2}{s}})^2} \qquad \text{A-32}$$

$$\sigma_{\gamma_m} = 1.1\ x\ 10^{-2} \qquad \text{A-33}$$

With γ_m now calculated, the calculations will focus solely on 2-MHA retention and diffusion data in order calculate the surface diffusion properties. First it is necessary to calculate $\sigma_{k'}$.

$$\sigma_{k'} = k'\left(\frac{\sigma_{t_R - t_m}}{t_R - t_m}\right) = 0.87\left(\frac{2.31\ x\ 10^{-3}\ min}{2.08\ min}\right) = 9.6\ x\ 10^{-4} \quad \text{A-34}$$

From here, $\sigma_{\gamma_s D_s}$ can be calculated by calculating the individual contributions of each term in the following equation.

$$\gamma_s\ D_s = \left(D_{eff,2MHA} - \frac{\gamma_m\ D_{m,2MHA}}{1 + k'}\right)\left(\frac{1 + k'}{k'}\right) \quad \text{A-35}$$

$$\psi = \frac{\gamma_m D_{m,2MHA}}{1 + k'} \quad \text{A-36}$$

$$\sigma_{1+k'} = \sigma_{k'} \quad \text{A-37}$$

$$\sigma_\psi = \psi\sqrt{(\frac{\sigma_{\gamma_m}}{\gamma_m})^2 + (\frac{\sigma_{D_{m,2MHA}}}{D_{m,2MHA}})^2 + (\frac{\sigma_{1+k'}}{1 + k'})^2} \quad \text{A-38}$$

$$\sigma_\psi = \left(2.46\ x\ 10^{-6}\ \frac{cm^2}{s}\right)\sqrt{(\frac{0.011}{0.48})^2 + (\frac{1.7\ x\ 10^{-7}\ \frac{cm^2}{s}}{9.6\ x\ 10^{-6}\ \frac{cm^2}{s}})^2 + (\frac{9.6\ x\ 10^{-4}}{1.87})^2} \quad \text{A-39}$$

$$\sigma_\psi = 7.26\ x\ 10^{-8}\ \frac{cm^2}{s} \quad \text{A-40}$$

$$\sigma_{D_{eff,2MHA}-\psi} = \sqrt{\sigma^2_{D_{eff,2MHA}} + \sigma^2_\psi} \quad \text{A-41}$$

$$\sigma_{D_{eff,2MHA}-\psi} = \sqrt{(7.9\ x\ 10^{-8}\ \frac{cm^2}{s})^2 + (7.3x\ 10^{-8}\ \frac{cm^2}{s})^2} \quad \text{A-42}$$

$$\sigma_{D_{eff,2MHA}-\psi} = 1.1\ x\ 10^{-7}\ \frac{cm^2}{s} \quad \text{A-43}$$

$$k'_{total} = \frac{1 + k'}{k'} \quad \text{A-44}$$

$$\sigma_{k'_{total}} = k'_{total}\sqrt{(\frac{\sigma_{1+k'}}{1 + k'})^2 + (\frac{\sigma_{k'}}{k'})^2} \quad \text{A-45}$$

$$\sigma_{k'_{total}} = 2.15\sqrt{(\frac{9.6\ x\ 10^{-4}}{1.87'})^2 + (\frac{9.6\ x\ 10^{-4}}{0.87})^2} \quad \text{A-46}$$

$$\sigma_{k'_{total}} = 2.6\ x\ 10^{-3} \quad \text{A-47}$$

Combining all of these terms together allows for the calculation of $\sigma_{\gamma_s D_s}$.

$$\sigma_{\gamma_S D_S} = \gamma_S D_S \sqrt{(\frac{\sigma_{D_{eff,2MHA}-\psi}}{D_{eff,2MHA}-\psi})^2 + (\frac{\sigma_{k'_{total}}}{k'_{total}})^2} \quad \text{A-48}$$

$$\sigma_{\gamma_S D_S} = (9.9\ x\ 10^{-7}\ \frac{cm^2}{s}) \sqrt{(\frac{1.1\ x\ 10^{-7}\ \frac{cm^2}{s}}{4.6\ x\ 10^{-7}\ \frac{cm^2}{s}})^2 + (\frac{2.6\ x\ 10^{-3}}{2.15})^2} \quad \text{A-49}$$

$$\sigma_{\gamma_S D_S} = 2.3\ x\ 10^{-7}\ \frac{cm^2}{s} \quad \text{A-50}$$

The error in $\frac{\gamma_S D_S}{\gamma_m D_{m,2MHA}}$ can be calculated as follows.

$$\frac{\sigma_{\gamma_m D_{m,2MHA}}}{\gamma_m D_{m,2MHA}} = \sqrt{(\frac{\sigma_{\gamma_m}}{\gamma_m})^2 + (\frac{\sigma_{D_{m,2MHA}}}{D_{m,2mHA}})^2} \quad \text{A-51}$$

$$\sigma_{\gamma_m D_{m,2MHA}} = (4.6\ x\ 10^{-6}\ \frac{cm^2}{s}) \sqrt{(\frac{1.1\ x\ 10^{-2}}{0.478})^2 + (\frac{1.7\ x\ 10^{-7}\ \frac{cm^2}{s}}{9.6\ x\ 10^{-6}\ \frac{cm^2}{s}})^2} \quad \text{A-52}$$

$$\sigma_{\gamma_m D_{m,2MHA}} = 1.4\ x\ 10^{-7}\ \frac{cm^2}{s} \quad \text{A-53}$$

$$\sigma_{\frac{\sigma_{\gamma_S D_S}}{\gamma_m D_{m,2MHA}}} = \frac{\gamma_S D_S}{\gamma_m D_{m,2MHA}} \sqrt{(\frac{\sigma_{\gamma_S D_S}}{\gamma_S D_S})^2 + (\frac{\sigma_{\gamma_m D_{m,2MHA}}}{\gamma_m D_{m,2MHA}})^2} \quad \text{A-54}$$

$$\sigma_{\frac{\sigma_{\gamma_S D_S}}{\gamma_m D_{m,2MHA}}} = \frac{9.9\ x\ 10^{-7}\ \frac{cm^2}{s}}{4.60\ x\ 10^{-6}\ \frac{cm^2}{s}} \sqrt{(\frac{1.9\ x\ 10^{-7}\ \frac{cm^2}{s}}{9.9\ x\ 10^{-7}\ \frac{cm^2}{s}})^2 + (\frac{1.4\ x\ 10^{-7}\ \frac{cm^2}{s}}{4.6\ x\ 10^{-6}\ \frac{cm^2}{s}})^2} \quad \text{A-55}$$

$$\sigma_{\frac{\sigma_{\gamma_S D_S}}{\gamma_m D_{m,2MHA}}} = 5.1\ x\ 10^{-2} \quad \text{A-56}$$

These calculations were performed for each mobile phase and analyte in order to determine the error associated with the plotted data in Figures 3-6 and 3-7.